Optimizing the Purification and Investigating the Function of Rhodoquinone Biosynthesis Enzyme A

by

Emma Michele Ferguson

Submitted in partial fulfilment of the requirements

for the degree of Master of Science

at

Dalhousie University

Halifax, Nova Scotia

August 2023

Dalhousie University is located in Mi'kma'ki, the ancestral and unceded territory of the Mi'kmaq. We are all Treaty people.

Table of Contents

List of Tables

List of Figures

Abstract

Organisms require a constant supply of energy to survive, and they store this energy in the form of adenosine triphosphate (ATP). Cellular respiration is the major source of energy; however, in many organisms it requires oxygen to continue. Organisms that reside in oxygen deficient environments have adapted to continue ATP production by using the electron carrier rhodoquinone instead of ubiquinone. Rhodoquinone has a much lower reduction potential than ubiquinone allowing for fumarate to be reduced and the production of ATP to continue in the absence of oxygen. *Rhodoquinone biosynthesis enzyme A* (*RquA*) was the first gene discovered that was required for rhodoquinone biosynthesis. RquA requires *S*-adenosylmethionine and Mn^{2+} to catalyze the conversion of ubiquinone to rhodoquinone. In this thesis an optimal method was created to purify RquA from *Euglena gracilis* and isolated RquA was used for functional assays. High performance liquid chromatography was used to perform functional based assays to determine the production of rhodoquinone. The optimal condition required for the activity of RquA was determined and *S*-adenosyl-l-homocysteine and sinefungin were identified as weak inhibitors of RquA. The solubility of RquA was increased by creating two mutants that either deleted a predicted key α-helix or the amino acid sequence was mutated to make it more hydrophilic. This research is the first characterization of RquA from a protist to enable future structural studies.

List of Abbreviations and Symbols Used

ACN	Acetonitrile
ATP	Adenosine Triphosphate
βME	Betamercapoethanol
C12E8	Anapoe-C12E8
CD	Circular Dichroism
CMC	Critical Micelle Concentration
CTAB	Cetyltrimethylammonium Bromide
DDM	n-Dodecyl-B-D-Maltoside
DTT	Dithiothreitol
ETC	Electron Transport Chain
FPLC	Fast Protein Liquid Chromatography
GSH	Reduced Glutathione
HPLC	High Performance Liquid Chromatography
IPTG	Isopropyl β-D-1-thiogalactopyranoside
MBP	Maltose Binding Protein
MCB	Multi Component Buffer
MK	Menaquinone

MRE	Mean Residue Ellipticity
O_2	Oxygen
OD_{600}	Optical Density at 600 nm
PQ	Plastoquinone
UQ	Ubiquinone
UQH_2	Ubiquinol
RQ	Rhodoquinone
RquA	Rhodoquinone Biosynthesis Enzyme A
RquA_HD	Helix Deletion Mutant of RquA
RquA_MH	Mutated Helix Mutant of RquA
RquA_WT	Wild Type RquA
SAM	*S*-Adenosyl-l-Methionine
SAH	*S*-Adenosyl-l-Homocysteine
SDS-PAGE	Sodium dodecyl-sulfate polyacrylamide gel electrophoresis
SEC	Size Exclusion Chromatography
TCEP	Tris-(2-carboxyethyl)-phosphine
TFA	Trifluoroacetic Acid

Acknowledgments

First, I would like to acknowledge my supervisor, Dr. David Langelaan, for taking me on as a Master student in September 2021. I have greatly appreciated his guidance and support throughout these last two years. I knew I could always count on his wisdom and knowledge if I came to him with any issue. He was always there to help me troubleshoot any problems that occurred, both experimental and mechanical, especially mechanical. I greatly appreciated his help in fixing the multiple problems that occurred on the HPLC machine. Without his ability to fix them, most of the functional assays might not have worked out the way they did. So, thank you David for allowing me to grow both as an individual and as a scientist.

Secondly, I would like the members of the Langelaan Lab for all their help and guidance over the last two years. I have thoroughly enjoyed working and getting to know everyone in the lab. In particular I would like to thank Trilok Neupane for his help at the start of my Masters degree and answering any questions I had throughout these last two years.

Thirdly, I would like to thank my supervisory committee, Dr. Jan Rainey, and Dr. Andrew Roger, for their knowledge and support throughout these last two years of my degree. Thank you for always making sure that I was always on track and being there if I had any questions.

Lastly, I would like to thank my family and friends who have supported me these last two years. Thank you all for your encouragement and allowing me to explain my research to you, even though most had no clue of what I was saying.

Chapter 1 Introduction

1.1 Energy Production in Organisms

Organisms require a constant supply of energy to survive, reproduce, and perform normal biological processes (Alberts et al, 2002). Organisms obtain energy either by electromagnetic radiation or through chemical energy obtained through food (Muller, 1983). When the chemical bonds of proteins, lipids, and polysaccharides found in food are reduced through a series of biochemical pathways, such as proteolysis, lipolysis, and glycolysis, respectively, cells use the energy produced to perform their biological processes (Alberts et al, 2002, Igelsrud, 1989). In the simplest form, through a series of reduction/oxidation (redox) reactions, lipids, and carbohydrates are oxidized to CO_2 (Alberts et al, 2002). Through oxidation of these molecules, adenosine triphosphate (ATP) is produced (Hinkle et al, 1978).

Plants, bacteria, and animals produce ATP in different ways depending on oxygen availability. Plants and algae use a process called photosynthesis to generate ATP (Allen, 2002). Photosynthesis uses the energy from sunlight to generate ATP and NADPH, which is then coupled to the formation of O_2 from H_2O (Cooper, 2000). Bacteria are classified as aerobes, anaerobes, or facultative based on how they generate energy and the availability of oxygen (Schmitz et al, 2006). Aerobic bacteria require oxygen to generate energy and can generate ATP either from photosynthesis or from the oxidation of organic compounds (Jurtshuk, 1996, Schmitz et al, 2006). Facultative bacteria can use alternate molecules as final electron acceptors, such as nitrate, methane, and fumarate, when oxygen is not readily available. Anaerobic bacteria do not require oxygen to generate ATP and tend to use fermentation as the source for energy (Hentges, 1996). Cellular respiration using oxygen is the main pathway that eukaryotic species use to

generate ATP. However, certain eukaryotic species, such as yeast, can use fermentation to generate ATP without oxygen (Voidarou et al, 2020).

1.2 Aerobic Respiration

1.2.1 Oxygen as the Terminal Electron Acceptor

Aerobic organisms obtain their energy through cellular respiration and require oxygen (Figure 1.1). Cellular respiration consists of four steps with the end goal to generate enough energy (ATP) for cells to use. Glycolysis is the first step of cellular respiration and takes place in the cytosol. Glycolysis is a series of reactions that convert one molecule of glucose to two molecules of pyruvate while generating two molecules of ATP that are formed through substrate-level phosphorylation and two molecules of nicotinamide adenine dinucleotide (NADH). The NADH molecules produced in glycolysis are shuttled to the final step of cellular respiration, the electron transport chain (ETC), as electron carriers (Alberts et al, 2002). The energy that is released from the oxidation of the molecules along the glycolytic pathway are stored in the electron carrier (NADH) and allows for ATP to be made directly through substrate-level phosphorylation (Alberts et al, 2002). Substrate-level phosphorylation does not require oxygen to produce ATP, and, therefore, glycolysis is the only step in cellular respiration that does not need oxygen.

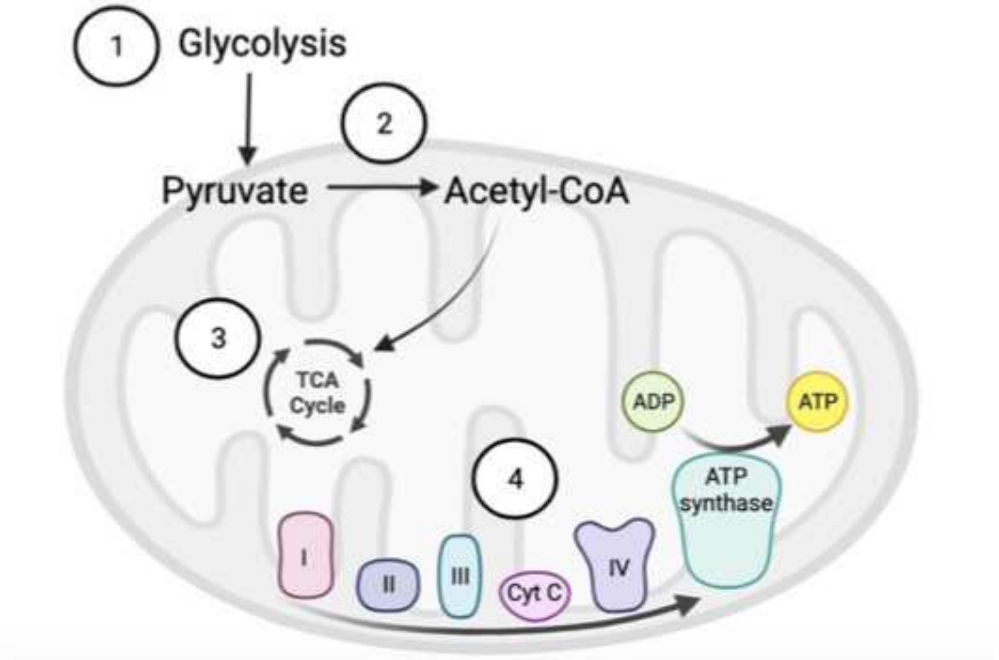

Figure 1.1 General Overview of Cellular Respiration. There are four steps of cellular respiration: glycolysis (1), converting pyruvate to acetyl-CoA (2), citric acid cycle (3), and the electron transport chain (ETC) (4). Glycolysis is the only step that does not require oxygen and is able to produce ATP through substrate level phosphorylation. If oxygen is not available, cellular respiration comes to a halt and the products from glycolysis will enter fermentation. The first three stages generate the electron carriers NADH and $FADH_2$ which are shuttled to the final stage, the electron transport chain. The end goal of cellular respiration is to generate ATP. Imagine created with biorender.com.

The next step of cellular respiration occurs in the mitochondrial matrix. Since glycolysis takes place in the cytosol, the pyruvate that was generate must first be transported into the mitochondrial matrix before it is oxidized further. The oxidization of pyruvate is catalyzed by the enzyme pyruvate dehydrogenase and results in one molecule each of CO_2, NADH, and acetyl-CoA per molecule of pyruvate. Like the NADH produced in glycolysis, the NADH produced in the step is shuttled to the ETC to act as electron carriers.

The third step of cellular respiration takes place in the mitochondrial matrix and is referred to as tricarboxylic acid cycle (TCA). The TCA cycle is a series of reactions that oxidize acetyl-CoA to form two molecules of CO_2, three molecules of NADH, one molecule of GTP - which gets converted to ATP by the enzyme nucleoside-diphosphate kinase - and one molecule of flavin adenine dinucleotide ($FADH_2$) per molecule of acetyl-CoA. The NADH and $FADH_2$ produced in the TCA are then shuttled to the ETC to act as electron carriers.

The electron transport chain (ETC) is a series of membrane bound proteins found along the inner mitochondrial membrane (Figure 1.2A). The electron carriers NADH and $FADH_2$ are oxidized, and the electrons are shuttled through a series of redox reactions that results in protons being pumped out into the intermembrane space (Alberts et al, 2002). The reduction potential of each complex in the ETC is increased to allow for the transfer of electrons (Figure 2.1B). Complex I in the ETC is known as ubiquinone oxidoreductase and comprises of NADH dehydrogenase, flavin mononucleotide (FMN), and eight iron-sulfur (Fe-S) clusters (Ahmad et al, 2023). NADH produced in the earlier steps is oxidized at complex I and donate two electrons from NADH to FMN to the Fe-S clusters and finally to ubiquinone (Ahmad et al, 2023). During the transfer of electrons, four protons are pumped into the intermembrane space of the mitochondria. Ubiquinone acts as an electron carrier that shuttles electrons from complex I to

complex III where it is reduced to ubiquinol.

A

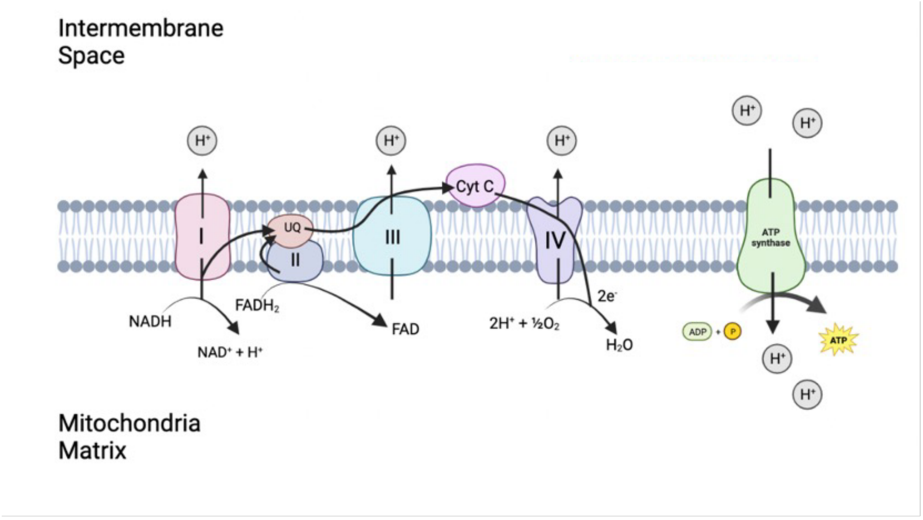

B

Complex in the ETC	Standard Reduction Potential (E °) (mV)
$NADH/NAD^+$	-320
Complex I	-300
$FADH_2/FAD$	-180
Complex II	+30
UQ/UQH_2	+100
Complex III	+200
Cytochrome C	+254
Complex IV	+562
O_2/H_2O	+800

Figure 1.2. Overview of the Electron Transport Chain. A. Electrons are reduced as they passed through the four complexes (I-IV), and electron carriers' ubiquinone (UQ) and cytochrome c (Cyt C). As they get reduced at complexes I, III, and IV, protons are pumped into the intermembrane space which creates a difference in proton concentration between the mitochondrial matrix and the intermembrane space creating an electrochemical gradient which drives the formation of ATP from ADP and P_i through ATPase. **B.** Standard reduction potentials of each complex found in the ETC (Ballard & Youngson, 2015). Image created with biorender.com.

The $FADH_2$ produced in the TCA cycle enters the ETC through complex II, also known as succinate dehydrogenase. Succinate dehydrogenase oxidizes succinate to fumarate and reduces ubiquinone (UQ) to ubiquinol (UQH_2) as two electrons are accepted by $FADH_2$. The electrons are then passed to the Fe-S clusters and finally to ubiquinone; however, no protons are pumped across the membrane during this process (Ahmad et al, 2023). Ubiquinone is then reduced to ubiquinol and transfers the electrons to complex III.

The electrons donated from NADH and $FADH_2$ are then shuttled to complex III, also known as cytochrome c reductase. Complex III is made up of cytochrome b, two Fe-S clusters, and cytochrome c proteins (Ahmad et al, 2023). The electrons are then passed to cytochrome c, which is another electron carrier that shuttles one electron at a time from complex III to complex IV (Yeagle, 2016). As the electrons are being shuttled, complex III pumps four protons into the intermembrane space.

The final complex in the ETC is complex IV, also known as cytochrome c oxidase, which oxidizes cytochrome c and transfers the electrons to oxygen and pumps four protons into the intermembrane space (Ahmad et al, 2016). Oxygen is the final electron acceptor where it gets reduced to water, and if oxygen is not available the ETC and associated ATP production will come to a stop.

1.2.2 Alternate Terminal Electron Acceptors

Certain anaerobic bacteria use other molecules as the final electron acceptor of the electron transport chain instead of oxygen. Methanogens, like *Methanobacterium thermoautotrophicum,* can reduce carbon dioxide to methane through a series of redox reactions in the absence of oxygen to continue ATP production (Thauer et al, 1977). Anaerobic bacteria, like *Paracoccus denitificans*, can reduce nitrate to nitrite to produce ATP when oxygen is absent

(Stouthamer, 1991).

The ETC can also use fumarate as the final electron acceptor in the absence of oxygen. Fumarate is reduced by the enzyme fumarate reductase. Fumarate reductase is found to be homologous to the enzyme succinate-dehydrogenase, which catalyzes the conversion of succinate to fumarate (Karavaeva et al, 2022). In these organisms, complex II runs in reverse to reduce fumarate to succinate. The high reduction potential of fumarate (+33 mV) allows fumarate to be a good electron acceptor and for that reason alternate quinones are used as electron carriers (Thauer et al, 1977).

1.3 Quinones in Organisms

Quinones are part of the family of quinoids that are widely distributed across nature and are found in natural products, endogenous biochemicals, drugs, and environmental chemicals ranging from yellow to black in colour (Bolton et al, 2016, El-Najjar et al, 2011, and Thomson, 1971). Isoprenoid quinones are important in biological process and are one of the most important compounds that are found in membranes of living organisms (Nowicka et al, 2010). Isoprenoid quinones consist of a hydrophilic head group and a hydrophobic isoprenoid side chain which allows them to be lipid soluble (Nowicka et al, 2010). Ubiquinone (UQ), menaquinone (MK), plastoquinone (PQ), and rhodoquinone (RQ) ae all classified as isoprenoids with very similar structures (Figure 1.3).

Quinones as electron carriers in biological pathways are conserved between all organisms (Milshteyn et al, 2019). Quinones act as lipid soluble hydrogen shuttles that diffuse across the membrane to carry electrons between complexes in the ETC (Milshteyn, et al, 2019). Quinones can accept two electrons and two protons, one at a time, the first protonation is through a semiquinone and the second protonation is to a hydroquinone (Figure 1.4) (Kishi et al, 2017).

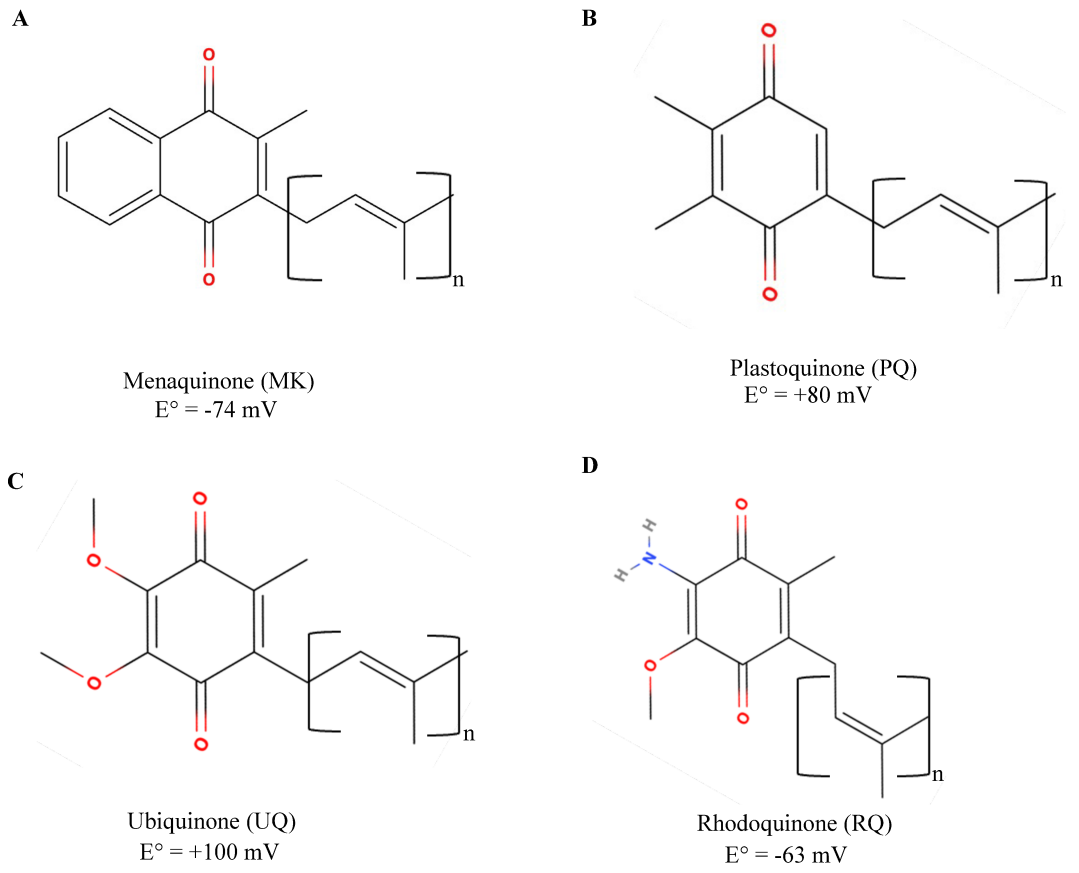

Figure 1.3 Structures of Isoprenoid Quinones A. Menaquinone (MK) is the electron carrier in bacteria that undergo anaerobic respiration with a reduction potential of -74 mV. n represent the number of isoprenoid units. Bacteria that use MK tend to have 6-10 isoprenyl units. **B.** Plastoquinone (PQ) is the electron carrier in organisms that participate in photosynthesis with a reduction potential of +80 mV. n represents the number of isoprenyl units, which plants typically have nine units. **C.** Ubiquinone (UQ) is the electron carrier in organisms that undergo aerobic respiration with a reduction potential of +100 mV. n represents the number of isoprenyl units with most mammals, including humans have 10. **D.** Rhodoquinone (RQ) is the electron carrier found in certain bacteria, eukaryotes, and helminths that undergo anaerobic respiration with a reduction potential of -63 mV. n represents the number of isoprenyl units. n = 10 *Rhodospirillum rubrum* n = 9 *Euglena gracilis* n = 9 or 10 in helminths. Figure made with MolView.

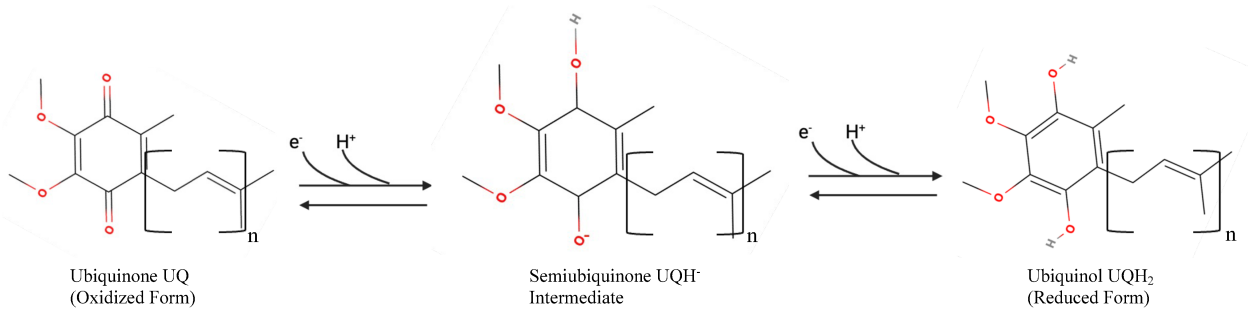

Figure 1.4 Oxidized/Reduced Forms of Ubiquinone. In the ETC, the reduction of ubiquinone occurs in two steps transferring one electron at a time forming an intermediate of a semiubiquinone. Ubiquinone is in constant equilibrium between a reduced (ubiquinol) and oxidized (ubiquinone) after receiving the two electrons (Alcázar-Fabra et al, 2016). Figure made with MolView and biorender.com

1.3.1 Menaquinone

Menaquinone (MK) tends to have 6-10 isoprenyl units; however, certain species have been found to contain as little as one unit to at most 14 units (Figure 1.3A) (Nowicka et al, 2010). MK is thought to be the evolutionary ancestor to all isoprenoid quinones (Nowicka et al, 2010). MK is the major quinone used in prokaryotic respiratory chains of Gram-positive and anaerobically respiring Gram-negative bacteria (Boersch et al., 2018, Walther et al 2013). The early occurrence of MK in the evolutionary time span and its low redox potential (-74 mV) is predicted to be attributed to the reducing characteristics of the atmosphere before oxygen was introduced (Nowicka et al, 2010). As an adaptation to aerobic respiration, the evolution of MK to other quinones with higher reduction potential occurred independently in a few groups of prokaryotic and eukaryotic species (Nowicka et al, 2010). MK acts as the first electron carrier between complex I (NADH dehydrogenase) and complex II (succinate dehydrogenase), as well as fumarate reductase enzymes in the absence of O_2 (Boersch et al., 2018). Archaea and prokaryotic species typically use MK as their electron carrier instead of UQ under anaerobic conditions to produce ATP (Dairi, 2012, Nowicka et al, 2010, and Verberne et al 1999). MK has a much lower redox potential (-74 mV) than UQ (+100 mV), which allows fumarate to be reduced. Fumarate has a reduction potential of +33 mV, which makes the reaction with UQ unfavourable due to its positive free energy (+6.116 kcal/mole) (Figure 1.5A). The lower reduction potential of MK results in a favourable negative free energy (-1.886 kcal/mole), allowing fumarate to be reduced (Figure 1.5B).

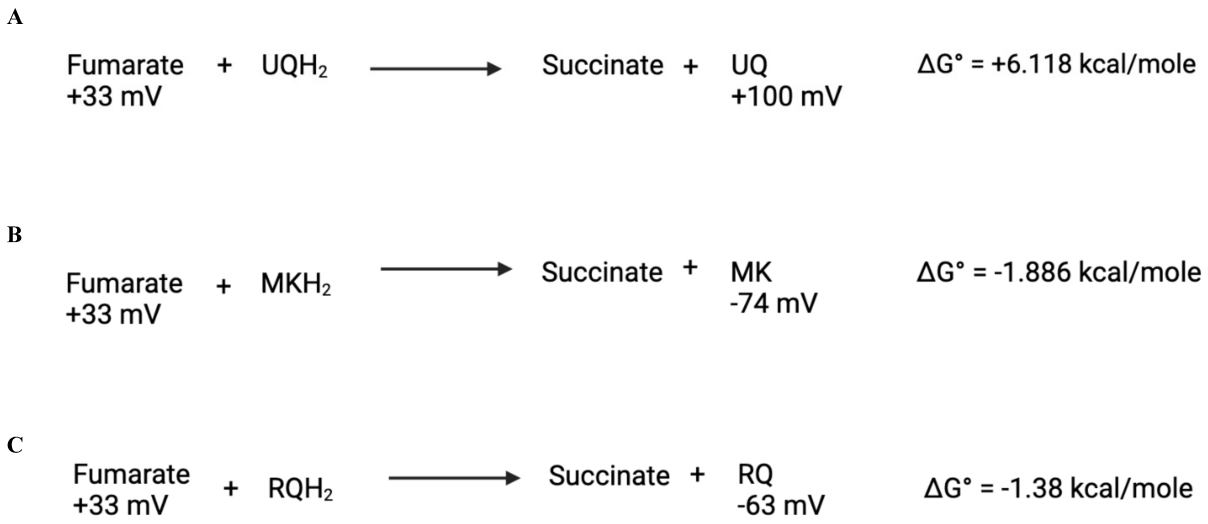

Figure 1.5 Reactions of Complex II Succinate Dehydrogenase/Fumarate Reductase A. Reaction with UQ as the electron carrier. This reaction in unfavourable due to the positive free energy of this reaction. $\Delta G°$ of each reaction was determined using this equation $\Delta G° = n(0.023)\Delta E°$, where n represents the number of electrons and $\Delta E°$ is the redox potential change (Alberts et al, 2002). Two electrons are transferred for each reaction (n=2). The $\Delta E°$ for UQ/fumarate would be +133 mV, resulting in a positive $\Delta G°$. **B.** Reaction with MK as the electron carrier. This reaction is favourable due to the negative free energy from this reaction. The $\Delta E°$ with fumarate is -41 mV, resulting in a negative free energy. **C.** Reaction with RQ as the electron carrier. This reaction is also favourable due to the negative free energy. The $\Delta E°$ with fumarate is -30 mV, resulting in a negative free energy. Figure made with biorender.com

1.3.2 Plastoquinone

Plastoquinone (PQ) has two methyl groups on the quinone ring and typically consists of nine isoprenyl units; however, some plant species have smaller isoprenyl lengths consisting of only three, four, or eight units (Figure 1.3B) (Havaux, 2020). PQ is the major isoprenoid quinone in oxygenic photosynthesis in cyanobacteria and plants, however it has not been found in photosynthetic bacteria (Amesz, 1983, Bentley et al, 1982). PQ acts as an electron carrier that shuttles electron between protein complexes found along the membrane of chloroplasts and pumps out protons (Bentley et al, 1982).

1.3.3 Ubiquinone

Ubiquinone (UQ) has two methoxy groups and a methyl group on the quinone ring and has a polyisoprenyl ring of varying length (Figure 1.3C) (Dykens, 2007). Most mammals, including humans have 10 isoprenyl units, with a few species containing nine isoprenyl units (Bentley et al, 1982). UQ is thought to have evolved from MK during the evolution of proteobacteria, making it evolutionary younger than MK (Bentley et al, 1982). UQ is found along the inner mitochondrial membrane and acts as an electron carrier in the ETC during aerobic respiration (Figure 1.6A).

UQ aids in pumping protons into the intermembrane space through what is called the Q cycle. The Q cycle consists of two steps that results in two protons being pumped across the membrane for each step, resulting in a total of four protons being pumped. The first step in the Q cycle involves ubiquinol (UQH_2) and UQ binding on two different sites in complex III of the ETC. UQH_2 moves the two electrons on a different path within complex III. The first electron goes to the Fe-S cluster and then to cytochrome c, whereas the second electron is transferred to cytochrome b and then to UQ (Ahmad et al, 2023). UQH_2 is now oxidized to UQ, as it lost both

of its electrons and can dissociate from the complex, where UQ bound at the second site is now in its semiubiquinone form, UQH^- (Ahmad et al, 2023). As both electrons are transferred to either cytochrome c or UQ, two protons are pumped across the membrane. A new UQH_2 binds to the first site again and the cycle repeats itself and two more protons are pumped across the membrane (Ahmad et al, 2023).

1.3.4 Rhodoquinone

RQ has a very similar structure to UQ, only differing at one position on the quinone ring. Where UQ has a methoxy group, RQ has an amino group (Figure 1.3D). This change in structure gives RQ a much lower reduction potential (-63 mV) compared to UQ (+100 mV) allowing for the reduction of fumarate to occur due to the favourable negative free energy (-1.38 kcal/mole) (Figure 1.5C). RQ is found in prokaryotes, bacteria, and certain eukaryotes (Salinas et al, 2020). RQ was discovered in the phototrophic purple non-sulfur bacteria *Rhodospirillum rubrum* and was first thought to play a role in its' photosynthetic ability (Salinas et al, 2020). However, *R. rubrum*'s photosynthetic ability was only restored when UQ was re-added, suggesting that RQ could be involved in a different pathway (Salinas et al, 2020). RQ can exist in both the oxidized and reduced forms, RQ/RQH_2, however, the reduced form is very unstable and short lived (Salinas et al, 2020). The oxidized and reduced forms of RQ could play a role in the redox balance in photosynthesis; however, this theory has not been proven yet (Salinas et al, 2020). These results suggest that RQ in *R. rubrum* could participate in an alternate electron transport chain. RQ could act as the electron carrier in the fumarate reductase pathway found in *R. rubrum* (Ferguson et al., 1987, Salinas et al, 2020). A mutant of *R. rubrum* that lacked RQ showed a decrease in fumarate reductase activity, suggesting that RQ could play a role in this pathway (Ferguson et al, 1987). The fumarate reductase pathway has been shown to be active in strains of

R. rubrum that contain RQ and MK, but not UQ.

Since its initial discovery, RQ has been found in a few unicellular protists, nematoda, mullosca, and platyhelminthes, but has not been found in any mammals or plants (Salinas et al, 2020). RQ is thought to be evolutionary younger than MK and UQ, as it was predicted that UQ evolved from MK first and then RQ evolved after UQ (Salinas et al, 2020). The function of RQ in protists has not been fully determined; however, it is predicted to function like RQ found in helminths (Salinas et al, 2020). In helminths, RQ is involved in a modified ETC where fumarate is the terminal electron acceptor and is reduced to succinate (Figure 1.6B). In these organisms, RQ is reduced to RQH_2 by complex I and is then re-oxidized back to RQ by complex II (Figure 1.6B). The low reduction potential of RQ (-63 mV), allows fumarate to be reduced to succinate, as the reduction potential of RQ is much lower than that of fumarate (+33 mV). This allows protons to continue to be pumped across the membrane to regenerate NAD^+ and ATP when oxygen is absent.

It has been proposed that demethyldemethoxyubiquinone (DDMQ), demethoxyubiquinone (DMQ), demethylubiquinone (DMeQ), or UQ could be precursors to RQ (Figure 1.7) (Brajcich et al, 2010). To determine which predicted compound is the direct precursor of RQ, feeding assays were done on *R. rubrum* cells to determine if RQ was produced when each compound was fed. No RQ_3 production was seen when *R. rubrum* cells were fed $DDMQ_3$ and DMQ_3, indicating that these compounds are not a precursor of RQ_3. When *R. rubrum* cells were feed $DMeQ_3$, both UQ_3 and RQ_3 were detected, indicating that $DMeQ_3$ could be the precursor. When UQ_3 was fed to *R. rubrum*, RQ_3 was detected, suggesting that UQ_3 could also be the direct precursor of RQ_3. To determine if $DMeQ_3$ or UQ_3 is the direct precursor of RQ_3, S-Adenosyl-L-homocysteine (SAH) inhibition assays were done. SAH was used as it is a

competitive inhibitor of the *O*-methyltransferase that is required for the conversion of $DMeQ_3$ to UQ_3 (Brajcich et al, 2010). UQ_3 synthesis was inhibited, RQ_3 was not detected, indicating that RQ_3 cannot be made directly from $DMeQ_3$. These results indicated that UQ_3 is the direct precursor of RQ_3 biosynthesis (Brajcich et al, 2010).

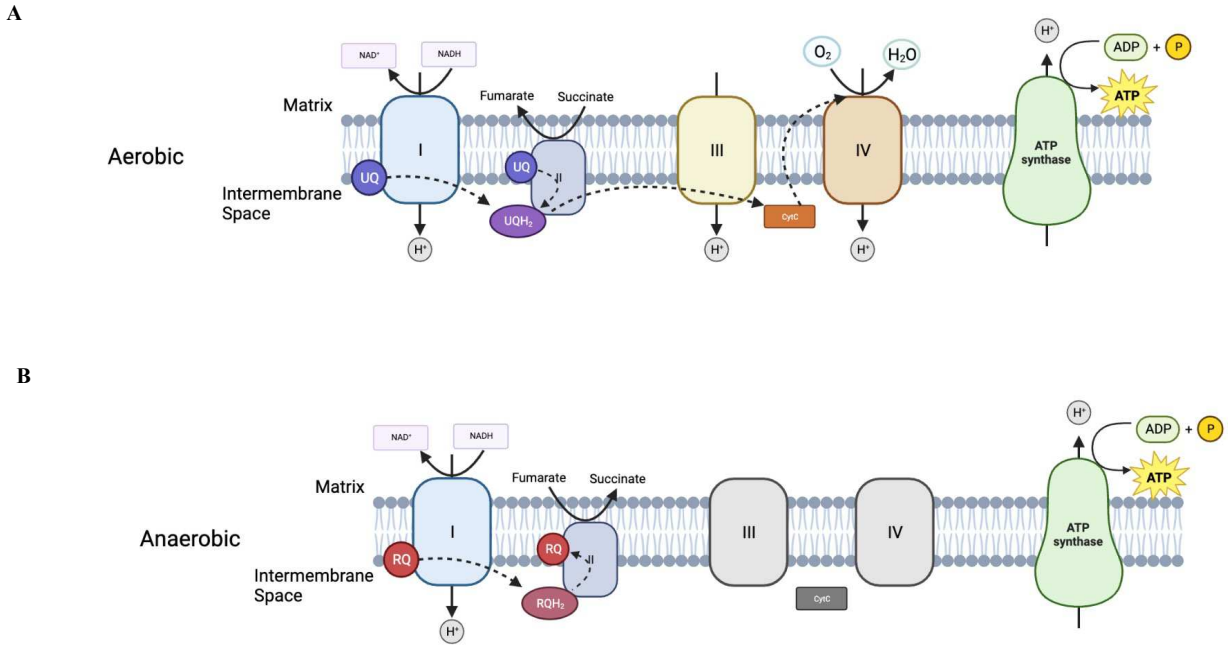

Figure 1.6 Electron Transport Chain Under Aerobic vs Anaerobic conditions A. Under aerobic conditions, the electron carrier UQ is used to shuttle electrons from complex I and II to complex III. In this case, oxygen is the final electron acceptor and is reduced to water. **B.** Under anerobic conditions, the electron carrier RQ is used. RQ has a lower redox potential (-63 mV) than UQ (+100 mV), which allows fumarate to act as the final electron acceptor and is reduced to succinate. This allows the ETC to continue and ATP production to continue in oxygen deficient environments. Figure made with biorender.com.

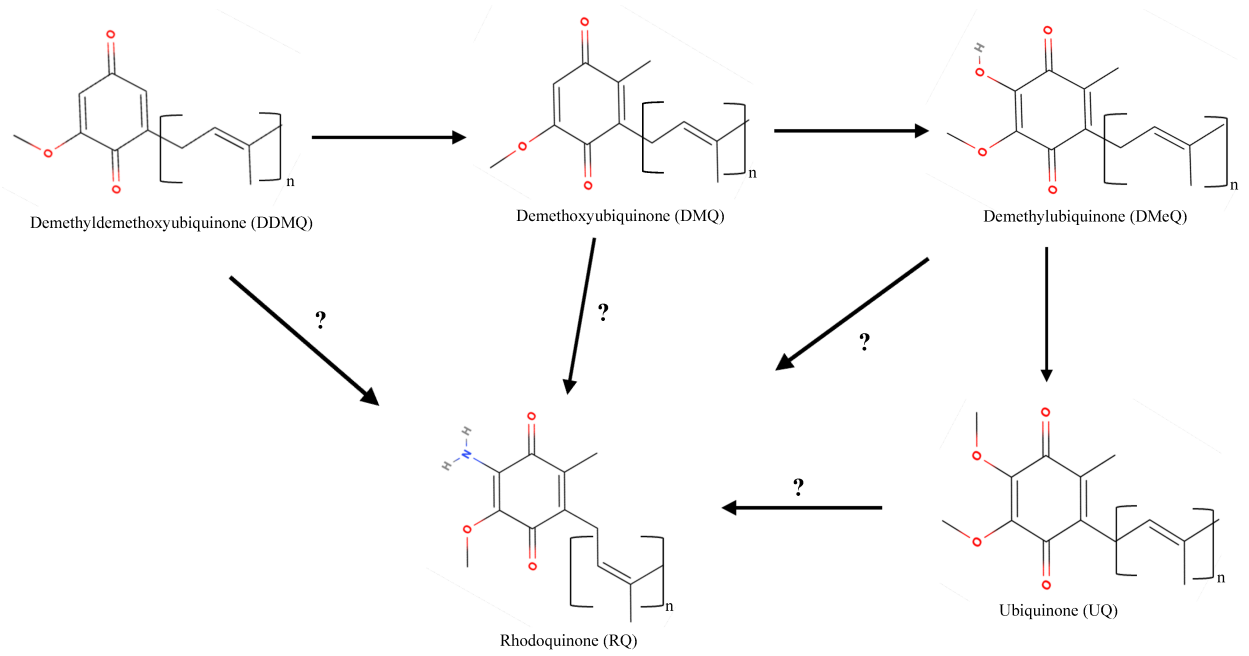

Figure 1.7 Proposed Pathway for RQ Biosynthesis. It was proposed that RQ could arise from a few compounds, demethyldemethoxyubiquinone (DDMQ), demethoxyubiquinone (DMQ), demethylubiquinone (DMeQ), or ubiquinone (UQ). Through feeding assays done with *R. rubrum,* it was determined that $DDMQ_3$ and DMQ_3 are not the direct precursors of RQ_3, as RQ_3 was not detected. However, when *R. rubrum* was fed with $DMeQ_3$, UQ_3 and RQ_3 was detected and when it *R. rubrum* was fed UQ_3, RQ_3 was also able to be detected. To distinguish if $DMeQ_3$ or UQ_3 is the direct precursor of RQ_3 S-Adenosyl-L-homocysteine (SAH) inhibition assays were done. SAH inhibits the conversion of $DMeQ_3$ to UQ_3, allowing to see which compound produces RQ_3. From these assays, it was determined that when UQ_3 is inhibited, RQ_3 synthesis did not occur, indicating that UQ_3 is the direct precursor of RQ_3. Figure made with MolView.

1.4 *Rhodoquinone Biosynthesis Enzyme A (RquA)*

1.4.1 *RquA* is Required for Rhodoquinone Biosynthesis

Rhodoquinone Biosynthesis Enzyme A (*RquA*) was the first gene discovered that was required for RQ biosynthesis. Lonjers et al created a mutant strain of *R. rubrum* (F11) that cannot grow anaerobically or produce RQ and compared to the genome sequence of the wild type (ATTC11170), which can grow anaerobically and produce RQ. The two genomic sequences only differ in one base pair, which caused a nonsense mutation in *RquA* in F11. The mutant strain F11 was still able to produce UQ, however was no longer able to produce RQ, suggesting that *RquA* could be required for RQ biosynthesis. A mutant with *RquA* deleted entirely (ATTC11170Δ*rqua*) was subsequently created to determine if *RquA* is required for RQ biosynthesis. Through liquid chromatography-mass spectrometry (LC-MS), it was determined that the mutant ATTC11170Δ*rqua* was no longer able to produce RQ, indicating that *RquA* is required for RQ biosynthesis (Lonjers et al, 2012). Not only is *RquA* required for RQ biosynthesis, the presence of *RquA* is sufficient to produce RQ. An experiment done with *E. coli* cells showed that *RquA* can drive the formation of RQ. *E. coli* cells do not contain the gene *RquA* and do not produce RQ_8 when fed UQ_8. However, RQ_8 is produced when *RquA* is expressed in *E. coli* BL21 cells that are fed UQ_8 (Bernert et al 2019). Combined these results indicate that *RquA* is directly involved in RQ biosynthesis.

Phylogenetic analyses of *RquA* showed that both prokaryotic and eukaryotic homologs of *RquA* evolved from a group of bacterial ubiquinone/menaquinone biosynthesis C-methyltransferase proteins (Stairs et al 2018). Homologs of *RquA* consist in two distinct groups, group A and group B. Group A consists of *RquA* homologs from alphaproteobacteria, betaproteobacteria, and five eukaryote lineages - breviate *Pygsuia*, stramenphiles *Blastocystis*

and *Proteromonas*, three amoebozoans *Mastigamoeba*, *Copromyxa* and a *Neoparamoeba + Paramoeba* group, euglenids and rhizarian *Brevimastigamonas.* Group B was found to consist of homologs from alpha-, beta-, and gammaproteobacterial homologs, candidate phylum radiation bacterial sequences and four independent eukaryotic lineages - opisthokont *Monosiga ovata*, a ciliate clade, a diatom group and a rhizarian amoebae. The wide distributions between different eukaryotic lineages suggest that eukaryotes acquired *RquA* from bacteria through multiple independent lateral gene transfers (Stairs et al, 2018).

1.4.2 RquA is Homologous to class I SAM-dependent methyltransferases

The gene *RquA* encodes for the protein RquA, and is related to the quinone biosynthesis enzymes UbiE, Coq5, and UbiG and was shown to share a 16% homology to UbiG (Lonjers et al, 2012, Neupane et al, 2022, and Stairs et al, 2018). RquA is homologous to and predicted to belong to the class I S-adenosylmethionine (SAM)-dependent methyltransferases (Lonjers et al, 2012, Stairs et al, 2018). The primary structures of proteins that belong to this family are not well conserved, however, the secondary and tertiary structures of these proteins are better conserved (Lonjers et al, 2012). Sequence analyses of RquA homologs have identified four distinct motifs – motif I, motif post-I, motif II, and motif post-II – that most class I SAM-dependent methyltransferases are known to have and that are critical for protein folding and SAM binding (Stairs et al, 2018). Three of those motifs were found to be conserved in *RquA* homologs; however, motif I was found not to be conserved (Lonjers et al, 2012, Stairs et al, 2018). The SAM-binding motif usually consists of the consensus sequence GxGxG, but the three glycine residues are not universally conserved between all SAM-binding proteins and the residues can be replaced with small chain amino acids or amino acids with propensity of bending the main chain (Kozbial et al, 2005). Motif I contains the SAM-binding motif of SAM-dependent

methyltransferases, and since RquA homologs were found to have substitutions in this motif, this suggests that RquA might bind SAM in a different manner than most SAM-dependent methyltransferases.

The structure of RquA has not yet been determined but can be predicted using AlphaFold2 (Figure 1.8A) (Jumper et al, 2021). RquA is predicted to adopt a Rossmann Fold, which is a common characteristic for SAM-dependent methyltransferases. The Rossmann Fold consists of alternating β-strands and α-helices, with all the strands forming a central planar β-sheet with the α-helices on each side of the sheet (Figure 1.9) (Kozbial et al, 2005). RquA is predicted to have a disordered N-terminal region, which is not required for its activity as seen with mutants with the N-terminal region deleted (Figure 1.8A) (Neupane et al, 2022). The confidence of the predicted structure is indicated by local Distance Difference Test (IDDT) scores with red being the highest confidence (>90%) and blue being the least confident (<50%) (Figure 1.8A). The regions with the lowest IDDT scores are the N-terminal region, with it coloured in blue, and a few helices that are coloured in orange/green (Figure 1.8A). Most of the structure is coloured in red, indicating a high confidence prediction (Figure 1.8A).

RquA is predicted to be associated with a membrane as it converts UQ to RQ, which are both integral membrane lipids (Figure 1.8B) (Hebditch et al. 2019). At the protein surface, one side of RquA is very hydrophobic and the other side is more hydrophilic, which could indicate that RquA could be acting as a monotopic membrane protein (Figure 1.8B), where the hydrophobic surface of RquA would interact with the membrane where UQ and RQ are located.

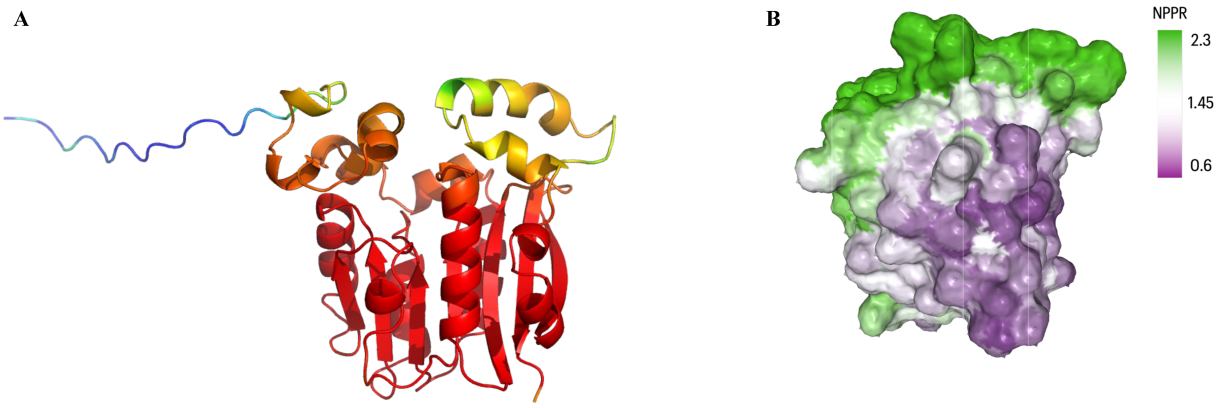

Figure 1.8 Predicted Structure of RquA. A. The structure of RquA has not been determined as of now, however, its structure was predicted using AlphaFold2 (Jumper et al, 2021). RquA is predicted to have a disordered N-terminal region and is predicted to consist of a Rossmann Fold, which is a tertiary fold that consists of alternating alpha helices and beta strands that is characteristic of methyltransferases. Red indicates a high confidence (>90%) whereas blue indicates a low confidence (<50%) of the predicted structure. **B**. RquA is predicted to be associated with a membrane, and for that reason, consists of hydrophobic patches. This diagram represents the predicted non-polar polar ratio (NPPR) of RquA (Hebditch et al. 2019). The green represents non-polar regions and purple represents polar regions.

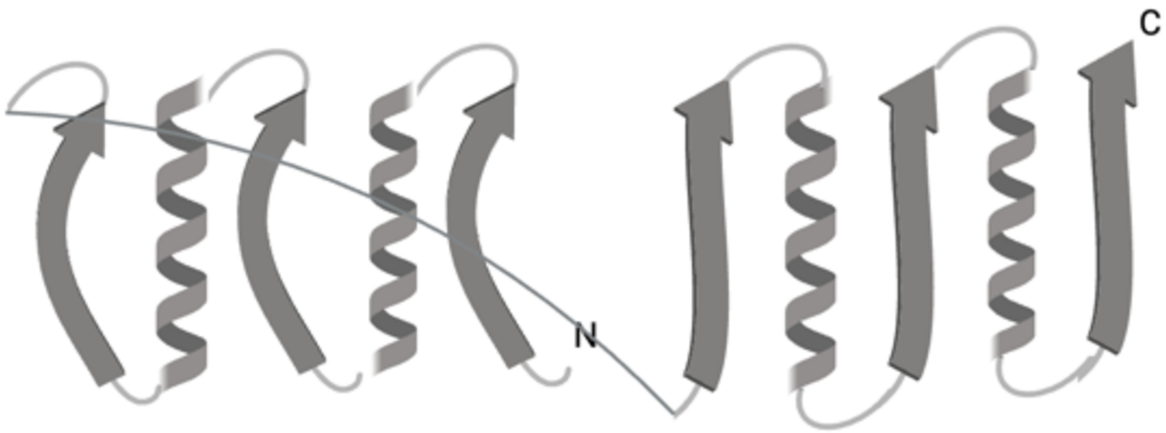

Figure 1.9 Depiction of a Rossmann Fold. A Rossmann fold is a common characteristic of methyltransferases and consists of alternating β-strands and α-helices, with all the strands forming a central planar β-sheet with the α-helices on each side of the sheet (Kozbial et al, 2005). Figure made with biorender.com.

1.4.3 RquA Catalyzes to Reaction of UQ to RQ

RquA catalyzes the formation of RQ from UQ, using SAM as an amino donor for the reaction but the exact mechanism of the reaction remains unknown (Figure 1.10). What is known regarding the reaction are the substrates and a few products of the reaction (Figure 1.10). Through liquid chromatography – mass spectrometry (LC-MS) and nuclear magnetic resonance (NMR) spectroscopy it was determined that 5′-methylthioadenosine (MTA) and CO_2 were the products derived from SAM and methanol was the product derived from UQ (Neupane et al, 2022).

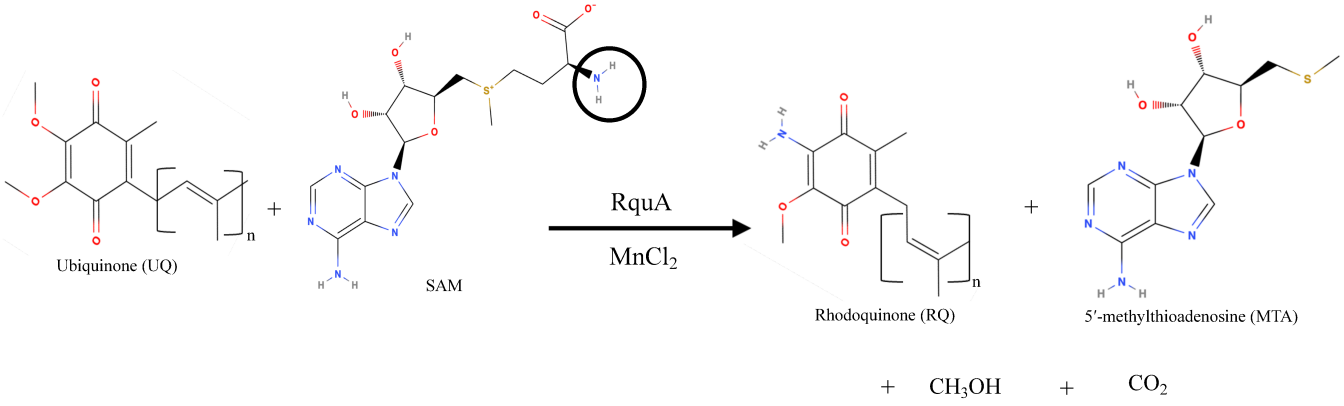

Figure 1.10 Known Substrates and Products of the RquA Reaction. Ubiquinone, SAM, and $MnCl_2$ are required for RquA to convert UQ to RQ. SAM does not participate in a typical methyltransferase reaction, but instead donates its amino group, circled in black, to generate RQ. The products 5'-methlythioadenosine and CO_2 are the byproducts of this amino transfer of SAM and methanol was determined as the byproduct coming from UQ (Neupane et al, 2022). Figure made with MolView.

Previous studies have determined that SAM and Mn^{2+} are required for the reaction (Neupane et al, 2022). Both SAM-dependent methyltransferases and RquA have a well conserved acidic residue (D or E) found in motif I and a second one in motif II that are essential for SAM binding (Figure 1.11). Mutants of both aspartic acid residues replaced with alanine residues resulted in loss of RquA function, indicating they are required for SAM binding (Neupane et al, 2022). Reactions done without SAM or with SAM analogs - *S*-adenosyl-l-homocysteine (SAH) and sinefungin – resulted in no RQ production, indicating that SAM is required for RQ biosynthesis. To determine where the amino group comes from in RQ, reactions done with exogenous NH_4^+ with and without SAM were done to see if free ammonia could act as the amino source. Reactions that were done with free ammonia and no SAM resulted in no RQ production, suggesting that the amino group of RQ comes from SAM (Neupane et al, 2022). A typical SAM-dependent methyltransferase removes the methyl group of SAM; however, that is not seen with the RquA reaction. RquA seems to catalyze the transfer of the amino group of SAM, indicating that RquA does not participate in a typical SAM-dependent methyltransferase reaction.

RquA reaction requires $MnCl_2$ to be active. Different metals with a 2^+ charge – Mn^{2+}, Mg^{2+}, Zn^{2+}, Fe^{2+}, Ca^{2+}, Cu^{2+}, Cd^{2+}, Co^{2+}, and Ni^{2+} - were tested to see if RquA is active in other divalent metal ions. However, RquA activity was only seen when Mn^{2+} was present in the reaction mixture (Neupane et al, 2022). Divalent metal ions are important for both the structure and catalysis functions of proteins (Sissi et al, 2009). Often Mg^{2+} and Mn^{2+} are used

interchangeably if they play strictly a structural role. However, since RquA is only active with Mn^{2+}, that suggests that Mn^{2+} does not play a role for the structure but could play a role in the catalysis of the RquA reaction.

```
Coq5_S.c  163       FIDVAGGSGDIAFGLLDHAESKFGDTESTMDIVDINPDMLKEGEKRAMEQGKYFKDPRVRFLVSWGEKLE         232
UbiE_E.c  66        VLDLAGGTGDLTAKFSR-----LVGETGKVVLADINESMLKMGREKLRNIGVI---GNVEYVQANAEAL-         226
UbiG_E.c  60        VLDVGCGGGILAESMAR-----E-GATVTGLDMDFEPLQVAKLHALESGIGVDYVQE--------VEEHA         120
RquA_R.r  106       VLQPACVYGPFSRHLAE-----RLGPEGYLEVHDVAPVQIHHTRRKVE--GLPQVT--LR--RA--DA-A         167
RquA_E.g  74        AIQVGHTHGGLVPKAAA-----AIGEAGDFTVVDVTPIQADHAQVKLQ---ASPW-----SRVRLGDA-C         135

     SAM-binding motif: GxGxG
```

Figure 1.11 Sequence Alignment of Multiple SAM-dependent methyltransferases. A sequence alignment was done with the methyltransferases Coq5 from *Saccharomyces cerevisiae*, UbiE from *Escherichia coli,* UbiG from *Escherichia coli, RquA* from *Rhodospirillum rubrum*, and *RquA* from *Euglena gracilis* using ClustalOmega. The SAM-binding motif in each sequence is highlighted in yellow and the key acidic residues required for SAM binding are coloured red.

1.5 Objectives

The RquA homolog from *Rhodospirillum rubrum* has been studied extensively as this was the first RquA homologue characterized *in vitro.* However, RquA homologs exist in different organisms ranging from prokaryotes to eukaryotes. My research focuses on characterizing the RquA homolog found in the unicellular protist *Euglena gracilis* to see if other RquA homologs can be purified and are functional. The overall goal of studying this protein is to determine its structure through x-ray diffraction to determine how UQ and SAM bind to RquA. Previous studies of RquA from *R. rubrum* have failed to result in any crystals, so using a different homolog might result in a structure. There has been no previous research regarding the purification or enzymatic activity of this RquA from *E. gracilis.* My thesis is focused on determining the optimal purification method needed to solubilize RquA, determining the optimal conditions for enzymatic activity, and creating structural modifications to improve its solubility. Chapter 2 focuses on determining the optimal purification method required for RquA. RquA has a very hydrophobic patch as it is predicted to be associated with a membrane, therefore, detergents were used to solubilize RquA, and an optimal purification method was determined for RquA_Euglena. The optimal reaction conditions required for RquA activity were also determined. Finally, I investigated the potential of SAM analogues as potential inhibitors of RquA.

Chapter 3 investigated modifying the sequence of RquA to improve RquA for crystallization studies. RquA contains an α-helix of mostly hydrophobic amino acids that potentially interacts with a membrane. A homologous protein to RquA, UbiG, has a similar α-helix to RquA, and once deleted, was able to be solubilized without detergent and still bind its substrates (Zhu et al, 2016). I generated two mutants of *RquA*, one with the helix deleted and one

with the amino acids mutated to hydrophilic amino acids, to see if these modifications can improve the solubility of RquA while maintaining its catalytic activity.

Chapter 2 Purification and Functional Assays of Wild Type RquA

2.1 Introduction

A surface scan using the sequence of RquA predicts one side of the protein to be non-polar and one side to be polar (Figure 2.1A). This predicted surface polarity of RquA suggests that it could be associated with a membrane as a monotopic protein. UbiG and UbiE are two methyltransferases that participate in ubiquinone biosynthesis in prokaryotes (Stefely et al, 2017). UbiG and UbiE are found to be homologous to RquA and are both monotopic membrane proteins. RquA, UbiG, and UbiE all have similar surface polarity, suggesting that RquA could also be a monotopic memnbrane protein (Figure 2.1). Monotopic membrane proteins are not always soluble in water alone and may require detergent to extract them (Allen et al 2019 and Carpenter et al 2008).

Detergents can act as tools to help isolate, solubilize, and aid membrane protein characterization (Garavito et al 2001). Detergents consist of a polar head group and a hydrophobic tail, which allows them to bind to hydrophobic surfaces (Garavito et al 2001). Detergents can self-associate to form structures called micelles, which are amphiphilic spheres that have a hydrophobic core and a hydrophilic shell (Aguilar, 2013, Joseph et al., 2017).

Common detergents used to solubilize hydrophobic proteins are Brij-35, n-Dodecyl-β-D-Maltoside (DDM), and Anapoe-C12E8 (C12E8) (Figure 2.2). Brij-35 and C12E8 are both polyglycol ether detergents with similar structures, with Brij-35 having 23 polyethylene glycol groups and C12E8 having 8 (Figure 2.2AC). The detergent DDM has a hydrophilic maltose head group and a 12-carbon tail (Figure 2.2B). The characteristics of these detergents are outlined in Table 2.1. These detergents were used in a detergent screen to determine the optimal detergent

required for RquA as there is not a universally optimal detergent for all proteins.

Table 2.1 Detergent Characteristics from Anatrace and ThermoFisher Scientific

Detergent Name	Molecular Weight (Da)	Aggregation Number	Critical Micelle Concentration mM (%w/v)
Brij-35	1125	20-40	0.09 (0.01%)
Anapoe C12E8	539.1	123	0.09 (0.005%)
DDM	510	98	0.17 (0.009%)

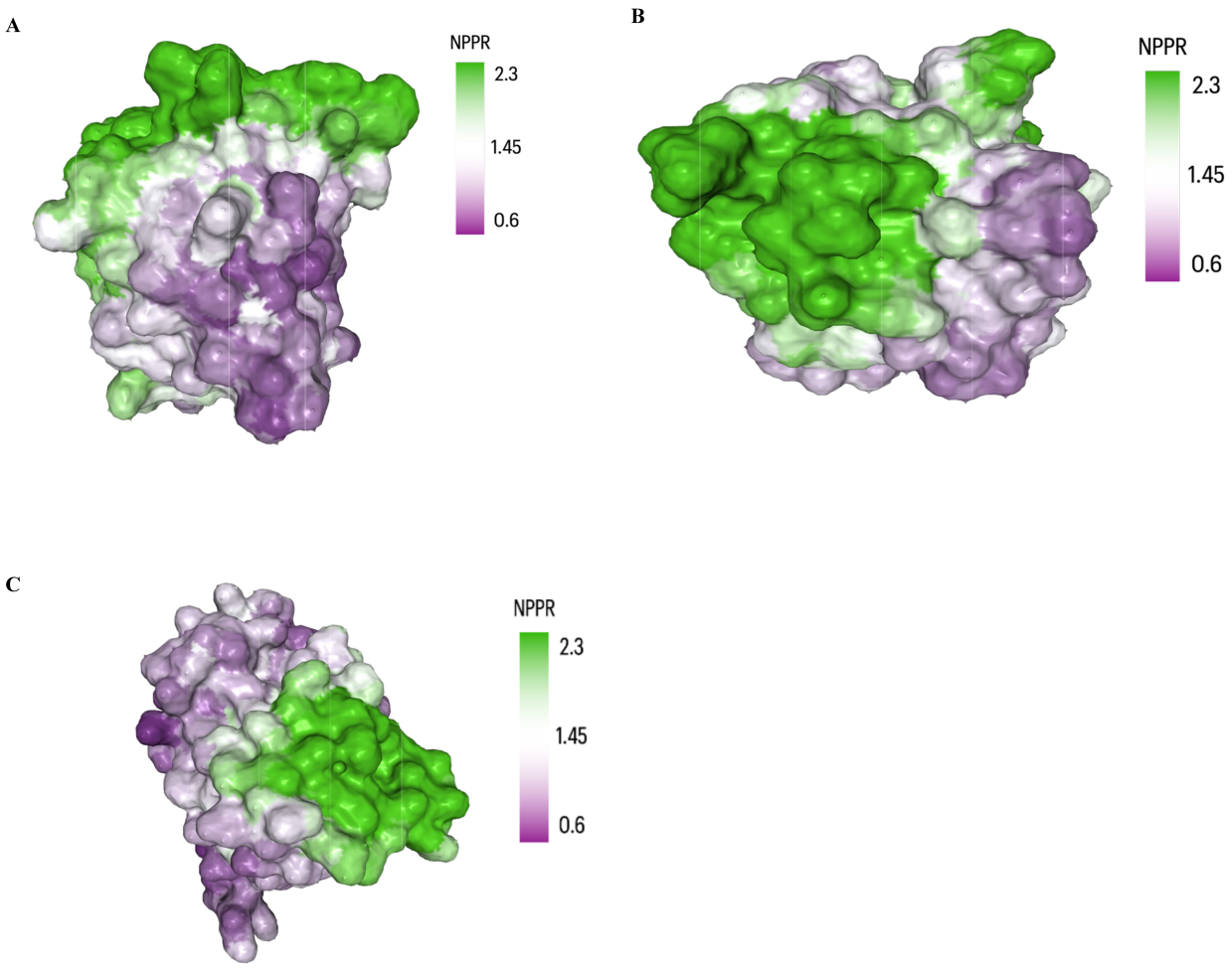

Figure 2.1 Surface Polarity of RquA, UbiG and UbiE. **A.** Predicted surface polarity of RquA using the non-polar polar ratio (NPPR). RquA has a polar region (purple) and a non-polar region (green). **B.** Like RquA, UbiG has non-polar (green) and polar (purple) surfaces, suggesting it may interact with a membrane. **C.** UbiE also has a non-polar region (green) and a polar region (purple) like RquA, however the non-polar region is much smaller than that of UbiG and RquA.

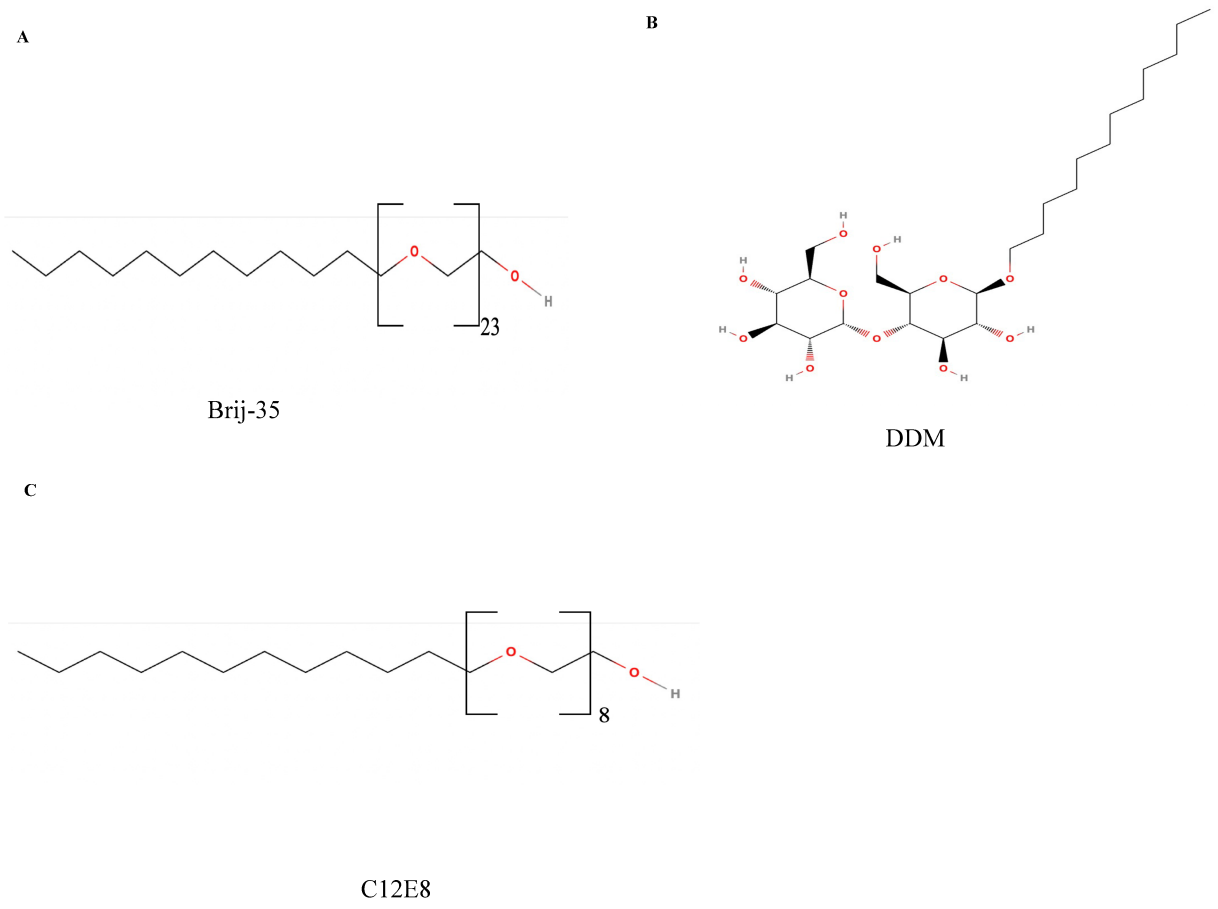

Figure 2.2 Structures of Detergents A. Brij-35 consists of a polar head group of 23 polyethylene glycol repeats and a hydrophobic alkyl chain. **B.** n-Dodecyl-β-D-Maltoside (DDM) consists of a maltose head group and a long alkyl tail. **C.** Anapoe-C12E8 consist of a polar head group of eight polyethylene glycol repeats and a hydrophobic alkyl chain. Structures made with MolView.

Previous studies regarding RquA have been done on the homolog from *Rhodospirillum rubrum* (Bernert et al, 2019, Brajcich et al, 2010, Lonjers et al, 2012, Neupane et al 2022, and Salinas et al, 2020). There are many homologs of RquA that have not been studied and learning more about this protein and its different homologs will help us gain insight into how RquA works. Studying RquA from *E. gracilis* will determine if a different homolog can be solubilized and also functional. RquA from *Euglena gracilis* will be the second RquA protein that has been characterized for future crystallography studies. This research will aim to develop methods to express and isolate this homolog of RquA to determine if it is functional. Once it is determined that it is functional, the kinetic parameters needed to obtain optimal activity will be determined and to see if it can be inhibited.

SAM analogs will be tested as potential inhibitors of RquA since SAM is required for the RquA reaction. S-adenosyl-L-homocysteine (SAH) and sinefungin will be used as potential SAM analog inhibitors. These two compounds were chosen as potential inhibitors due to having a similar structure to SAM (Figure 2.3). Where SAM has a methyl group on the sulfur, SAH does not, and sinefungin has a carbon with an amine group (Figure 2.3). Potentially inhibiting SAM by using SAM analogs, we can learn more about how RquA works in general and more about the active site of RquA that may be involved in the binding of SAM.

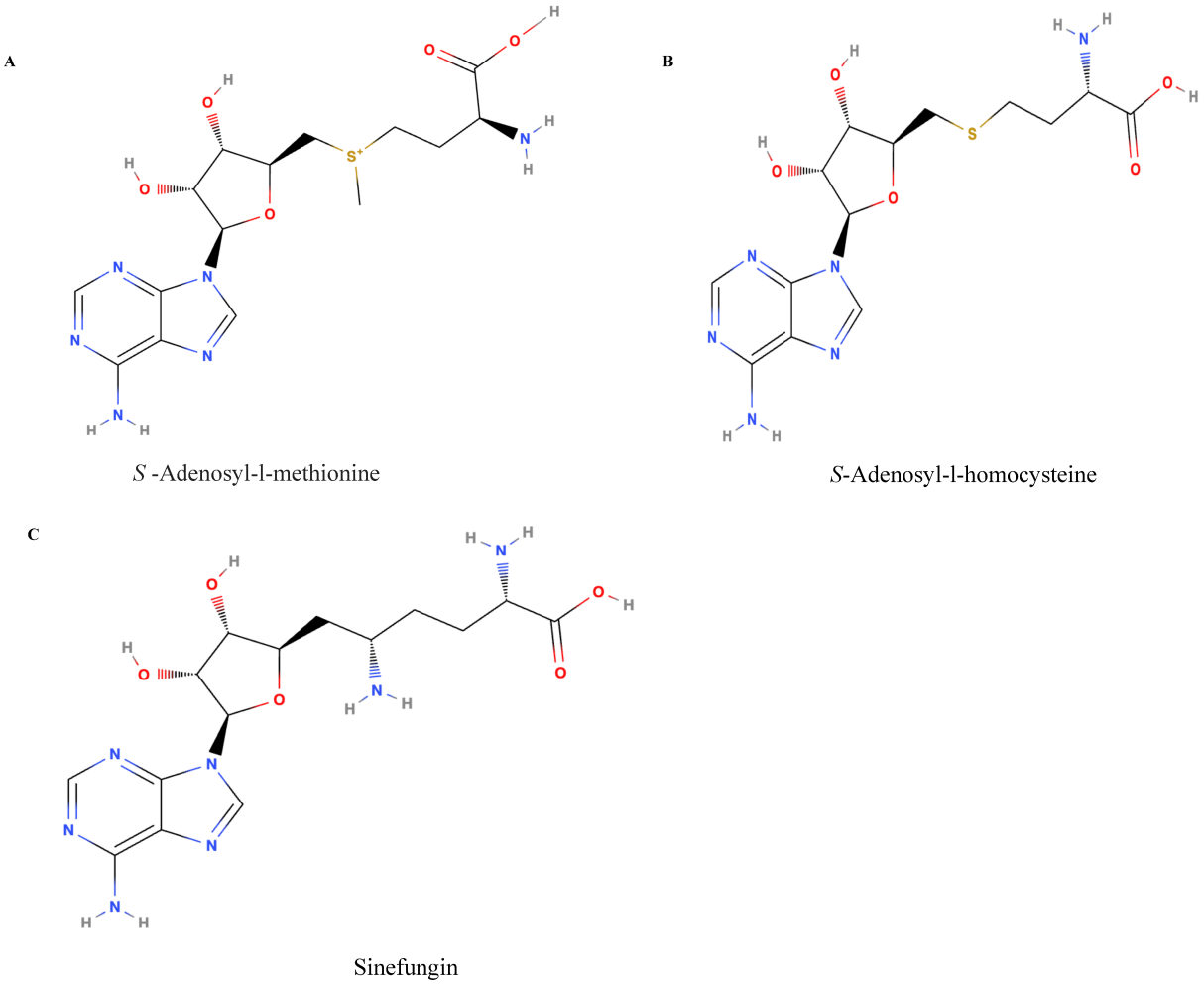

Figure 2.3 Structures of Potential Inhibitors of RquA A. Structure of SAM **B.** Structure of SAH **C.** Structure of Sinefungin. SAM is required for the activity of RquA, and its binding site could be a target for inhibition. Both SAH and sinefungin have very similar structures to SAM and these minor changes in structures allows them to potentially compete with SAM in binding to the SAM-binding site of RquA. Structures made with MolView.

2.2 Methods

2.2.1 Plasmid Construction

A codon optimized plasmid coding for *RquA* from *Euglena gracilis* was purchased from Bio Basic Inc. with 5' and 3' BamHI and XhoI recognition sites, respectively. The plasmid was digested with restriction enzymes BamHI and XhoI and ligated into a modified pET21 vector with T4 DNA ligase (New England Biolabs) using manufacturers' protocols. The final expression plasmid contained an open reading frame coding for a hexahistadine tag on the N-terminal region of RquA (pET21_His-RquA). A second plasmid was created and contained an open reading frame coding for a hexahistadine tag, maltose binding protein (MBP), a tobacco etch virus (TEV) protease recognition site, and RquA (pET21_MBP-RquA).

2.2.2 Purification and Refolding RquA from Inclusion Bodies

Chemically competent *E. coli* BL21 (DE3) cells were transformed with pET21_His-RquA. Individual bacterial colonies were grown at 37 °C in Lennox Broth (LB) media with ampicillin (100 µg/ml) until optimal density at 600 nm (OD_{600}) of ~ 0.6 was reached. Gene expression was induced by addition of 0.5 mM isopropyl β-D-1-thiogalactopyranoside (IPTG) and were left at 37 °C for 4 h before centrifugation. Cell pellets were resuspended in 30 mL of lysis buffer (100 mM Tris pH 8, 50 mM NaCl, and 1 mM EDTA). The resuspension was lysed via sonication and centrifuged at 4 °C at 25,000 × g for 20 min and repeated three times to harvest inclusion bodies. For the third resuspension, EDTA was removed from the buffer. Inclusion bodies were denatured in an 8 M urea solution (100 mM Tris pH 8, 50 mM NaCl, 1 mM TCEP, and 8 M urea). The denatured His-RquA was diluted 20-fold with refolding buffer (20 mM Tris pH 8, 200 mM NaCl, 1 mM TCEP, 1 mM $MnCl_2$, and 0.25% Brij-35) and left for 24 hours at room temperature. Refolded His-RquA was passed through a nickel-nitriloacetic acid

(NTA) affinity column washed with refolding buffer containing 20 mM imidazole pH 8 and eluted with refolding buffer containing 300 mM imidazole pH 8. His-RquA was then purified by FPLC using the HiLoad 16 60 Superdex 300 column. The purification process was confirmed by SDS-PAGE and visualized by Coomassie brilliant blue.

2.2.3 Additive Screening of RquA

An additive screen was carried out for RquA, adapted from Leibly et al, 2012. Additives 0.75 M trehalose, 0.5 M mannitol, 1 M xylitol, 0.1 M potassium citrate, 0.01 M sodium selenite, 1 M betaine, 0.375 M L-arginine, 1 M trimethylamine N-oxide, 1M 1,6-hexanediol, 0.01% cetyltrimethylammonium bromide (CTAB) and 0.5% CTAB were tried to increase the solubility of RquA. Briefly, after protein expression 500 µL of culture was collected via centrifugation at 4,000 × g for 20 min at 4 °C. Cell pellets were resuspended in 450 µL lysis buffer containing 25 mM HEPES pH 7, 500 mM NaCl, 10% Glycerol, and 0.1% lysozyme and 50 µL of an additive. The cells were lysed via shaking for 60 min at room temperature and collected by centrifugation at 4,000 × g for 30 min at 4 °C. The supernatant was taken from each additive sample and analyzed by SDS-PAGE visualized by Coomassie brilliant blue.

2.2.4 Native Expression and Purification of RquA

Chemically competent *E. coli* BL21 (DE3) cells were transformed with pET21_MBP-RquA. Individual bacterial colonies were grown at 37 °C in Lennox Broth (LB) media with ampicillin (100 µg/ml) until optimal density at 600 nm (OD_{600}) of ~ 0.6 was reached. Gene expression was induced by addition of 0.5 mM isopropyl β-D-1-thiogalactopyranoside (IPTG) and were left to grow at 20 °C overnight before centrifugation. Cell pellets were resuspended in 30 mL of lysis buffer (20 mM Tris pH 8, 200 mM NaCl, 1 mM tris(2-carboxyethyl) phosphine (TCEP), and detergent (either 0.1% Brij-35, 0.05% n-Dodecyl-B-D-Maltoside (DDM), or 0.05%

Anapoe-C12E8 (C12E8))) (MJS Biolynx Inc). The resuspension was lysed via sonication and centrifuged at 4 °C at 25,000 × g for 20 minutes. The supernatant was applied to an amylose resin column (NEB Biolabs), washed with lysis buffer, and eluted with lysis buffer (5 mL) containing 10 mM maltose. The eluted protein was incubated with 38 μM of TEV-protease and left overnight at 4 °C. The cleaved protein was passed through a nickel-NTA affinity column (IMAC Sepharose, Cytiva), washed with lysis buffer containing 20 mM imidazole pH 8 and eluted with lysis buffer containing 300 mM imidazole pH 8. The flow-through and wash samples were pooled together and concentrated before further purification by fast protein liquid chromatography (FPLC) using the preparatory size exclusion chromatography sepharose column Superdex 300 (Cytiva). The fraction(s) containing RquA were collected, flash frozen in liquid nitrogen, and stored at -20 °C until further analysis. The purification process was confirmed by SDS-PAGE visualized by Coomassie brilliant blue.

2.2.5 Circular Dichroism (CD) Spectroscopy

RquA was purified in the presence of 0.1% Brij-35, and then dialyzed overnight in buffer containing 20 mM Tris pH 8, 200 mM NaF, 1 mM TCEP, and 0.1% Brij-35. Data were collected on a CD spectropolarimeter (Olis DSM20) using a 0.5 mm quartz cuvette. Six scans of the buffer sample and RquA sample from 270 nm – 180 nm with 90 increments and an integration time of 20 seconds. The buffer's raw data was subtracted from RquA raw CD data before being analyzed. The raw CD data in millidegrees (θ) was first converted to Δε using equation 2.1 before being converted to mean residue ellipticity (MRE) using equation 2.2.

$$\text{Equation 2.1: } \Delta\varepsilon = \theta * \frac{0.1 * \text{MRW}}{\text{P} * \text{C} * 3298}$$

$$\text{Equation 2.2: } \text{MRE} = \Delta\varepsilon * 3298$$

where the mean residue weight (MRW) is in atomic mass units/daltons (amu), P is the path length (cm), and C is the concentration of the protein (mg/ml). The calculated MRW of RquA was 113.581274 amu, the path length was 0.05 cm, and the concentration of RquA was 0.1536 mg/ml. The concentration of RquA was determined using the Beer-Lambert law to obtain a concentration in μM. The concentration of RquA in μM was converted to mg/ml using the molecular weight of RquA in mg/mmol. The raw data was then analyzed by BeStSel to determine the distributions of secondary structure (Micsonai et al, 2015).

2.2.6 Functional Assays of RquA

Functional assays of RquA were adapted from Neupane et al, 2022 and were prepared in base reaction buffer containing 20 μM UQ_3, 40 μM SAM, 1 mM $MnCl_2$, 1 μM RquA in assay buffer (20 mM Tris pH 8, 200 mM NaCl, 1 mM TCEP, and 0.1% Brij-35). The reaction was left to react in the dark at room temperature (21-24 °C) and aliquots of the reaction are removed at subsequent time points (0 min, 5 min, 10 min, 20 min, 30 min, 45 min, and 60 min) and quenched with an equal volume of acetonitrile. Triplicate RquA reactions were performed. RQ_3 and UQ_3 content were analyzed on the Waters 2695 Separation Module and Waters 2487 Dual λ Absorbance Detector at 280 nm. A set of rhodoquinone-3 (RQ_3) standards (1 μM, 5 μM, 10 μM, 15 μM, 20 μM, and 30 μM) were analyzed to generate a standard curve. The area under the curve for the RQ_3 peak was determined by the Empower Software integration function. The areas corresponding to their respective concentrations generated the equation $y = 10055x + 4252.8$, which was used to convert the area under the curve generated from the RquA reactions into a concentration to determine how much RQ_3 was produced. The initial velocities for each reaction were determined using the time points 0 min and 20 min, as this represents the linear

region of the RquA reaction given by the R^2 value of 0.9 indicating that this region is linear. RquA ability to convert UQ_3 to RQ_3 for each condition was calculated using equation 2.3:

$$\text{Equation 2.3: Conversion} = \frac{[\text{RQ}_3\ \text{Produced}]}{[\text{UQ}_3\ \text{Provided}]} * 100$$

To assess the influence of different UQ_3 and SAM concentrations on RquA reaction rates, the concentrations of UQ_3 and SAM were varied to 1 µM, 3 µM, 5 µM, 7 µM, 10 µM, 15 µM, 20 µM, and 40 µM of UQ_3 and 1 µM, 5 µM, 10 µM, 15 µM, 20 µM, 30 µM, 40 µM, 50 µM, 60 µM, 70 µM, and 80 µM of SAM in base reaction buffer. The initial velocities of the reactions were analyzed using GraphPad Prism and fit to either a Michaelis-Menten or allosteric sigmoidal model. The Michaelis-Menten model is fitted to equation 2.4,

$$\text{Equation 2.4 } V_0 = {}^{V_{max}[S]}\Big/_{K_M + [S]}$$

where v_0 is the initial velocity, V_{max} is the maximum velocity, [S] is the substrate concentration, and K_M is Michaelis constant. The allosteric sigmoidal model is fitted to equation 2.5,

$$\text{Equation 2.5 } V_0 = {}^{V_{max} * [S]^h}\Big/_{K_{half}^h + [S]^h}$$

where V_0 is the initial velocity, V_{max} is the maximum velocity, [S] is the substrate concentration, h is the hill slope, when h = 1 this model is equivalent to Michaelis-Menten, but when it is >1, the curve is sigmoidal, and K_{half} is the concentration of substrate that produces half of the V_{max}. The standard deviation values for the Michaelis-Menten constant (K_M) and maximum velocity (V_{max}) values were calculated from the 95% CI values obtained using equation 2.6:

$$\text{Equation 2.6: SD} = \sqrt{\text{N}} * \frac{\text{Upper CI} - \text{Lower CI}}{\text{t}_{\alpha,\text{df}} * 2}$$

where N equals the number of samples (3), t is the distributions of α, α equals 0.05 as this was a done with a 95% CI, and df equals the degrees of freedom (N-1) (2).

The data collection and analysis procedure were repeated to assess the effect of other reaction components on RquA activity. To assess the effect of pH on RquA activity, a multicomponent buffer (MCB) comprising of 100 mM MES, 100 mM HEPES, and 100 mM CHES, 1 mM TCEP, 200 mM NaCl, and 0.1% Brij-35 was used and adjusted to pH 6, pH 7, pH 8, pH 9, and pH 10. The RquA reaction contained 20 μM UQ_3, 40 μM SAM, 1 mM $MnCl_2$, 1 μM RquA, and 50 mM of MCB for each pH being tested. To assess the influence of different $MnCl_2$ concentrations on RquA activity, the concentration of $MnCl_2$ was adjusted to 0 μM, 25 μM, 75 μM, 250 μM, 750 μM, 1 mM, and 2 mM with base reaction buffer. To assess the effects of salt concentration and Brij-35 concentration the final concentrations of NaCl and Brij-35 were 50 mM, 100 mM, 200 mM, and 400 mM and 0.05%, 0.1%, and 0.2%, respectively with base reaction buffer. The determine the effects of different buffers at pH 8, the buffers Tris, HEPES, and bicarbonate were added to a final concentration of 20 mM in base reaction buffer.

To assess the effects of reducing agents, the reducing agent was varied to 1 mM TCEP, 1 mM DTT, 5 mM GSH, and 5 mM BME with base reaction buffer, or dialyzed overnight in buffer containing 20 mM Tris pH 8, 200 mM NaCl, and 0.1% Brij-35 to remove TCEP. To assess the amount of reducing agent required to support RquA function, 5 μM, 10 μM, 15 μM, 25 μM, 50 μM, 75 μM, 125 μM, 200 μM, 500 μM, and 1 mM TCEP were added back to the reaction after removal of TCEP through dialysis. Finally, the effect of sinefungin and S-adenosyl-L-homocysteine (SAH) on the reaction rate of RquA was assessed at concentrations of 5 μM, 10 μM, 20μM, 40 μM, 80 μM, 500 μM, 1 mM, and 2 mM with base reaction buffer.

2.3 Results and Discussion

2.3.1 Purification of RquA from Inclusion Bodies

One method used to try to isolate and purify RquA was first denaturing it and then refolding RquA in 0.25% Brij-35. This yielded around 0.99 mg of RquA per L of culture. RquA was purified and refolded successfully through this method, as seen with the bands with the red box on the SDS-PAGE gel around 25 kDa (Figure 2.4A). There was a large shoulder on the SEC chromatogram leading up to the RquA peak, indicating some possible aggregation (Figure 2.4B). As well, there were multiple proteins present in the final sample, as seen with the multiple bands after the band representing RquA (Figure 2.4A). The bands could be proteins that contain histidine's, as RquA was purified using a Ni^{2+}-NTA affinity column, which does not have the highest selectivity as it selects for any proteins that contain histidine's.

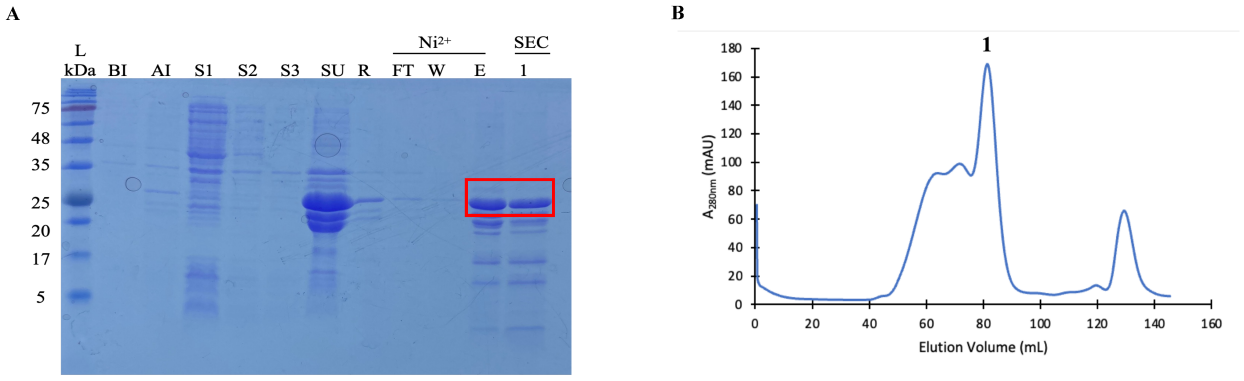

Figure 2.4 Purification of RquA Through Refolding in 0.25% Brij-35. A. His-RquA was expressed BL21 (DE3) *E. coli*. His-RquA was isolated through a denaturing purification before being refolded by dilution into 0.25% Brij-35. **B.** Resulting SEC chromatogram after RquA was refolded in 0.25% Brij-35 and purified via Ni^{2+} affinity chromatography. Gel Lanes: **L:** FroggaBio BLUelf protein ladder **BI:** before induction **AI:** after induction **S1-S3:** supernatants from each inclusion body washes **SU**: supernatant of inclusion bodies in the presence of 8 M urea **R:** refolded sample **FT:** flow-through **W:** wash **E:** elution **1:** His-RquA sample from SEC.

2.3.2 0.01% and 0.5% CTAB Added to the Lysis Improves the Solubility of RquA

In an alternate approach, an additive screen was carried out during cell lysis to increase the solubility of MBP-RquA (Leibly et al, 2012). Leibly et al chose additives that are natural ligands, detergents, salts, buffers, and chemicals that have previously shown to increase the stability of proteins *in vivo* (Leibly et al, 2012). The additives trehalose, mannitol, xylitol, potassium citrate, sodium selenite, betaine, L-arginine, 1,6-hexanedial, 0.01% CTAB, 0.5% CTAB and trimethylamine N-oxide were added to the lysis buffer following the protocol from Leibly et al, 2012. From the additives, the solubility of MBP-RquA, which can be seen around 75 kDa ladder, is increased when 0.01% and 0.5% CTAB are present in the lysis buffer as seen with the more prominent bands on the SDS-PAGE compared to the no additives added (Figure 2.5).

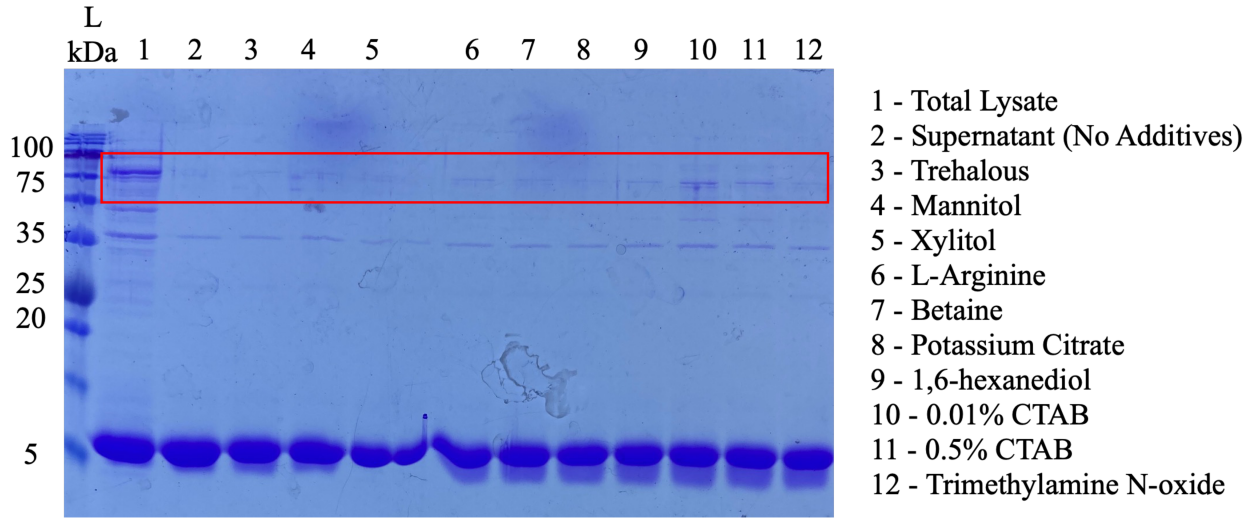

Figure 2.5 Additive Screen of MBP-RquA. MBP-RquA was prepared following the protocol from Leibly et al, 2012, and lysis supernatants were analyzed by SDS-PAGE. Gel lanes are labelled 1 – 12 with the respective additive indicated. From this additive screen, the solubility of MBP-RquA is increased in the presence of 0.01% and 0.5% CTAB.

2.3.3 RquA Requires a Detergent to be Soluble

MBP-RquA was first purified without detergent present in the lysis buffer. There was a large MBP-RquA band after the elution off the amylose affinity, indicating that MBP-RquA was purified (~80 kDa) (Figure 2.6A). However, there was not efficient TEV cleavage as seen with the three bands, representing MBP-RquA, MBP, and RquA, after incubation with TEV protease overnight (~80 kDa, 40 kDa, and 30 kDa) (Figure 2.6A). The combined flow-through/wash was loaded onto the FPLC column to further separate MBP-RquA, MBP, and RquA. The peak corresponding to RquA (1) seemed to contain MBP-RquA, MBP, and RquA, on the SDS-PAGE indicating a poor separation (Figure 2.6A). RquA and maltose binding protein (MBP) have a size of around 29 kDa and 42 kDa, respectively, and can be seen around the 30 kDa and 40 kDa ladder bands of the SDS-PAG analysis respectively (Figure 2.6A). MBP-RquA has a size of around 71 kDa and can be seen around the 80 kDa ladder band (Figure 2.6A). The resulting peak on the chromatogram representing RquA was a very broad peak on the SEC chromatogram, indicating that RquA is not soluble and became aggregated (Figure 2.6B). The peak containing MBP (2) was much thinner, indicating that MBP was soluble (Figure 2.6B).

To see if detergents would help the solubility of RquA, I purified RquA in 0.1% Brij-35, 0.05% DDM, and 0.05% C12E8. In Figure 2.7D there were two resolved peaks indicating that there was a clear separation between RquA and MBP. The peak representing RquA was much cleaner and sharper than when purified without detergent (Figure 2.6B and Figure 2.7D). This indicates that RquA requires a detergent to be solubilized. The resulting yields of RquA purified in 0.1% Brij-35, 0.05% DDM, and 0.05% C12E8 were 1 mg, 0.34 mg, and 0.67 mg of RquA per L of culture, respectfully. RquA purified in 0.1% Brij-35 produces the highest yield as seen with the largest absorbance value, highest yield, and the darkest SDS-PAGE band compared to when

RquA is purified in 0.05% DDM and 0.05% C12E8 (Figure 2.7).

MBP has a larger mass (42 kDa) than RquA (29 kDa), meaning it should elute off the SEC first. However, that is not the case. RquA elutes first at around 87 mL (Brij-35), 86 mL (DDM), and 85 mL (C12E8) and MBP second at around 95 mL, suggesting that RquA is larger in size. This may in part be because RquA is purified with detergent, resulting in the RquA eluting off the column incorporated in detergent micelles, thereby making it seem larger than MBP.

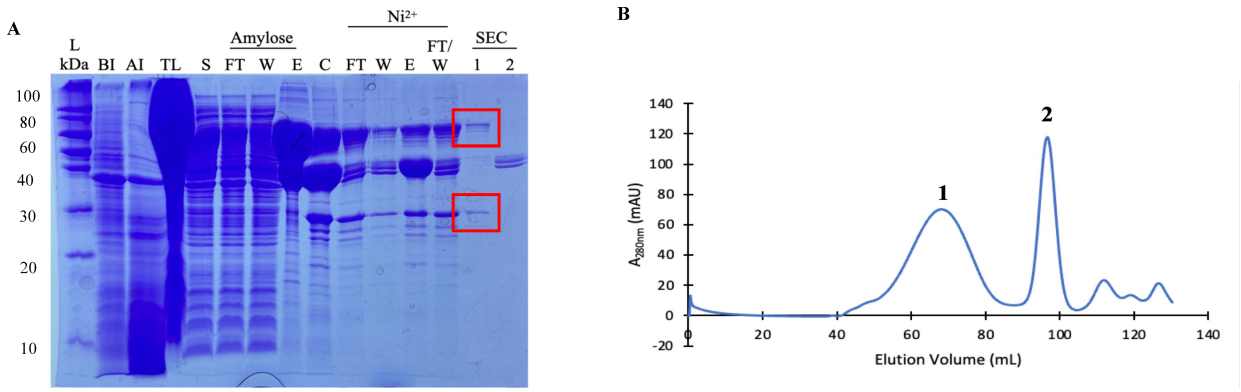

Figure 2.6 Purification of RquA without Detergent. A. SDS-PAGE analysis of RquA purified without detergent. MBPRquA was expressed in BL21 (DE3) *E. coli* cells, lysed, purified with amylose resin, cleaved with TEV protease, and further purified with Ni^{2+} resin and SEC. **B.** Resulting size exclusion chromatogram of RquA when no detergent is present. Gel lanes: **L:** Penn State protein ladder **BI:** before induction **AI:** after induction **TL:** total lysate **S:** supernatant **FT:** flow-through **W:** wash **E:** elution **C:** cleaved Protein **FT/W:** combined flow-through and wash **1:** RquA **2:** MBP.

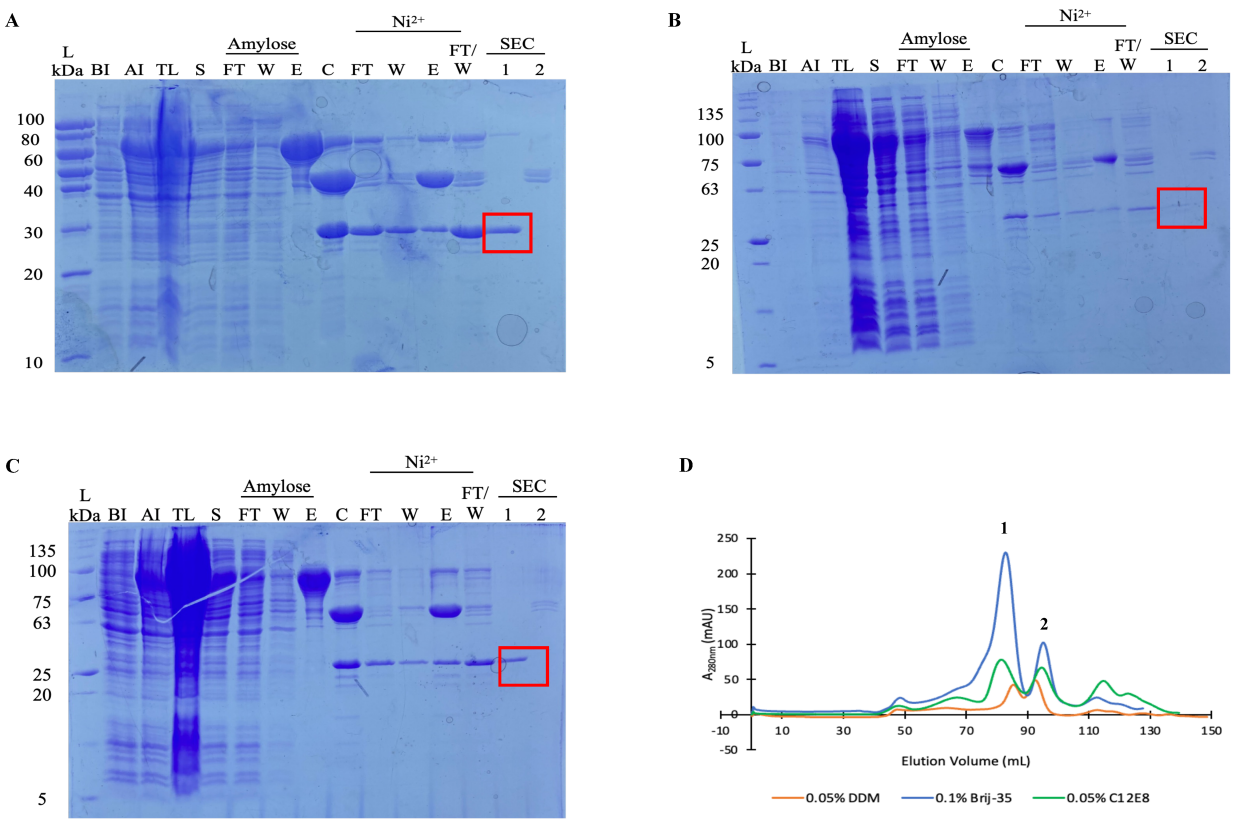

Figure 2.7 Purification of RquA. SDS-PAGE analysis of RquA solubilized in the presence of **A.** 0.1% Brij-35 **B.** 0.05% DDM **C.** 0.05% C12E8. MBP-RquA was expressed in BL21 (DE3) *E. coli* cells, lysed, purified with amylose resin, cleaved with TEV protease and further purified with Ni^{2+} resin and SEC. **D.** Resulting SEC chromatograms of the FT/W collected from RquA being solubilized in 0.1% Brij-35 (blue), 0.05% DDM (orange), and 0.05% C12E8 (green). Peak 1 represents RquA and peak 2 represents MBP. Gel lanes: **L:** Penn State protein ladder **BI:** before induction **AI:** after induction **TL:** total lysate **S:** supernatant **FT:** flow-through **W:** wash **E:** elution **C:** cleaved Protein **FT/W:** combined flow-through and wash **1:** RquA **2:** MBP

2.3.4 RquA is Folded when Purified in 0.1% Brij-35

Since RquA was found to be soluble when purified in 0.1% Brij-35, I next wanted to determine if it was folded. Using circular dichroism (CD) spectroscopy, the secondary structure of RquA was assessed (Figure 2.8A). There is a positive band at around 190 nm, which is indicative of an alpha helix or a beta strand. There seems to be a negative band(s) between 210-220, which is also indicative of an alpha helix and a beta strand (Figure 2.8A). The resulting distributions of secondary structures obtained from BeStSeL predicts that RquA consists of 21% alpha helices and 36% beta strands (Figure 2.8B). These deconvolution results appear consistent with the CD spectra, where the bands around 190 nm and 220 nm are consistent with a mixture of α-helix and a β-strands.

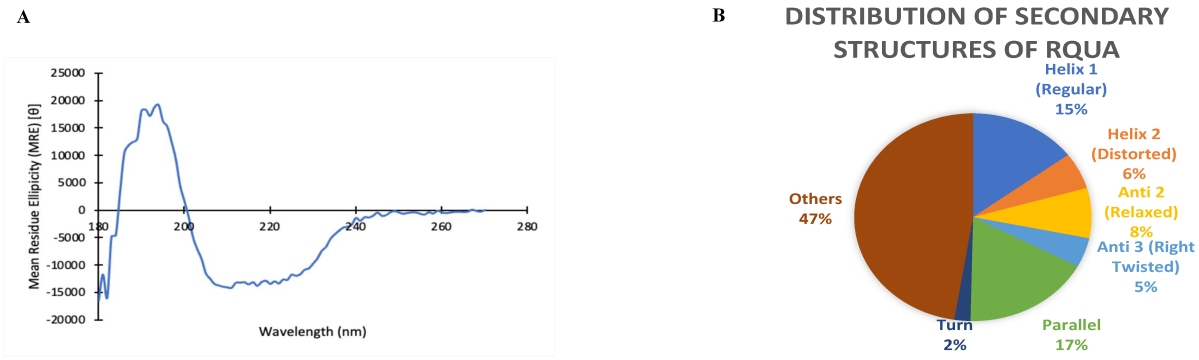

Figure 2.8 RquA is Folded when Purified in 0.1% Brij-35. A. Resulting CD spectrum obtained from *RquA* purified in 0.1% Brij-35. Six runs were averaged, and the resulting CD results were converted to mean residue ellipticity. The corrected CD Data was then analyzed by BeStSeL. The negative and positive peaks represent a spectrum of a protein with mixed alpha-helices and beta-strands. **B.** The deconvoluted distribution of secondary structures within RquA. RquA is predicted to consist of 21% alpha-helices of 36% beta sheets, which appears consistent with the predicted structure of RquA.

2.3.5 RquA can Convert UQ3 to RQ3

Now that RquA was shown to be soluble and folded in 0.1% Brij-35, I wanted to determine if it was functional. I used high performance liquid chromatography (HPLC) to determine if RquA can convert UQ_3 to RQ_3. An isocratic method with 90% acetonitrile (ACN) and 10% water with trace amounts of trifluoroacetic acid (TFA) (0.05%) was able to efficiently separate RQ_3 and UQ_3. RQ_3 and UQ_3 eluted off the C_4 column at around 6.1 min and 6.8 min, respectively (Figure 2.9A). A series of RQ_3 standards were run to generate a RQ_3 standard curve to obtain a line of best fit (Figure 2.9B). The equation generated from the standard curve, $y = 10055x + 4252.8$, was used to convert the area under the curve of unknown samples to a concentration of RQ_3 (Figure 2.9B).

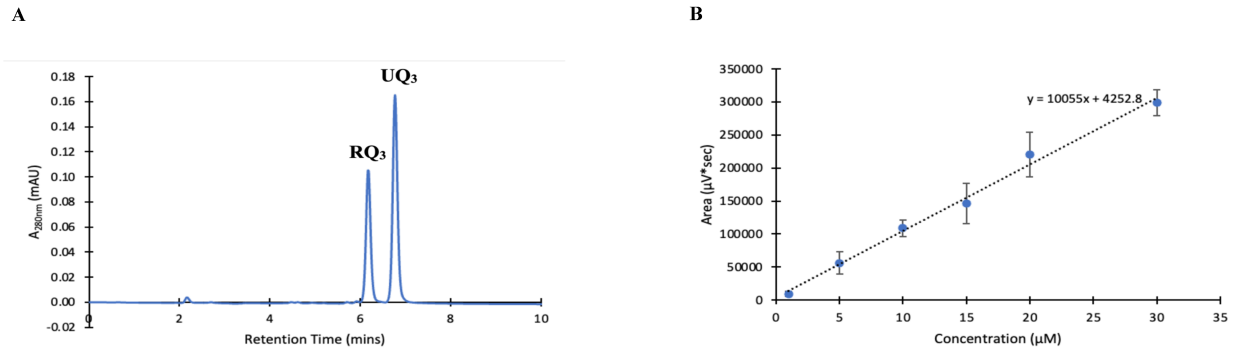

Figure 2.9 HPLC-Based Separation of Rhodoquinone-3 and Ubiquinone-3 Standards. A. An isocratic method was optimized to detect the separation of rhodoquinone-3 (RQ_3) and ubiquinone-3 (UQ_3). 20 µM of RQ_3 and UQ_3 were loaded onto a C_4 analytical HPLC column with 90% acetonitrile and 10% water with trace amounts of trifluoroacetic acid (0.05%) for 10 minutes. RQ_3 and UQ_3 eluted off the column at ~6.1 min and ~6.8 min respectively. **B.** A set of rhodoquinone-3 standards (1 µM, 5 µM, 10 µM, 15 µM, 20 µM, and 30 µM) were used to generate a standard curve. Triplicate assays were done to ensure accuracy. The equation generated from the line of best fit (y = 10055x + 4252.8) was used to determine the concentration rhodoquinone-3 produced in future functional assays.

A control reaction without RquA was prepared and left to react for 60 min before being quenched with acetonitrile (ACN). Figure 2.10A shows that only UQ_3 and ubiquinol (UQ_3H_2) were present in the reaction (Figure 2.10A). A control UQ_3 sample with 1 mM TCEP showed two peaks, one at 6.8 min that we attribute to UQ_3, and another at 5.8 min, which we attributed to UQ_3H_2. This suggests that when a reducing agent is present in solution, UQ_3 is being reduced to UQ_3H_2.

To determine at what times of the RquA reaction RQ_3 formation is linear, a time course assay was conducted. Aliquots of the reaction were quenched at 0 min, 5 min, 10 min, 20 min, 30 min, 45 min, and 60 min. Over the 60 min reaction RquA was shown to convert UQ_3 to RQ_3 or it was reduced to UQ_3H_2 (Figure 2.10B). As the time course went on, more RQ_3 production was observed with increasing RQ_3 peak area and decreasing UQ_3 peak area (Figure 2.10B). A linear regression was done to determine the R^2 value to determine the linear region of the reaction, with a value closer to 1 indicating a linear relationship. The R^2 value for the full 60 min reaction was 0.96, which indicates a linear model (Figure 2.10C). To further confirm that the first 30 min is in the linear region, a second linear regression was done with just the data points from the first 30 min (Figure 2.10D). This obtained a R^2 value of 0.992, which is very close to 1, indicating a linear relationship (Figure 2.10D). To ensure that, for future experiments, the reaction is always in the linear region, the first 20 min of the reaction will be used to determine the initial velocities.

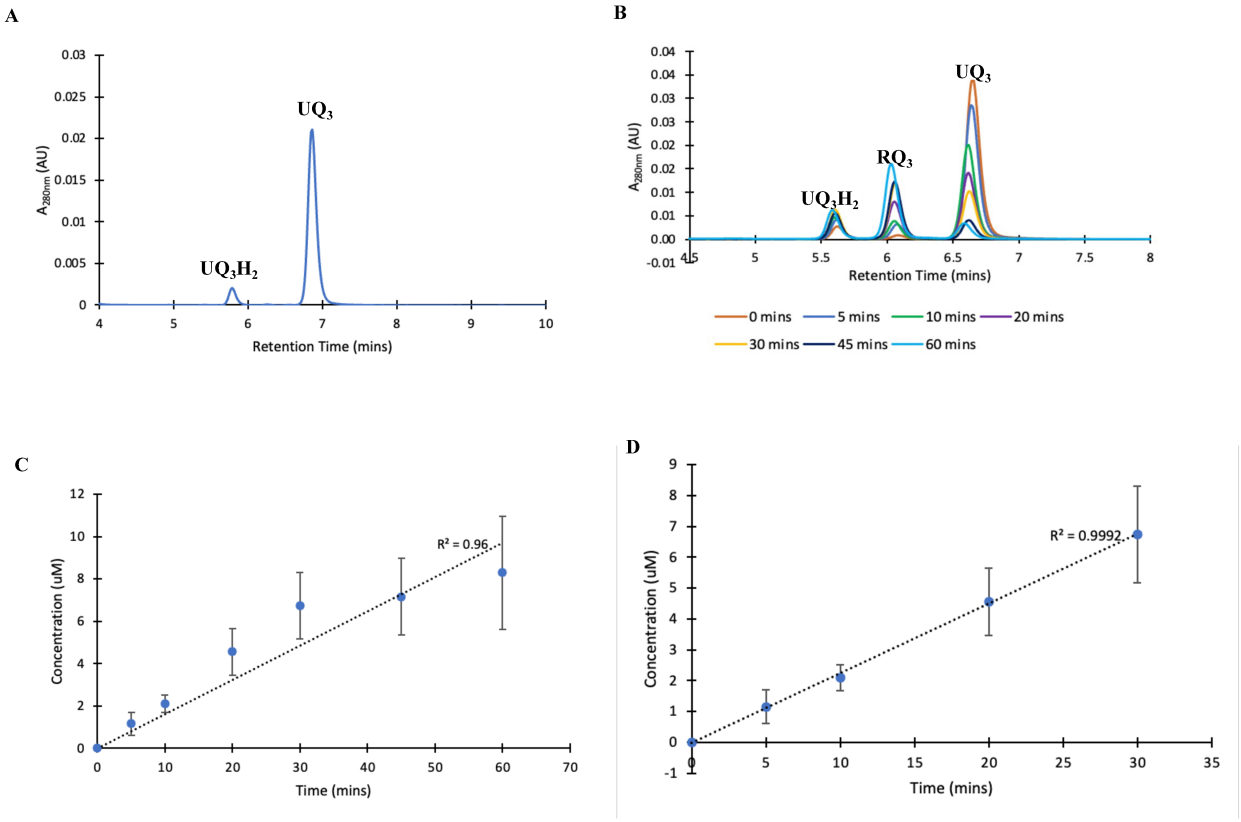

Figure 2.10 RquA is Required for the Conversion of UQ_3 to RQ_3. A. A reaction without RquA, but instead equal parts water, was done containing 20 µM UQ_3. 40 µM SAM, 1 mM $MnCl_2$, H_2O, and assay buffer containing 20 mM Tris pH 8, 200 mM NaCl, 1 mM TCEP, and 0.1% Brij-35. The reaction took place in the dark at room temperature for 60 min after which it was quenched with equal parts acetonitrile. Peaks corresponding to UQ_3 and UQ_3H_2 are labelled. **B.** Over the course of the 60-minute reaction, UQ_3 was converted to RQ_3 or reduced to ubiquinol (UQH_2). **C.** Concentration of RQ_3 (µM) produced throughout the time course plotted against time (min). The R^2 value of 0.96 does indicate that this reaction is linear. **D.** The first 30 min of the reaction is linear as seen with this high R^2 value of 0.9992. Triplicate assays were completed to ensure accuracy where error bars represent standard deviation.

2.3.6 Effect of UQ_3 Concentration on the Reaction Rate of RquA

Concentrations of UQ_3 ranging from 1 μM to 40 μM were tested to determine the apparent K_M and V_{max} of RquA for UQ_3. A RquA reaction was done for each UQ_3 concentration and the initial rate of RQ_3 formation determined (Figure 2.11A). The reaction rate plateaued when 20 μM of UQ_3 was present (Figure 2.11A).

The initial velocities of UQ_3 were first fitted to a Michaelis-Menten model (Figure 2.11A). The Michaelis-Menten fit is used to describe an enzyme that catalyzes a reaction with one substrate and one product. The apparent K_M and V_{max} obtained from this fit were 9.2 ± 1.54 μM and 0.2599 ± 0.02 μM, respectively. When GraphPad Prism analyzes a non-linear fit, it performs a replicate test. A replicate test ensures that the average distance of the points from the curve is not too far compared to the scatter that is found among the replicates. GraphPad Prism calculates this first determining the standard deviation for each point. The standard deviations are then used to calculate the F ratio before determining the p-value of the set. The p-value is then used to determine if the fit used is the best fit for the data. If the p-value is very small, then there is evidence of an inadequate fit. The p-value obtained from the Michaelis-Menten fit for UQ_3 concentrations was <0.0001, which indicates that there is evidence of an inadequate model.

The Michaelis-Menten fit was then compared to an allosteric sigmoidal model to determine the best model for when UQ_3 binds RquA (Figure 2.11B). The apparent K_{half} and V_{max} values of the allosteric sigmoidal fit are 5.179 ± 0.005 μM and 0.1928 ± 0.23 μM min^{-1}, respectively. An allosteric sigmoidal fit is for enzyme's that appear to have cooperative binding to its' active site. The replicates test was performed on the sigmoidal fit, and the p-value obtained from this fit was 0.1513, indicating that an allosteric model fits the data better than a Michaelis-Menten model.

Since the allosteric sigmoidal model is the best fit, this raises the question of how RquA is acting as an allosteric enzyme when it binds to UQ_3. One reason for why the allosteric sigmoidal fit is the best model could be is due to the hydrophobic nature of UQ_3 and RquA. For RquA to be soluble, detergent is required in the purification process and the reaction assay buffer. In solution, UQ_3 will also localize to the detergent micelles, resulting in a local concentration of UQ_3 in the micelle that is higher than in the bulk solution. This could potentially explain the sigmoidal fit, as the actual amount of UQ_3 being reacted would not be known, which would result in inaccurate results. Substrate activation of RquA caused by a non-optimal detergent environment could also result in an allosteric sigmoidal fit for when UQ_3 binds to RquA. Adding phospholipids into the solution to try to mimic the native membrane conditions of RquA might resolve the allosteric sigmoidal model.

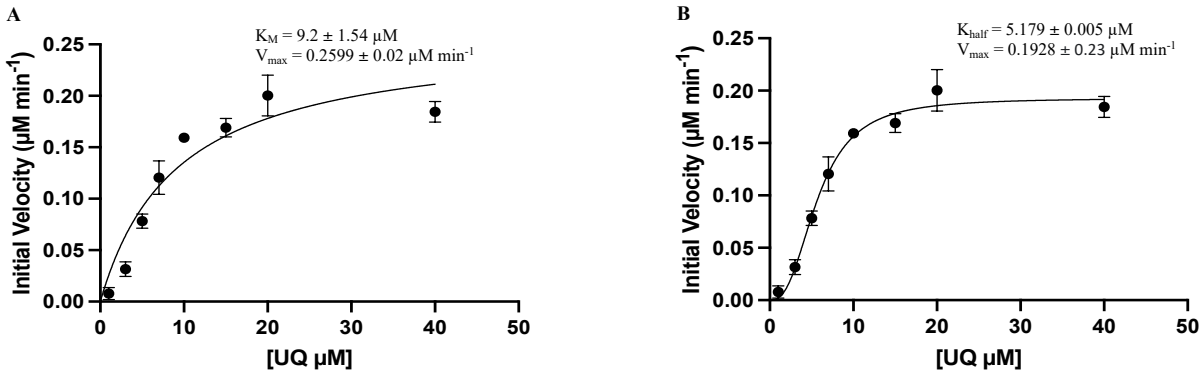

Figure 2.11 Kinetic Characterization of RquA with Respect to UQ_3. RquA was purified in the presence of 0.1% Brij-35 before the RquA functional assay was done with base reaction buffer (1 µM RquA, 40 µM SAM, 1 mM $MnCl_2$, and assay buffer (20 mM Tris pH 8, 200 mM NaCl, 1 mM TCEP, and 0.1% Brij-35)). 1 µM to 40 µM of UQ_3 were tested to determine the effects of UQ_3 concentration on the reaction rate of RquA. RQ_3 produced was quantified via an HPLC-based assay and fit to (**A)** a Michaelis-Menten model, with apparent K_M and V_{max} values of 9.2 ± 1.54 µM and 0.2599 ± 0.02 µM min^{-1}, respectively or (**B)** an allosteric model, with apparent K_{half} and V_{max} values of 5.179 ± 0.005 µM and 0.1928 ± 0.23 µM min^{-1}, respectively.

2.3.7 Effect of SAM Concentration on the Reaction Rate of RquA

Various concentrations of SAM ranging from 1 μM, to 80 μM were tested to determine the apparent K_M and V_{max} of RquA for SAM. The V_{max} of the reaction was approached when 40 μM of SAM was present in the reaction (Figure 2.12). A Michaelis-Menten and an allosteric sigmoidal fit were compared to determine the best fit using the p-values obtained from the standard deviations of each run. The p-value obtained from this comparison was 0.5693, indicating that a Michaelis-Menten fit an appropriate best model (Figure 2.12). The K_M and V_{max} value obtained from this fit was 14.72 ± 2.59 μM and 0.173 ± 0.01 μM min^{-1}, respectively. Many enzymes that use SAM as a substrate have a K_M between 0.2 and 15 μM (Horiuchi et al, 2013 and Ross et al, 1999). The relatively low K_M value obtained from this fit indicates that RquA has a high binding affinity for SAM.

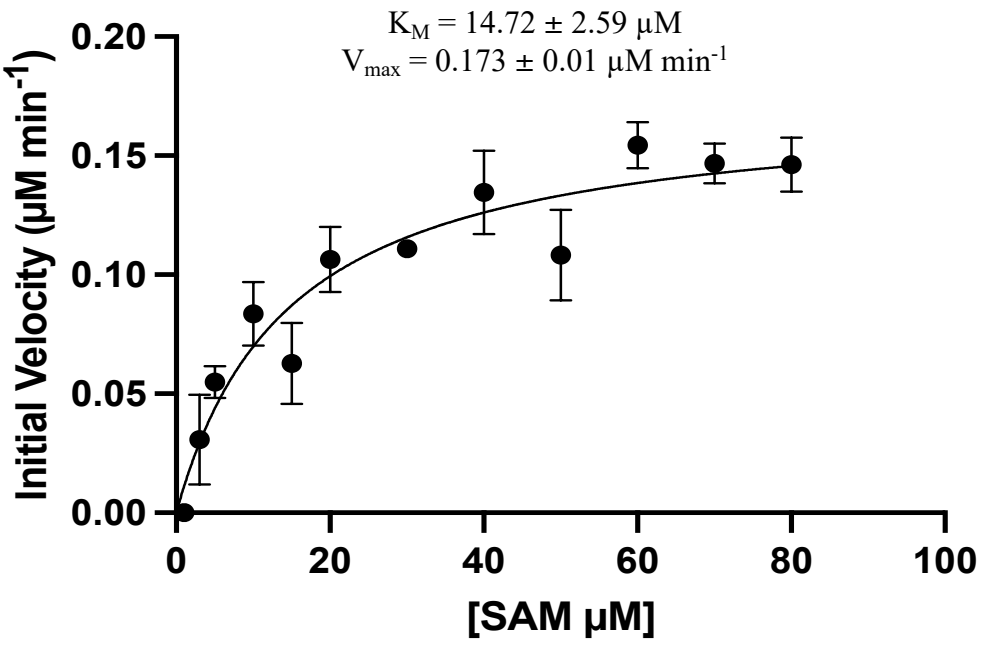

Figure 2.12 Kinetic Characterization of RquA with Respect to SAM. RquA was purified in 0.1% Brij-35 and assayed in base reaction buffer (1 µM RquA, 20 µM UQ_3, 1 mM $MnCl_2$, and assay buffer (20 mM Tris pH 8, 200 mM NaCl, 1 mM TCEP, and 0.1% Brij-35)). SAM concentration was varied from 1 µM to 80 µM of SAM to determine the effect of SAM on reaction velocity and the amount of RQ_3 produced was quantified. A Michaelis-Menten fit of initial reaction velocities. The apparent K_M and V_{max} from this fit were determined to be 14.72 ± 2.59 µM and 0.173 ± 0.01 µM min^{-1}, respectively.

2.3.8 Effect of $MnCl_2$ on RquA Activity

To determine if $MnCl_2$ is required for the activity of RquA like the homolog found in *R. rubrum*, a reaction lacking $MnCl_2$ and with 1 mM EDTA present was analyzed. When no $MnCl_2$ was present in the reaction RQ_3 biosynthesis no longer occurred, indicating that $MnCl_2$ is also required for the RquA homolog found in *E. gracilis* (Figure 2.13A). To determine the optimal amount of $MnCl_2$ needed for catalysis, reaction rates in the presence of 25 μM – 2 mM of $MnCl_2$ measured (Figure 2.13B). The activity of RquA was restored when various amounts of $MnCl_2$ were tested (Figure 2.13B).

Enzymes need divalent metals to stabilize the structure and/or for catalysis. If the divalent metal ion is there to stabilize its structure, $MnCl_2$ and $MgCl_2$ can be used interchangeable, however that is not the case with RquA. Studies done on *R. rubrum* determined that RquA was only active in $MnCl_2$ indicating that $MnCl_2$ is likely not required for the structure of RquA but could be involved in catalysis (Neupane et al, 2022). Manganese can exist in a few different oxidation states, the most common are a 2^+ and 3^+ charge, which could play a factor in the catalysis of RquA and help to keep the environment in a balanced redox state.

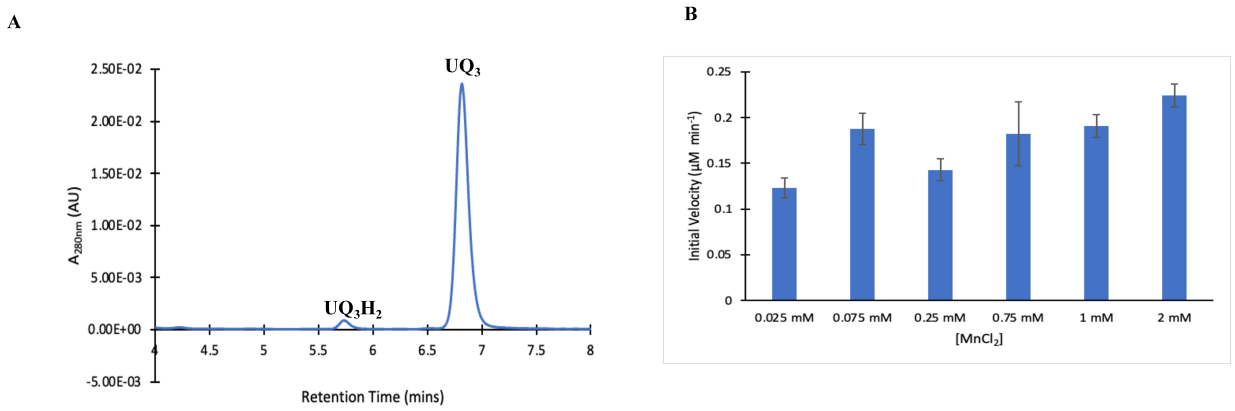

Figure 2.13 RquA Requires $MnCl_2$ for Catalysis. A. A reaction without $MnCl_2$ but instead 1 mM EDTA was completed to determine if $MnCl_2$ is required for catalysis. RquA was first purified in 0.1% Brij-35 and reacted in base reaction buffer lacking $MnCl_2$. After the reaction was complete there was no RQ_3 production, indicating that $MnCl_2$ is required for RQ_3 biosynthesis. **B.** To determine how much $MnCl_2$ is required for catalysis the activity of RquA in 25 μM to 2 mM of $MnCl_2$ was quantified. Triplicate assays were done to ensure accuracy with the error bars representing the standard deviation.

2.3.9 Optimizing the RquA Reaction Buffer

The base reaction for RquA contains 1 μM RquA, 20 μM UQ_3, 40 μM SAM, 1 mM $MnCl_2$ and assay buffer containing 20 mM Tris pH 8, 200 mM NaCl, 1 mM TCEP, and 0.1% Brij-35. The assay buffer can be manipulated to optimize the reaction to determine what conditions RquA is most active in to produce the most amount of RQ_3. Varying the pH, buffer identity, reducing agent, salt concentration, and Brij-35 concentrations were done to determine the optimal reaction conditions required for RquA.

To determine which pH RquA is most active in, the reaction was done in a multicomponent buffer to ensure that the chemical environment remains the same and the pH is changing. RquA activity was tested at pH 6, 7, 8, 9, and 10 and initial velocities were determined to be 0.01 μM min^{-1}, 0.14 μM min^{-1}, 0.13 μM min^{-1}, 0.08 μM min^{-1}, and 0.05 μM min^{-1}, respectively (Figure 2.14A). RquA was able to convert 1%, 26%, 33%, 24%, and 12%, of UQ_3 to RQ_3 pH 6, 7, 8, 9, and 10, respectively (Figure 2.14B).

Since RquA was most active at pH 8, different buffers at pH 8 were tested to determine if the chemistry of the buffer affected RquA function. The activity of RquA was tested at pH 8 in Tris, sodium bicarbonate, and HEPES buffers. The initial velocities of the reactions in Tris pH 8, bicarbonate pH 8, and HEPES pH 8 were determined to be 0.13 μM min^{-1}, 0.13 μM min^{-1}, and 0.14 μM min^{-1}, respectively (Figure 2.15A). The ability of RquA to convert UQ_3 to RQ_3 in Tris pH 8, Bicarbonate pH 8, and HEPES pH 8 was 38%, 28%, and 34%, respectively (Figure 2.15B). The initial velocities and UQ_3 to RQ_3 conversion in all buffers at pH 8 generally showed no statistical difference, indicating that the chemistry of the buffer chosen does not impact the activity of RquA.

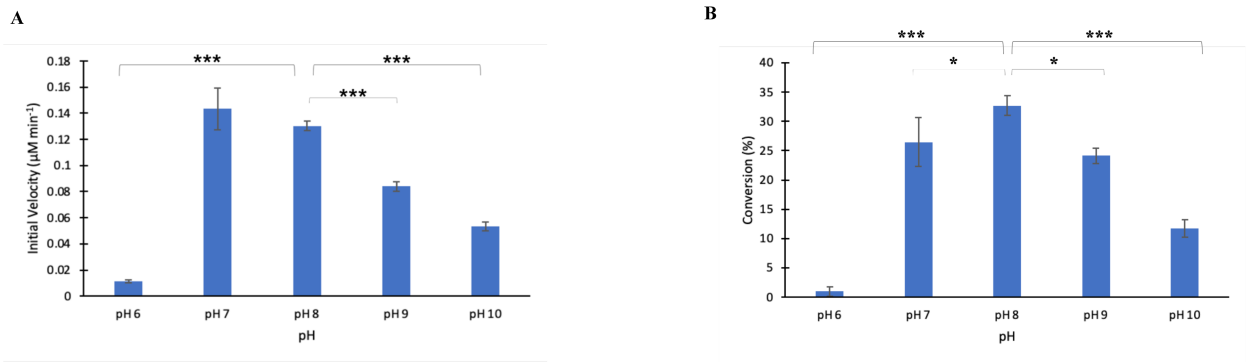

Figure 2.14 RquA is Most Active at pH 8. RquA activity was assayed in 20 μM UQ_3, 40 μM SAM, 1 mM $MnCl_2$, and assay buffer containing 50 mM Multi Component Buffer (MCB) which contained 100 mM HEPES, 100 mM MES, and 100 mM CHES, 200 mM NaCl, 1 mM TCEP, and 0.1 Brij-35 and adjusted to either pH 6, 7, 8, 9, or 10. Amount of RQ_3 produced was quantified to determine **A.** the initial velocities and **B.** ability to convert UQ_3 to RQ_3. From the initial velocities and ability to convert UQ_3 to RQ_3, it was determined that the optimal pH for RquA activity is pH 8. Triplicate assays were done to ensure accuracy with error bars representing standard deviation and significance was determined via one-way ANOVA and Dunnetts Test. An *, **, and *** represents the significance ($p<0.05$, <0.01, and <0.001, respectively) compared to pH 8.

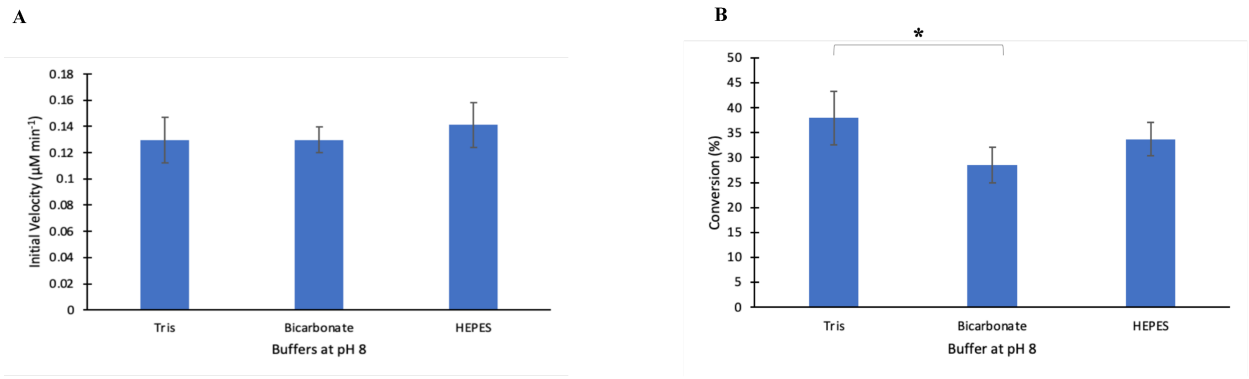

Figure 2.15 RquA is Active with Varying Buffers at pH 8. RquA first purified in 0.1% Brij-35 before being assayed in different buffers at pH 8. RQ_3 production was quantified to determine **A.** the initial velocities and **B.** ability to convert UQ_3 to RQ_3. From the initial velocities and ability to convert UQ_3 to RQ_3, the activity of RquA does not appear prefer a particular buffer composition. Triplicate assays were done to ensure accuracy with error bars representing standard deviation and significance was determined via a one-way ANOVA and Dunnetts Test. An * indicates significance ($p<0.05$) when compared to Tris.

To determine the effect of reducing agent, RquA activity was assayed in the presence of 1 mM TCEP, 1 mM DTT, 5 mM reduced glutathione (GHS), and 5 mM β-mercapoethanol (βME). The reaction was unaffected by the identity of the reducing agent (Figure 2.16A). The initial velocities of the reaction with reducing agents TCEP, DTT, GSH, and βME were 0.2 μM min^{-1}, 0.18 μM min^{-1}, 0.13 μM min^{-1}, and 0.14 μM min^{-1}, respectively (Figure 2.16A). The conversion efficiency of RquA was highest in TCEP and DTT, with 44% and 40% of UQ_3 converted to RQ_3 respectively. (Figure 2.16B). Since RquA is active in different reducing agents, the reducing agent isn't likely to bind directly to RquA but instead may have an indirect role in the reaction by keeping RquA reduced. RquA from *E. gracilis* contains two cysteine residues, which could impact its activity if disulfide bonds were to form. The two cysteine residues are exposed on the surface of RquA, which in an oxidizing environment could form intermolecular disulphide bonds thereby rendering RquA inactive (Figure 2.16C). To determine if RquA is forming intermolecular disulfide bonds, SDS-PAGE without the reducing agent βME present, could be done to determine if RquA is forming a dimer in the absence of a reducing agent.

To determine if a reducing agent is required for function, RquA was dialyzed overnight in a buffer lacking TCEP. After dialysis it can be seen that RquA was no longer active (Figure 2.16AB). RquA might require the two cysteine residues to be in their reduced forms to be active. When a reducing agent is present in solution, this ensures that the two cysteine residues are reduced and not forming an intermolecular disulfide bond. RquA activity was restored when 1 μM to 1 mM TCEP was added back into the reaction assay buffer (2.16D). Overall, these results suggest that the reducing agent is not directly involved in the reaction but ensures that RquA remains reduced during the reaction.

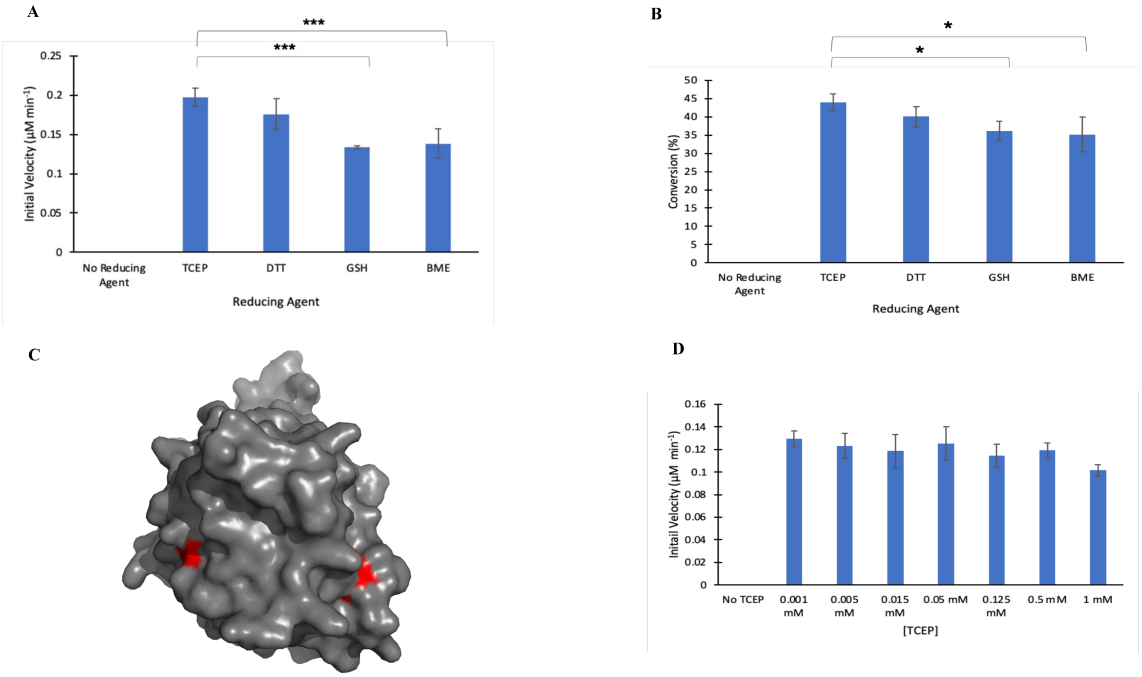

Figure 2.16 RquA Requires a Reducing Agent. RquA was purified in 0.1% Brij-35 then assayed in base reaction buffer with either no reducing agent, 1 mM TCEP, 1 mM DTT, 5 mM reduced glutathione, or 5 mM βME to determine the effects of a reducing agent. Amount of RQ_3 was quantified to determine **A.** the initial velocities and **B.** ability to convert UQ_3 to RQ_3. It was determined that a reducing agent is required for RquA to be active, as seen when no reducing agent was present. **C.** Surface representation of an AlphaFold2 prediction of RquA tertiary structure. RquA contains two cysteine residues, indicated by two red spots. The two cysteine residues are localized the surface of RquA, which when in an oxidizes environment, might participate in an intermolecular disulphide bond. **D.** RquA regains its activity when TCEP is added back into the reaction buffer. Triplicate assays were done to ensure accuracy and the bars represent the standard deviation Significance was determined via one-way ANOVA and Dunnetts Test. * and *** represents the significance ($p<0.05$and $p<0.001$, respectively) when compared to TCEP.

To determine the effect of salt concentration on RquA activity, RquA function was assayed in buffers with final concentrations of 50 mM, 100 mM, 200 mM, and 400 mM of NaCl to have initial velocities of 0.10 μM min^{-1}, 0.10 μM min^{-1}, 0.18 μM min^{-1}, and 0.15 μM min^{-1}, respectively (Figure 2.17A). Higher concentrations of NaCl also increased the conversion efficiency of the reaction, with the conversion efficiency being 36% for 200 mM and 400 mM and 25% and 27% for 50 mM and 100 mM respectively (Figure 2.17B). RquA was active in buffers containing all salt concentrations but was more active in higher salt concentrations as seen with the better initial velocities and conversions.

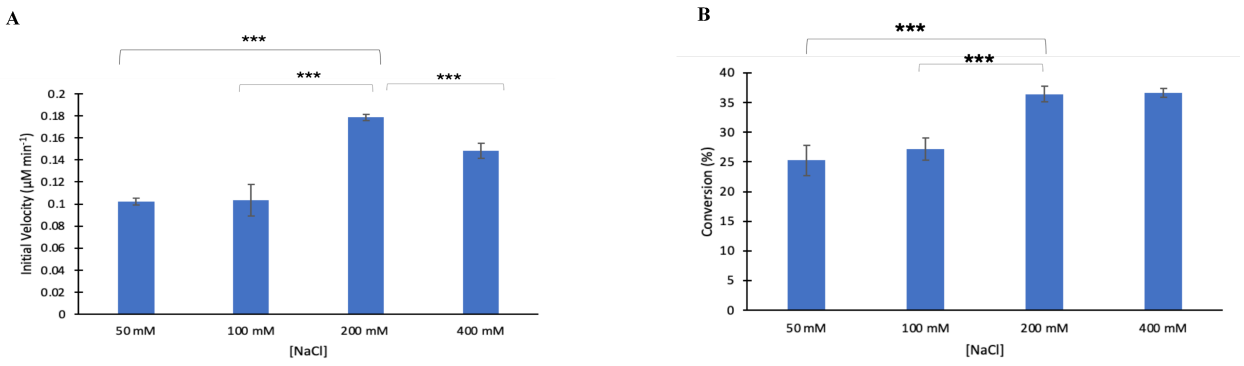

Figure 2.17 RquA is Active in Varying Salt Concentrations. RquA was first purified in 0.1% Brij-35 before being reacted in base reaction buffer with final concentration of NaCl either 50 mM, 100 mM, 200 mM, or 400 mM to determine the effects of salt concentration of the activity of RquA. The amount of RQ_3 produced was quantified to determine the **A.** initial velocities and **B.** ability to convert UQ_3 to RQ_3. Triplicate assays were done to ensure accuracy where the bars represent the standard deviation. A one-way ANOVA and Dunnett's Test was done on each salt concentration. An *** represents the significance ($p<0.001$) when compared to 200 mM NaCl.

I next investigated how much Brij-35 is required for RquA activity by assaying activity in buffers containing 0.05%, 0.1%, and 0.2% Brij-35. The initial velocities for each Brij-35 concentration were determined to be 0.14 μM min^{-1}, 0.14 μM min^{-1}, and 0.12 μM min^{-1} (Figure 2.18A) and conversion of UQ_3 to RQ_3 was 31%, 35%, and 30%, respectively (Figure 2.18B). The activity in all Brij-35 concentrations were similar, indicating that RquA is not sensitive to detergent concentration. However, when there was 0.2% Brij-35 present in the reaction buffer, the initial velocity and ability to convert UQ_3 to RQ_3 were the lowest, they were still comparable to the velocities measured in 0.05% and 0.1% Brij-35. This could suggest that when there are too many micelles present in solution, it could interfere with the activity of RquA through substrate dilution kinetics.

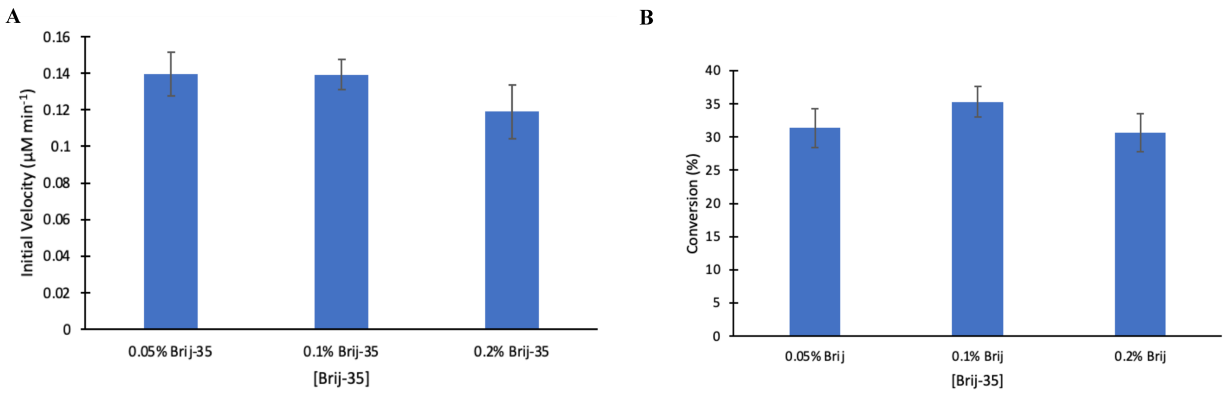

Figure 2.18 RquA is Active in Varying Detergent Concentrations. RquA was purified in 0.1% Brij-35 before being assayed in base reaction buffer with final Brij-35 concentrations of either 0.05%, 0.1% or 0.2% to determine the effects of Brij-35 on the activity of RquA. The amount of RQ_3 produced was quantified to determine **A.** the initial velocities and **B.** ability to convert UQ_3 to RQ_3. No significant differences in the activity of RquA in the different Brij-35 concentrations. Triplicate assays were done to ensure accuracy with error bars representing standard deviation.

2.3.10 S-adenosyl-l-homocysteine and Sinefungin Reduce RquA Activity

S-adenosyl-l-homocysteine (SAH) and sinefungin were tested as potential inhibitors of RquA due to their similar structures to SAM. Zero to 2 mM of each inhibitor were added to the base assay buffer to see what effect they have on the enzymatic activity of RquA. The enzymatic activity of RquA was inhibited when higher concentrations of SAH or sinefungin were added to the reaction, as seen with the decrease in initial velocities (Figure 2.19). It seems with both SAH and sinefungin, there needs to be a large excess of inhibitor compared to SAM for there to be any inhibition. Even then only a small decrease in reaction velocity was observed.

Enzyme inhibition can serve as a control mechanism for biological systems and can provide a better understanding of an enzymes activity by determining residues that are critical for catalysis (Mazzei et al., 2016). There have been no previous studies that identified inhibitors for RquA, so this research tried to look for potential inhibitors. The SAM-binding site was chosen as the target for inhibition as SAM is required for the RquA reaction and is the amino donor of the reaction. If SAM could no longer bind to RquA this would stop RQ biosynthesis. The SAM analogs SAH and sinefungin were chosen due to their similar structures to SAM, which could potentially allow them to bind to the SAM-binding site of RquA. Reactions done with no SAM and only SAH and sinefungin resulted in no RQ_3 production, indicating that they are unable to substitute for SAM in the reaction. By trying to inhibit SAM from binding to RquA, we might be able to gain insight into the active site of RquA and determine how SAM binds to it.

RquA was never fully inhibited by either SAH or sinefungin; however, the activity of RquA decreased with higher concentrations of inhibitor (Figure 2.19). Since the activity of RquA was only changed with high concentrations of SAH and sinefungin, this indicates that they are weak inhibitors for RquA. SAM/SAH based inhibitors have been shown to have very low

selectivity due to the high homology of the SAM-binding domains of different methyltransferases (Zhang et al, 2015).

Bisubstrate inhibitor analogs have the potential to increase the potency and selectivity of SAM/SAH based inhibitors (Zhang et al, 2015). By combining the free energies of the cofactor and substrate interactions, bisubstrate inhibitors can increase the selectivity of the inhibitors (Zhang et al, 2015). According to Zhang et al, an effective bisubstrate inhibitor should have an optimal linker between the compound that mimics the transition state of the methyl transfer reaction, or the amino transfer reaction in the case of RquA, where one part of the inhibitor targets the SAM-binding site and the other targets the substrate-binding site. For RquA, one target could mimic SAM to bind to the SAM-binding site and the other target could mimic UQ_3 to bind where UQ_3 binds to. The drawback to this method is the structure of RquA needs to be determined to fully understand how both SAM and UQ_3 bind to RquA. A way to overcome this is to create a general bisubstrate structure that mimics both SAM and UQ_3 to see if it can inhibit RquA.

UQ_3 is also required for the RquA reaction, and its binding site could be another target for inhibition. Quinone analogs could be tested to see if they inhibit UQ_3 from binding to RquA. Known quinone-site inhibitors that can be tested on RquA are rotenone, fenpyroximate, and bullatacin (Darrouzet & Dupuis, 1997, Uno et al, 2019). Another group has looked at potential inhibitors of UQ from binding to two UQ binding sites, A and B, found on complex I. Rolliniastatin, binds to site A, blocking UQ from binding to site A, and rotenone binds to site B, blocking UQ from binding to site B (Darrouzet & Dupuis, 1997). Since rolliniastatin and rotenone are known to inhibit UQ from binding to the two UQ binding sites on complex I, they could be assayed to determine if they block UQ from binding to its respective binding site on

RquA.

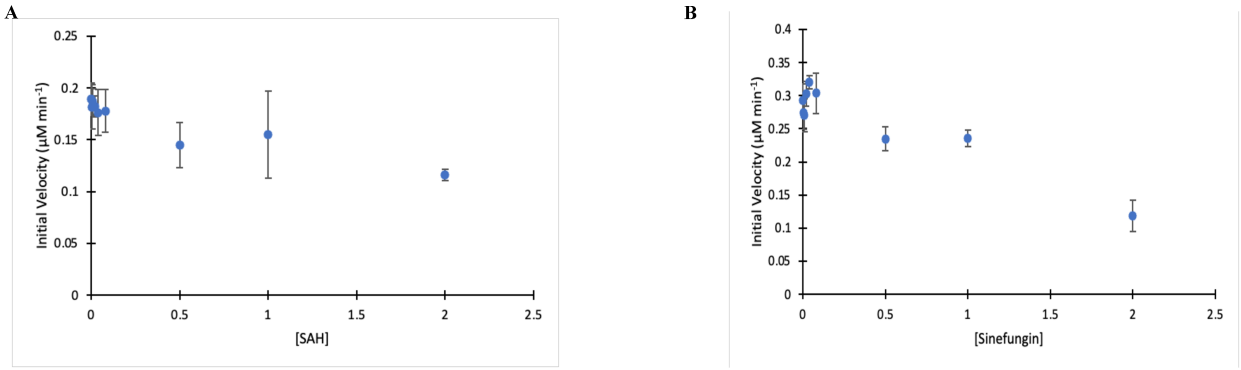

Figure 2.19 High Concentrations of SAH and Sinefungin Inhibit RquA. RquA was purified in 0.1% Brij-35 and then assayed for functional activity. **A.** Zero – 2 mM of SAH was added to the base assay buffer to determine if it inhibits RquA activity. **B.** Zero – 2 mM sinefungin was added to base assay buffer to determine if it inhibits RquA.

2.4 Summary

In this chapter I was able to determine the optimal conditions required for RquA to soluble and functional. I was able to determine that RquA is soluble in multiple detergents but has the highest yield when purified in 0.1% Brij-35 and that RquA has the highest activity at pH 8, requires a reducing agent, and is not sensitive to buffer composition, salt concentration, and Brij-35 concentration. Finally, I determined that SAH and sinefungin act as weak inhibitors for RquA only showing inhibition of RQ_3 production at concentrations of 500 μM or higher. The initial goal of this research was to determine a structure of RquA through x-ray diffraction; however, the detergent determined to produce the highest yield of RquA, Brij-35, is not the optimal detergent to use when trying to produce a crystal.

Chapter 3 Creating Mutants of RquA to Increase Solubility

3.1 Introduction

X-ray diffraction is a common structural biology technique used to determine a structure of a protein. To get a good crystal for x-ray diffraction, the protein needs to be soluble, homogenous, and have a high yield (Smyth et al, 2000). In the past, membrane proteins are difficult to crystalize from because of their poor solubility, and typically require detergents to aid in their solubility (Birch et al., 2018, Moraes et al, 2014). RquA is predicted to be a monotopic membrane and very few monotopic membrane proteins have been structurally characterized (Marcia et al, 2010). Monotopic membrane proteins cannot be isolated in a stable water-soluble form and typically require detergents to aid in their solubilization (Marcia et al, 2010). The choice of detergent is important when obtaining a good structure from a crystal. RquA is most soluble and has the highest yield when purified in the detergent Brij-35, however Brij-35 is a very large detergent with a tail consisting of 23 polyethylene glycol repeats (Figure 2.2A). Brij-35 is a very poor choice of detergent to use to produce a crystal, as the large micelles make it difficult for a good crystal to form. The detergent C12E8 and DDM are better for crystallography as they are much smaller than Brij-35 (Stetsenko & Guskov, 2017). However, with both C12E8 and DDM, the yield of RquA was insufficient. Instead of trying to screen multiple conditions to determine the optimal condition required to determine the structure of RquA through x-ray diffraction, another approach is needed.

RquA is a class I SAM-dependent methyltransferase, which consists of proteins like UgiG, UbiE, and Coq5. UbiG is also a monotopic protein that has been solubilized and its crystal structure determined (Zhu et al, 2016). UbiG shares a 16% homology to RquA and is a class I

SAM-dependent methyltransferase that catalyzes the transfer of two O-methyl groups for UQ biosynthesis in *E. coli* (Zhu et al, 2016). UbiG has a helix of interest between β4 and α10 which consists of hydrophobic amino acids used for membrane-lipid interaction (Figure 3.1A) (Zhu et al, 2016). Zhu et al created a UbiG mutant ($UbiG^{\Delta 165–187}$) by deleting this helix of interest. They found that the mutant $UbiG^{\Delta 165–187}$ was able to be solubilized and bind to its substrate SAH with a 58-fold higher binding affinity than wild type UbiG (Zhu et al 2016). Like UbiG, RquA has an analogous helix comprised of hydrophobic amino acids that may interact with a membrane (Figure 3.1B). The sequence of this helix is YWFNPTRYMPFVFWLEP and most of the amino acid side chains are predicted to be pointing outwards, indicating that they could be interacting with the membrane. The non-polar polar ratio (NPPR) of RquA indicates that this helix of interest is very non-polar, with a high score of around 2.3, which further suggests that this helix interacts with a membrane (Figure 2.1A). In this chapter I designed two mutants of RquA to help increase its solubility. I then purify these RquA mutants and determine if they are functional.

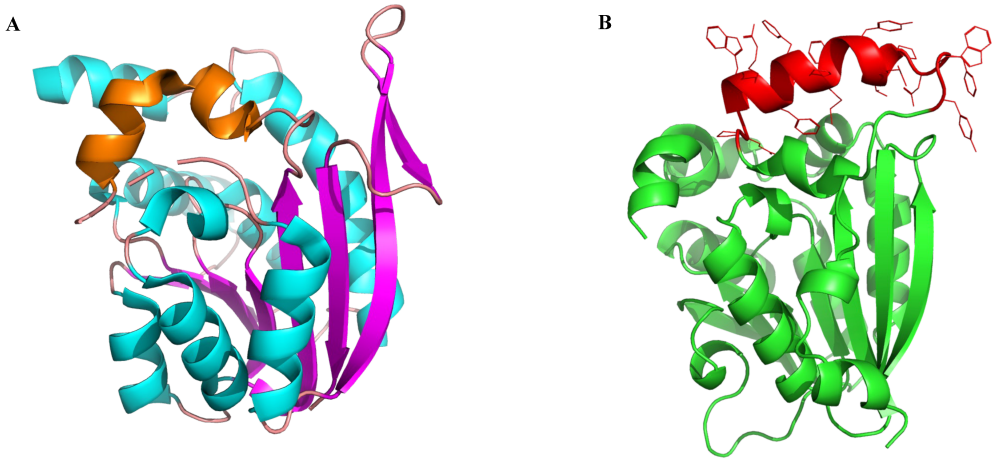

Figure 3.1 UbiG and RquA Share a Homologous Helix. A. Ribbon representation of UbiG (PDB 4KDC) from *E. coli*. The hydrophobic helix is coloured in orange. **B**. The AlphaFold2 predicted structure of RquA with the homologous helix coloured red. This helix region consists of a lot of hydrophobic amino acid side chains with most of them facing outwards, suggesting they may interact with the membrane. Figure was generated using PyMol.

3.2 Methods

3.2.1 Designing Soluble RquA

The *RquA Euglena gracilis* expression plasmid (pET21_MBP-RquA) and an empty vector (pET32_MBPTEV) were used as the template to create both mutants (*RquA_HD* and *RquA_MH*) used in this chapter (see 2.2.1).

The first mutant created has amino acids 119-217 deleted entirely (*RquA_HD*). A forward (RquA_EugΔ199-217_f) and a reverse (RquA_EugΔ119-217_r) primer were ordered from BioBasic Inc. (Table 3.1). The PCR overlap extension method of mutagenesis (Heckman et al, 2007) was done using the forward and reverse primers RquA_ EugΔ 99-217_f, RquA_EugΔ119-

217_r and the T7 Terminal Reverse and TEVins_f_SLIC forward and reverse primers following the Q5 polymerase protocol (Table 3.1). The final PCR product was digested with BamHI and XhoI restriction enzymes and ligated into the empty pET21_MBPTEV vector. The colonies were screened by PCR and verified via sequencing (BioBasic Inc).

Table 3.1 Sequences of the forward and reverse primers used to generate pET21_MBP-RquA_HD

Primer Name	Sequence (5' to 3')
RquA_EugΔ199-217_f	CAC GGT CCG CTG GAA CCG TTC CGC CTG
RquA_EugΔ199-217_r	CGG TTC CAG CGG ACC GTG ATA TTC AAC CC
TEVins_f_SLIC	TTG TAT TTC CAG GGA TCC
T7 Terminal Reverse	GCT AGT TAT TGC TCA GCG G

A second mutant of *RquA* was created by mutating the hydrophobic amino acids in segment 119-217 to hydrophilic amino acids (*RquA_MH*). A BLAST search was done using the amino acid sequence of *RquA* from *Euglena gracilis* to determine its closest homologs. The *RquA* sequences from *E. gracilis, R. rubrum, Pygsuia biforma, Blastocystis hominis,* and 10 sequences of homologs obtained from the BLAST search were aligned using Clustal Omega to determine which amino acids in the helix were conserved (Figure 3.2A). The amino acids that were conserved in all 14 sequences were kept, regardless of their polarity, and the amino acids that were not conserved were changed to hydrophilic amino acids that were found in other sequences or hydrophilic amino acids with helical propensity as this region is predicted to be a helix. The wild type residues of *RquA* were mutated to KEENPTREKMKEVFRELEP (Figure 3.2B). A plasmid with the modified *RquA* sequence was ordered from BioBasic Inc with BamHI and XhoI restriction enzyme sites. The plasmid was digested with the restriction enzymes

BamHI and XhoI and ligated into an empty pET21_MBPTEV vector following manufacturers protocols. The colonies were screened by PCR and verified via sequencing (BioBasic Inc).

A

```
Blastocystis spp.                                                LSFLLLHEVPDDTKRKVIDRIMMSVPVGGKAIFIEYHKPAWY-SPWRYMMPIVYWLLEPL  198
Euglena gracilis                                                 YAFMILHEVPDDRKHQIVNNMLKSVKTGGTVMWVEYHGPPYWFNPTRYFMPFVFRWLEPF  218
Pygsuia biforma                                                  CSFMLLHEIPDENKSSVVNNVLNSVKVGGKAVFIDYGRPSTL-HPVRPILSFVNDWLEPW  209
Rhodospirillum rubrum                                            CCFFLLHEVPDHVKSKIVDNMLSAVRPGGKVVFVDYHRYAAL-HPLRPIMAFVFRTLEPF  230
Jeongeupia sp. HS-3                                              CNFMLLHEVPDDWKRRIVDNMLAQMPAHGEVLFVDYHGPARW-QPVRYILKLVNRLLEPF  210
Class SAM-dependent methyltransferase [Proteobacteria bacterium] CSFFLLHEVPDDKKREIVDNMLAQLPKGGKVVFVDYHRPSMW-QPIRWILKAVNAWLEPF  196
Formivibrio citricus                                             CSFFLLHEVPDEKKRQILNNLLARLPKGGKLVLVDYHRPAWW-QPIRLILKVVNAWLEPF  197
Ubiquinone/menaquinone biosynthesis methylase [Chromobacterium vacinii] CSFFLLHEVPEGMKSAIVDNMLAQVAPGGRAMFVDYHRPRPW-QPIGWLLKWVNRALEPF  195
Paludibacterium paludis                                          VSFFLLHEVPDDLKCRIVDNMLSQLPEGGEALFVDYHKPAAW-QPIGWLLRGVNAWLEPF  194
Chitinibacter fontanus                                           CSFFLLHEVPDDKKREIVDHMLAKVPVGGKAVFVDYHNPRRW-QPIRYILKLVNHYLEPF  194
Candidatus Propionivibrio aalborgensis                           SSFFLLHEVPDEKKHEIVNNMLANLPKGGKAVFVDYHNPARW-QPVRYILKLVNRYLEPF  196
Betaproteobacteria bacterium                                     CSFFLLHEVPDDKKHQIVDHMLEKLPKGKKAIFIDYANPAKW-HPVRYILKIINHLLEPF  202
Betaproteobacteria bacterium                                     CNFFLLHEVPDDKKHQIVNQMLEKLPKKGKAIFVDYSNPAKW-HPVRYILKVVNHLLEPF  196
Proteobacteria bacterium                                         CSFFLLHEVPEDKKYQIVDHILKKLPKGGKAIFVDYANPAKW-QPIRYILKVVNHLLEPF  196
                                                                   *::***:*:  *  :::.::  :      : ::*        *   ::  :   ***
```

B

```
Original Sequence: YWFNPTRYFMPFVFRWLEP
Mutated Sequence:  KEENPTREKMKEVFRELEP
```

Figure 3.2 Sequence Alignment of RquA and its Closest Homologs. A. Alignment of *RquA* sequences and closely related sequences from a BLAST search to determine which amino acids are conserved in the 199-217 region of *RquA* from *Euglena gracilis*. The highlighted region is the region of interest (residues 199-217). Conserved residues (represented with an *) were kept and the amino acids that were not were changed to either hydrophilic amino acids present in the other homologs or amino acids with helical propensity. **B.** Amino acid sequences of the original sequence and the mutated sequence. The amino acids that were mutated to hydrophilic amino acids are coloured in red and the amino acids that were kept the same are coloured in black.

3.2.2 Purification of RquA_HD and RquA_MH

pET21_MBPRquA_HD and pET21_MBPRquAML were transformed into chemically competent BL21 (DE3) *E. coli* cells via heat shock. A single bacterial colony was grown in Lennox Broth (LB) media containing ampicillin (100 μg/mL) at 37 °C until optimal culture density was reached (OD_{600} ~0.6). Gene expression was induced with 0.5 M IPTG and were left to grow overnight at 20 °C before the cells were collected by centrifugation. Cell pellets were resuspended in 30 mL lysis buffer (20 mM Tris pH 8, 200 mM NaCl, 1 mM TCEP, and with or without 0.1% Brij-35). The resuspended cells were lysed via sonication and were centrifuged at 4 °C at 25,000 × g for 20 min. The supernatant was passed through an amylose resin column and the immobilized RquA proteins were washed with lysis buffer and eluted with lysis buffer (5 mL) containing 10 mM maltose. Eluted protein was then incubated with 38 μM of TEV protease overnight at 4 °C. Cleaved protein was applied to Ni^{2+} resin, washed with lysis buffer containing 20 mM Imidazole pH 8, and eluted with 300 mM imidazole pH 8. The flow-through and wash fractions were pooled together and concentrated before further purification by FPLC using the preparatory size exclusion chromatography (SEC) sepharose column Superdex 300 (Cytiva). The purification process was evaluated by SDS-PAGE and visualized by Coomassie brilliant blue.

In an alternate protocol, the purification of RquA_HD and RquA_MH was optimized to more efficiently separate MBP from RquA. The eluted protein (MBP-RquA) from amylose resin column was then purified by preparatory size exclusion chromatography. The fractions containing MBP-RquA were collected and cleaved with 38 μM TEV protease overnight at 4 °C. The cleaved protein was then purified by amylose resin and eluted with 10 mM maltose. The flow-through and wash fractions were pooled together and concentrated before a second round of size exclusion chromatography.

3.2.3 Functional Assays of RquA_HD and RquA_MH

To confirm if RquA_HD and RquA_MH are functional, an HPLC-based functional assay was performed. The functional assay was the same as for the wild type RquA described in 2.2.6, however only the time point of 60 min was analyzed.

3.3 Results and Discussion

3.3.1 RquA_MH is Soluble in 0.1% Brij-35 and No Detergent

AlphaFold2 predicts this helix with higher confidence than its prediction of the helix in RquA_WT (Figure 3.3AC). The WT sequence has three prolines – P203, P209, and P217 – which could cause the lower confidence in its prediction. Prolines are not usually found in the middle of the helices as they do not have an amide proton, preventing it from participating in hydrogen bonding (Wilman et al, 2014). In the mutated sequence the middle proline was mutated to a lysine, P209L, which could have caused the increase in the confidence of the predicted structure (Figure 3.3A).

To see if RquA_MH was expressed successfully, I first purified it in 0.1% Brij-35, like the wild type RquA (RquA_WT). RquA_MH was expressed successfully as seen by the soluble fraction elution band around 100 kDa (Figure 3.4A). The resulting SEC chromatogram produced a relatively broad peak with multiple shoulders leading up to the RquA_MH peak, which were confirmed by SDS-PAGE to be RquA_MH (Figure 3.4C). However, the SEC fraction was pure as seen by the single band on the SDS-PAGE as seen by the 25 kDa ladder band (Figure 3.4A). This purification yielded around 0.16 mg per L of culture, which is much lower than the RquA_WT purification in Brij-35, which typically yields around 0.8388 – 1 mg per L of culture.

I next purified RquA_MH without detergent to see if the mutations made in the helix

increased its solubility. RquA_MH was purified successfully without detergent, as seen with the large soluble fraction elution band on the SDS-PAGE around the 75 kDa ladder band (Figure 3.4B). Unfortunately, it was difficult to separate MBP from RquA during the SEC (Figure 3.4D). RquA seemed to be on the shoulder on the peak containing both MBP and RquA as seen on the SDS-PAGE (Figure 3.4BD). However, there did not seem to be any aggregation leading up to the combined peak of RquA and MBP, indicating that the RquA_MH is soluble without detergent.

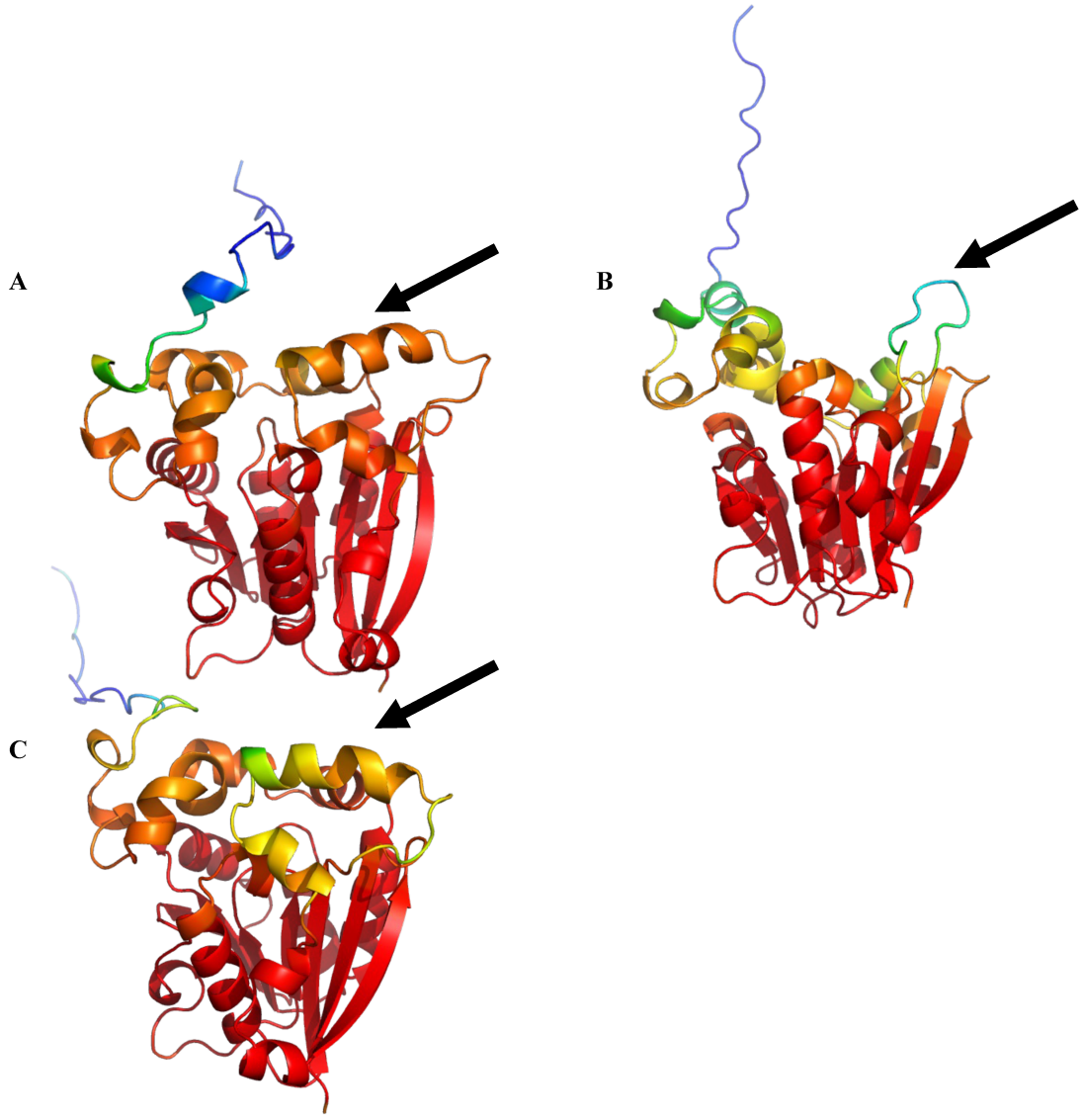

Figure 3.3 Predicted Structures of RquA. The predicted structures of RquA were predicted by AlphaFold2. **A.** RquA_MH **B.** RquA_HD and **C.** RquA_WT coloured by the confidence score of the prediction with red representing scores >90%, orange 80%, yellow 70%, green 60% and blue <50%. The hydrophobic helix is depicted by the black arrow. Figure was generated using PYMol.

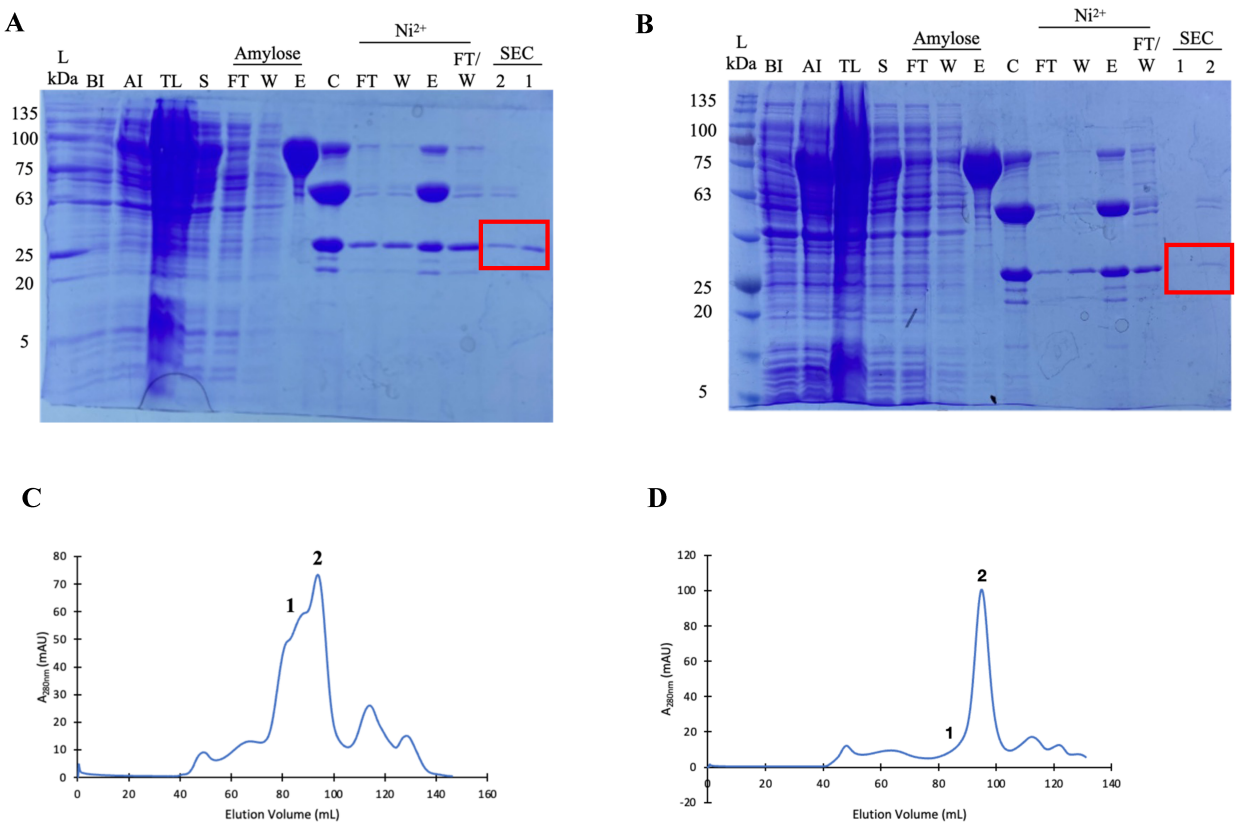

Figure 3.4 Purification of RquA_MH. SDS-PAGE analysis of RquA_MH purifications in the presence of **A.** 0.1% Brij-35 and **B.** no detergent. pET321_MBPRquA_MH cells were expressed in competent BL21 (DE3) *E. coli* cells, lysed, purified with amylose resin, cleaved with TEV protease, and further purified with Ni^{2+} and size exclusion chromatography (SEC). RquA_MH seems to be soluble in both 0.1% Brij-35 and no detergent as seen with the large soluble band after elution from the amylose resin. Gel Lanes: **L:** BLUelf Prestained protein ladder from FroggaBio **BI:** before induction **AI:** after induction **TL:** total lysate **S:** supernatant **FT:** flow-through **W:** wash **E:** elution **C:** cleaved protein **FT/W:** flow-through/wash **1** and **2:** SEC peaks. Resulting SEC chromatographs from RquA_MH purified in **C.** 0.1% Brij-35 and **D.** no detergent.

An alternate purification method was tried to further separate MBP from RquA. Since there seems to be a high yield of soluble MBP-RquA_MH after the amylose affinity chromatography, instead of cleaving the sample with TEV protease, it was first purified using SEC (Figure 3.5A). Afterwards, the fraction containing MBP-RquA_MH (70 kDa) was cleaved overnight with TEV protease (Figure 3.5B). The cleaved sample was then passed through an amylose resin column to remove MBP (Figure 3.5C). The flow-through and wash samples were combined before SEC to see if this helped with the separation. Unfortunately, RquA_MH was still not separated from MBP with this protocol as seen with the resulting SEC chromatogram (Figure 3.5D). There was only one peak observed that contained both MBP and RquA_MH, with RquA_MH alone only seen from the shoulder of the peak, which can be seen by the band around 30 kDa (Figure 3.5CD). Despite the low yield, around 0.162 mg per L of culture, with this protocol, RquA_MH was still soluble without detergent.

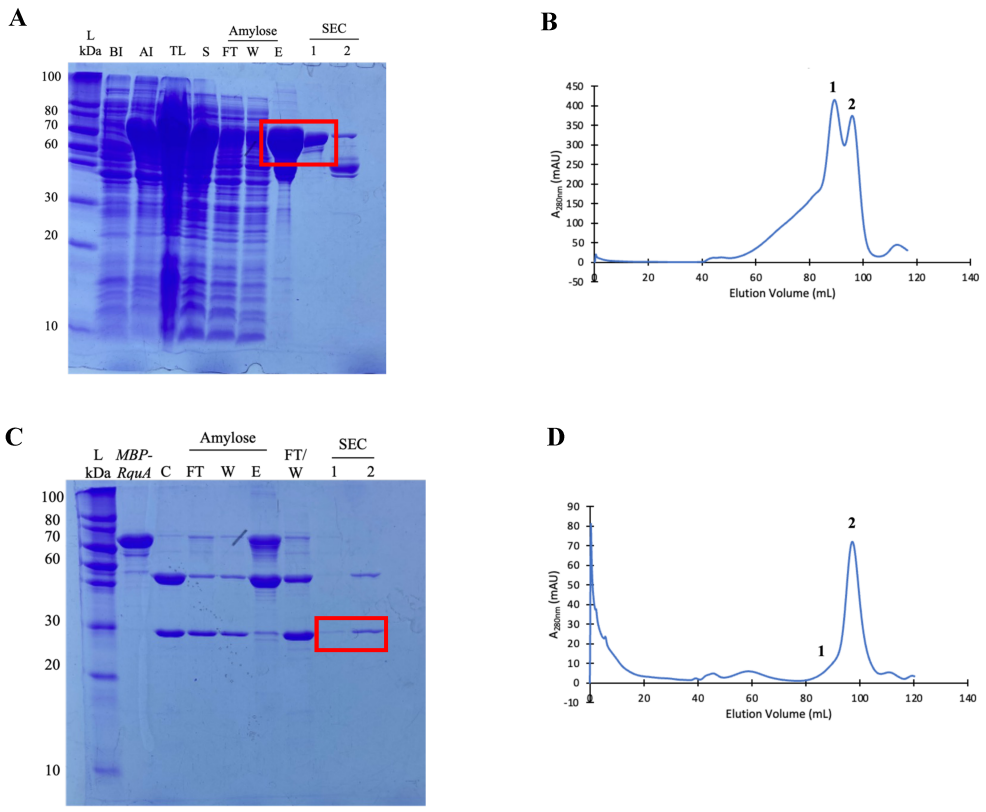

Figure 3.5 Optimization of the Purification of RquA_MH. pET21_MBPRquA_MH were expressed in competent BL21 (DE3) *E. coli* cells, lysed purified with amylose resin and SEC. **A.** SDS-PAGE analysis of MBP-RquA_MH purified without detergent. **B.** Resulting SEC chromatogram of elution from amylose resin purification of MBP-RquA_MH. MBP-RquA_MH (peak 1) was collected and cleaved with TEV protease overnight at 4 °C. **C.** SDS-PAGE analysis of cleaved MBP-RquA_MH. **D.** Resulting SEC chromatogram from FT/W sample of cleaved MBP-RquA_MH. Gel lanes: **L:** Penn State protein ladder **BI:** before induction **AI:** after induction **TL:** total lysate **S:** supernatant **FT:** flow-through **W:** wash **E:** elution **1:** Peak corresponding to MBP-RquA **2:** Peak corresponding to MBP. **MBP RquA**: peak 1 from **B** representing the un-cleaved MBP-RquA_MH sample **C:** cleaved protein **FT:** flow-through **W:** wash **E:** elution **FT/W:** flow-through/wash **1:** peak corresponding to RquA **2:** peak corresponding to MBP/RquA.

3.3.2 RquA_HD is Soluble in 0.1% Brij-35 and No Detergent

AlphaFold2 predicts RquA_HD can still adopt the proper tertiary structure despite the deletion of the hydrophobic helix (Figure 3.3B). This region is now predicted to be a loop with very low confidence (Figure 3.3B), possibly because it is just joining together the amino acids that were adjacent to the original hydrophobic helix to form this loop.

RquA_HD was first purified in 0.1% Brij-35 to determine if it is soluble in the presence of detergent. RquA_HD was soluble in the presence of 0.1% Brij-35 as seen with the large soluble band after elution from amylose affinity chromatography (Figure 3.6A). Unlike RquA_MH, there seemed to be more distinct peaks for RquA and MBP; however, the two peaks are not completely resolved (Figure 3.6C). As well, there is a large shoulder preceding the RquA peak on the SEC chromatogram, indicating some possible aggregation (Figure 3.6C).

RquA_HD was then purified without detergent to see if it is more soluble with less aggregation (Figure 3.6B). RquA_HD does seem to be soluble without detergent, as seen with the large single band present after amylose affinity chromatography (70 kDa) (Figure 3.6B). Like RquA_MH, RquA was not efficiently separated from MBP (Figure 3.6D). However, there does seem to be a small shoulder peak (1) at around 87 mL before the MBP peak (2) at around 95 mL, representing RquA, which can be seen around the 25 kDa ladder band (Figure 3.6BD). There seemed to be a very low yield of RquA_HD, around 0.150 mg per L of culture; however, this method was able to solubilize RquA without detergent.

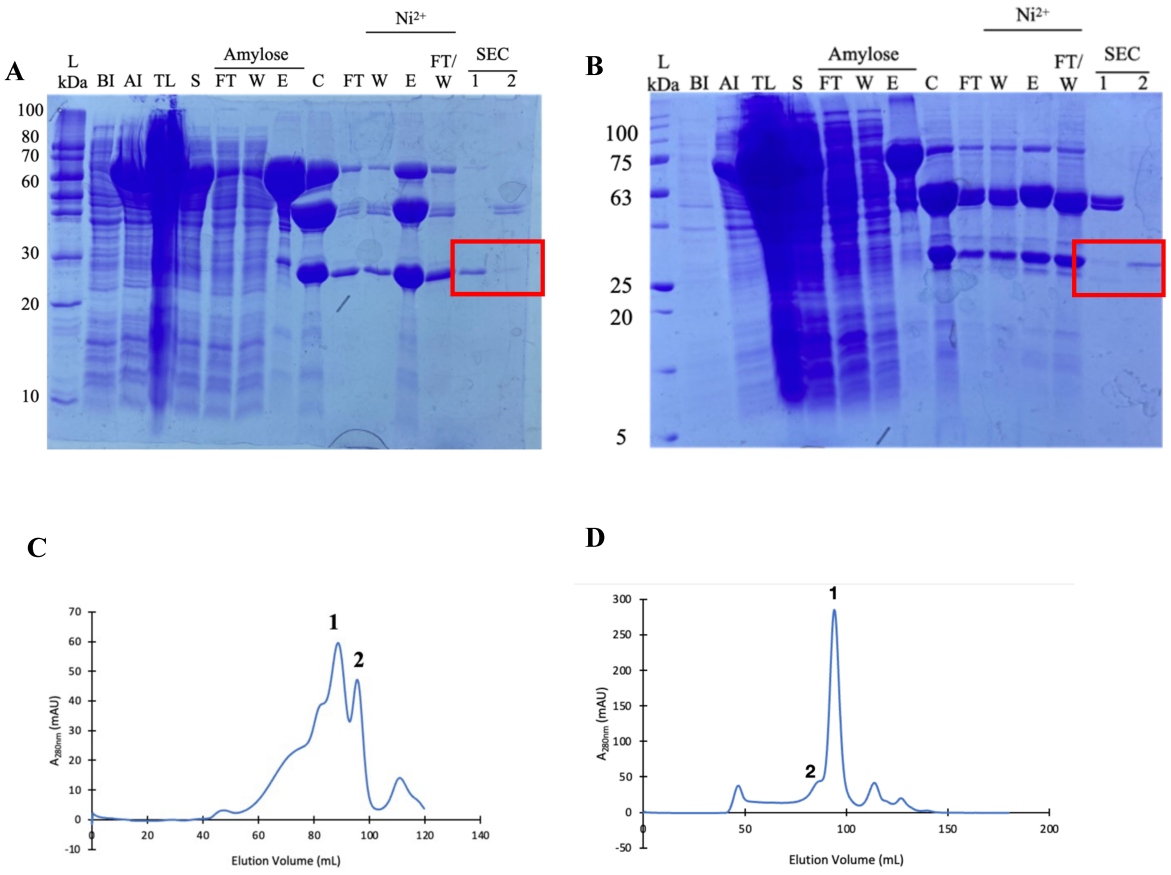

Figure 3.6 Purification of RquA_HD. SDS-PAGE analysis of RquA_HD with **A.** 0.1% Brij-35 and **B.** no detergent. pET21_MBPRquA_HD was expressed in competent BL21 (DE3) E. coli cells, purified with amylose resin, cleaved with TEV protease, and further purified by Ni^{2+} affinity chromatography and SEC. RquA_HD was soluble in both 0.1% Brij-35 and no detergent as indicated by the large soluble MBP-RquA_HD band from the amylose resin elution. Resulting SEC graphs of RquA_HD purified in **C.** 0.1% Brij-35 and **D.** no detergent. RquA was able to be separated when RquA_HD was purified in 0.1% Brij-35 but when purified without detergent. Gel lanes: **L:** Penn State protein ladder (**A**) or BLUelf Prestained protein ladder from FroggaBio (**B**) **BI:** before induction **AI:** after induction **TL:** total lysate **S:** supernatant **FT:** flow-through **W:** wash **E:** elution **C:** cleaved protein **FT/W:** flow-through/wash **1** and **2:** peaks corresponding to the SEC graphs for RquA_HD and MBP.

The alternative purification protocol was completed with RquA_HD to more efficiently separate MBP from RquA as there seemed to be a high yield of 2.54 mg of soluble MBP-RquA after amylose affinity chromatography (Figure 3.7A). I was able to obtain an isolated SEC peak of MBP-RquA (80 kDa), which was then cleaved with TEV protease (Figure 3.7B). After cleavage, MBP-RquA_HD was further purified with amylose affinity chromatography to separate MBP from RquA_HD (Figure 3.7C). Unlike with RquA_MH, this protocol did separate MBP from RquA_HD better to obtain a clean band of RquA_HD on the SDS-PAGE (30 kDa) (Figure 3.7C). The peak for RquA (1) eluted off the SEC around 87 mL and MBP (2) eluted off the SEC at around 96 mL (Figure 3.7D). Around 0.31 mg per L of culture of soluble RquA_HD was able to be isolated using this protocol.

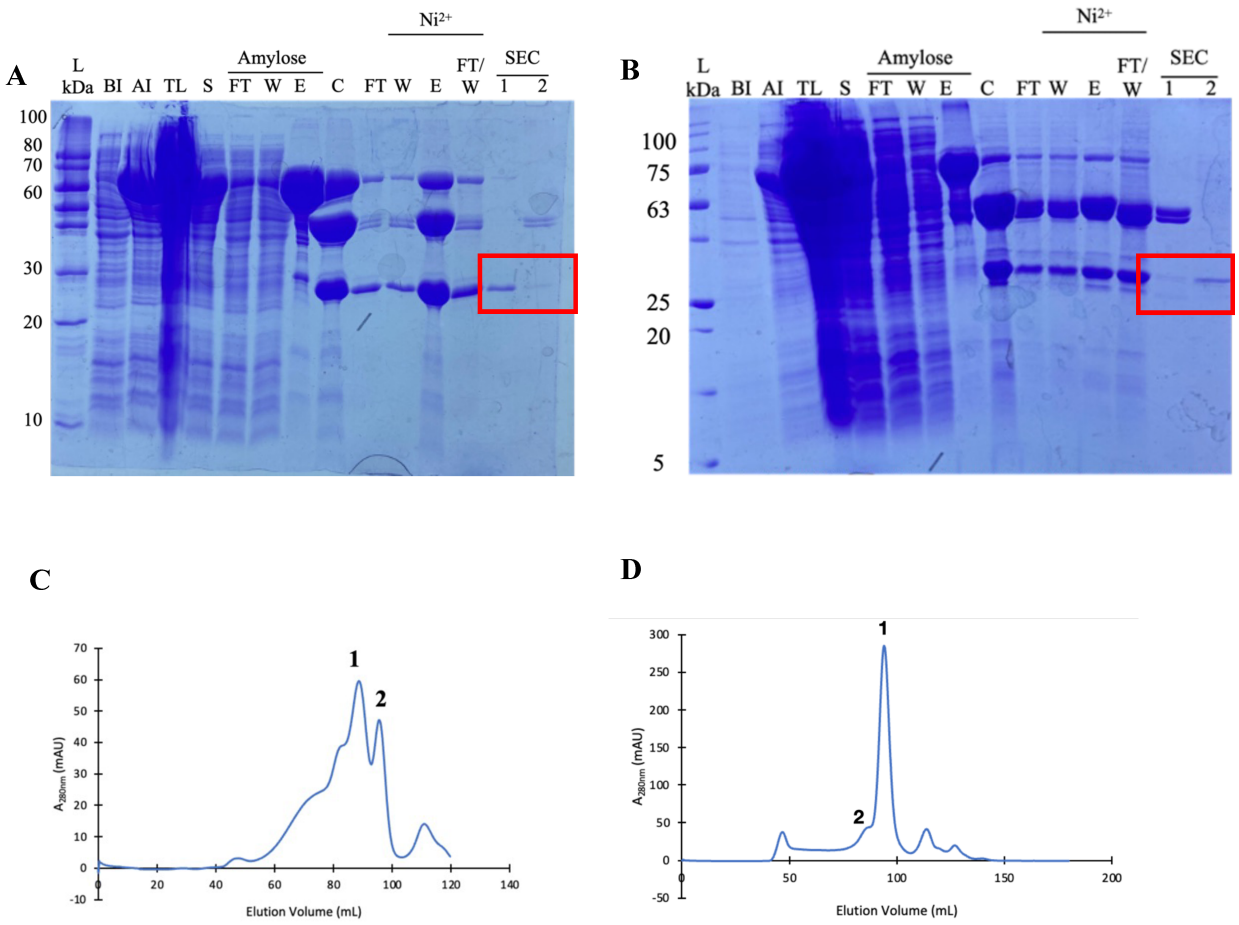

Figure 3.7 Optimization of RquA_HD purification. pET21_MBPRquA_HD was expressed in competent BL21 (DE3) E. coli cells, lysed, then purified with amylose resin and SEC. **A.** SDS-PAGE analysis of MBP-RquA_HD in no detergent. **B.** SEC graph of elution from amylose resin of MBP-RquA_HD. Peak 1, containing MBP-RquA_HD was cleaved with TEV protease overnight at 4 °C. **C.** SDS-PAGE analysis of cleaved MBP-RquA_HD. Gel Lanes **L:** Penn State protein ladder **BI:** before induction **AI:** after induction **TL:** total lysate **S:** supernatant **FT:** flow-through **W:** wash **E:** elution **1:** peak corresponding to MBP-RquA_HD **2:** peak corresponding to MBP **C:** cleaved protein **FT:** flow-through **W:** wash **E:** elution **FT/W:** flow-through/wash **1:** peak corresponding to RquA **2:** peak corresponding to MBP/RquA.

3.3.3 RquA_MH and RquA_HD are only Functional when Purified in 0.1% Brij-35

A RQ production assay was set up with both RquA_MH and RquA_HD to determine if they are functional. RquA_MH was only able to convert UQ_3 to RQ_3 when purified in 0.1% Brij-35 and did not convert UQ_3 to RQ_3 when purified without detergent (Figure 3.8AB). RquA_MH converted less UQ_3 to RQ_3 (3%) than RquA_WT (44%).

A similar result was observed with RquA_HD. RquA_HD was only able to convert UQ_3 to RQ_3 when it was purified with 0.1% Brij-35 and was inactive without detergent (Figure 3.8CD). RquA_HD converted less UQ_3 to RQ_3 than RquA_WT ability (2% vs. 44%, respectively). Even with the much lower ability to convert UQ_3 to RQ_3, these mutants were still functional in 0.1% Brij-35. Similar mutants in the homolog from *R. rubrum* showed no function when purified with detergent (Neupane, unpublished results). Even though these homologs have the same function and similar sequences, only the RquA mutants from *E. gracilis* were shown to be functional.

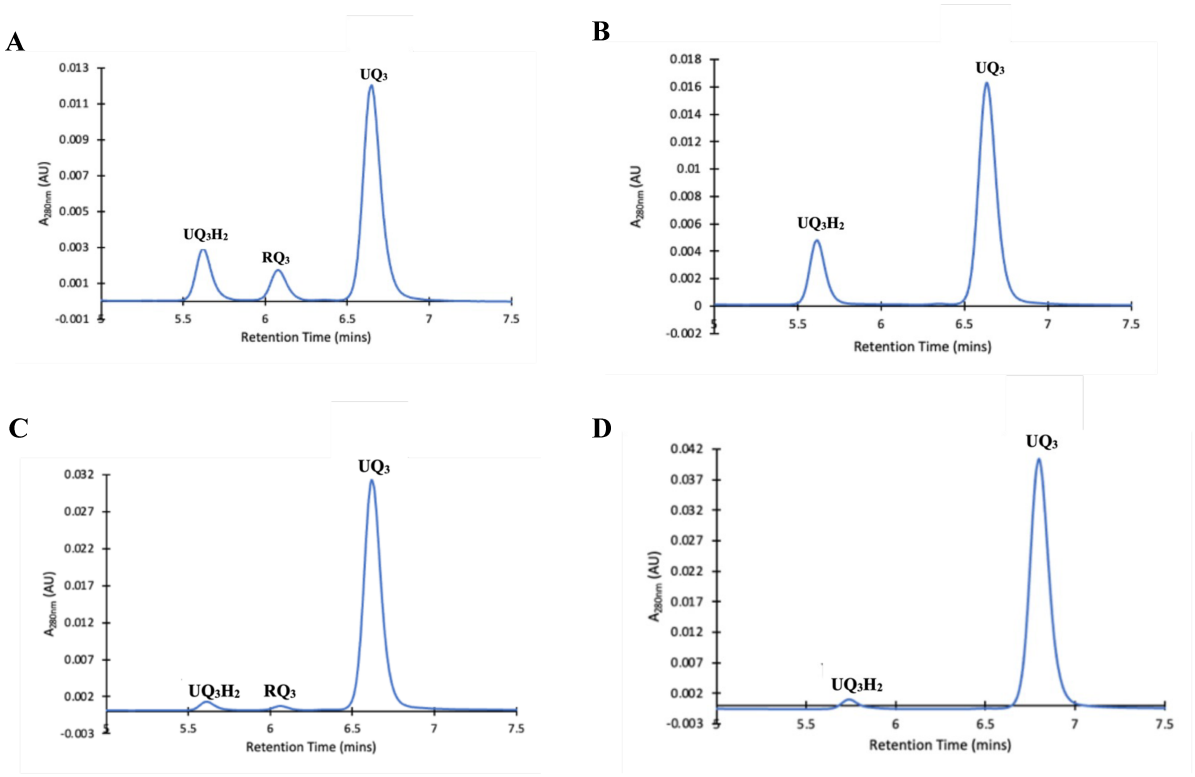

Figure 3.8 Functional Assays of RquA_MH and RquA_HD. Resulting HPLC chromatograms after RquA_MH was purified in **A.** 0.1% Brij-35 and **B.** no detergent. The reaction assay contained the base reaction buffer and RquA_MH was left to react for 60 min at room temperature in the dark before being quenched with acetonitrile. RquA_MH was able to convert UQ_3 to RQ_3 only when purified in 0.1% Brij-35. RquA_HD was purified in **C.** 0.1% Brij-35 and **D.** no detergent. RquA_HD was only able to convert UQ_3 to RQ_3 when it was purified in 0.1% Brij-35.

The reduced ability to convert UQ_3 to RQ_3 by both RquA_MH and RquA_HD compared to RquA_WT could be due to this helix being required for RquA to interact with UQ. This helix is predicted to interact with a membrane, which could be important when interacting with UQ, as UQ is found in a membrane. These changes to this helix to increase the solubility of RquA could have resulted in the diminished activity. UQ_3 is a hydrophobic molecule and might require micelles to be soluble. When a detergent is not present in the purification process, UQ_3 might not able to interact with RquA_MH and RquA_HD resulting in no RQ_3 production.

The amount of isoprenoid units increases the hydrophobicity of UQ. There are three isoprenoid units on the UQ being used in the RquA reactions (UQ_3). To see if a less hydrophobic UQ improves the activity of RquA_MH and RquA_HD, functional assays were attempted using UQ_1. However, the use of UQ_1 did not improve the activity of RquA_MH and RquA_HD (Figure 3.9AB). Interestingly, when UQ_1 is used in the reactions with RquA_MH and RquA_HD purified in 0.1% Brij-35, they are no longer active (Figure 3.9CD). The one isoprenoid unit tail might not be able to interact with RquA, resulting in it being unable to convert UQ_1 to RQ_1.

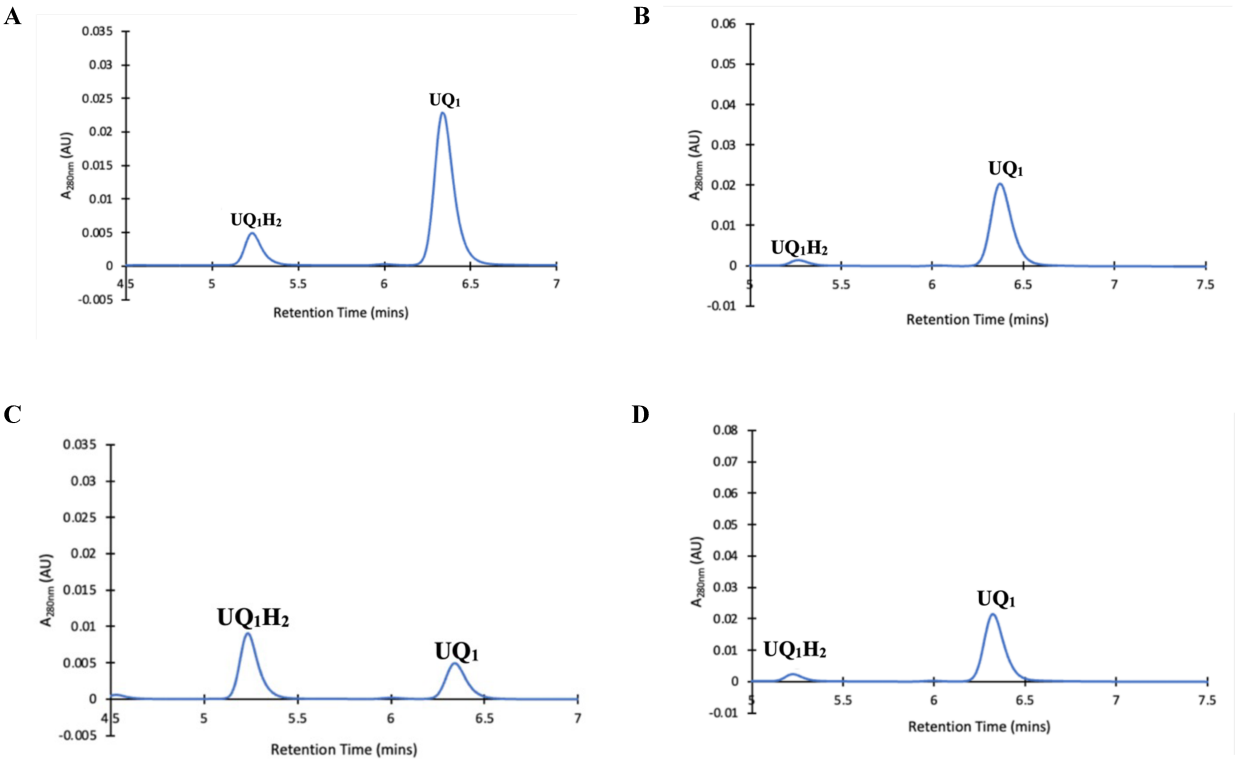

Figure 3.9 Functional Assays of RquA_MH and RquA_HD with UQ_1. HPLC chromatograms of functional assays involving UQ_1 are shown for **A.** RquA_MH purified without detergent. **B.** RquA_HD purified without detergent. **C.** RquA_MH purified with 0.1% Brij-35. **D.** RquA_HD purified with 0.1% Brij-35.

3.4 Summary

The aim of this research was to create two structural mutants of RquA to improve its solubility for future crystallography experiments. I chose a key helix that is comprised of mostly hydrophobic amino acids and predicted to interact with a membrane. I created two mutants by either mutating the helix to hydrophilic amino acids or deleting the helix. Both mutants were soluble with or without 0.1% Brij-3. However, it proved to be difficult to separate MBP from RquA_HD and RquA_MH. An alternate purification protocol created but did not completely resolve this issue. There was also very low yield after purification as I was only able to obtain about 0.l5 – 0.31 mg of protein per L of culture for both RquA_MH and RquA_HD. A good yield of RquA_HD and RquA_MH (~2.54 mg) were able to be solubilized without detergent up until the cleavage of MBP. This is an improvement compared to RquA_WT, as RquA_WT was insoluble without detergent. I was also able to determine that both RquA_MH and RquA_HD were only functional when purified in 0.1% Brij-35.

Chapter 4 Conclusions and Future Directions

4.1 Conclusions

This is the first research to show that the *RquA* homolog from *Euglena gracilis* can be produced recombinantly in *E. coli*, as past studies have focused on the *RquA* homolog from *Rhodospirillum rubrum* (Bernert et al, 2019, Brajcich et al, 2010, Lonjers et al, 2012, and Neupane et al, 2022). Both homologs are predicted to be associated with membranes and therefore require detergent to be soluble. I determined that RquA from *E. gracilis* is soluble in 0.1% Brij-35, 0.05% DDM, and 0.05% C12E8. I also determined that between those detergents, RquA had the highest yield when purified in 0.1% Brij-35. Based on circular dichroism spectroscopy and functional assays, RquA is folded when purified in 0.1% Brij-35. The apparent K_M and V_{max} values of UQ_3 and SAM binding to RquA were 9.2 ± 1.54 μM and 14.72 ± 2.59 μM, respectively. The maximum velocities of RquA when titrating UQ_3 and SAM were 0.2599 ± 0.017 μM min^{-1} and 0.173 ± 0.01 μM min^{-1}, respectively. Mn^{2+} was found to be required for RquA activity as, when it was absent, RQ_3 was no longer produced. I determined that RquA was most active at pH 8 but was not very sensitive to the chemical composition of the buffer, type of reducing agent used, concentration of NaCl, or concentration of Brij-35. Lastly, chapter 2 investigated two SAM analogs, SAH and sinefungin, as potential inhibitors of RquA. Both inhibitors were only able to slightly inhibit RquA at a concentration of 500 μM to 2 mM, indicating that they could be weak inhibitors of RquA.

Chapter 3 focused on creating structural mutants to improve the solubility of RquA to aid in future studies investigating its structure. RquA has a helix that is comprised of mostly hydrophobic amino acids and is predicted to interact with membranes. A similar helix was found

in UbiG and once it was removed, UbiG was more soluble (Zhu et al, 2016). The helix in RquA was either deleted or the amino acids were mutated with hydrophilic amino acids to try to improve its solubility. RquA_MH and RquA_HD were able to be solubilized without detergent, however they were not functional. These mutants were functional when they were purified in 0.1% Brij-35, indicating that this helix is not required for its activity. However, both mutants showed a lower ability to convert UQ_3 to RQ_3 compared to the wild type.

4.2 Future Directions

Unfortunately, I was unable to determine if SAH and sinefungin are competitive or non-competitive inhibitors of RquA. The HPLC instrument broke and for that reason complete inhibition assays were not carried out. I would like to determine what class (i.e., competitive, non-competitive, etc) of inhibitors SAH and sinefungin are by determining the effect of inhibitor concentration on the K_M and V_{max} of RquA. Since both SAH and sinefungin have very similar structures to SAM, I anticipate that they would inhibit in the same manner and act as competitive inhibitors competing with SAM to bind to the SAM binding site of RquA.

Mutants of RquA from *R. rubrum* had the aspartic acid residues required for SAM binding and found that they are required for activity (Neupane et al, 2022). RquA_Euglena also has two aspartic acid residues, so I would predict if they were also mutated, RquA_Euglena would also no longer be active. However, no work has looked at the SAM-binding motif consensus sequence of RquA. It would be interesting to see if mutating this consensus sequence, GHTHG, of RquA_Euglena would prevent SAM binding. I would like to specifically change the GxTxG to see if it would disrupt SAM from binding. GxGxG is the SAM-binding consensus sequence and it is not universally conserved, but the glycine residues are usually replaced with small chain, so it would be interesting to mutate those amino acids with long chain amino acids

to see if that affects SAM from binding to RquA. I would infer that changing the SAM-binding motif consensus sequence, would result in SAM no longer being able to bind RquA. RquA homology to other SAM-dependent methyltransferases is quite low, so mutagenesis on this sequence to try to narrow the location of this putative SAM-binding site is very beneficial. Since RquA does not participate in a typical methyltransferase reaction, SAM might bind to RquA in a different manner than most SAM-dependent methyltransferases to facilitate this amino transfer. The RquA mechanism remains unknown, but this research could provide some answers to how SAM is involved in the reaction, specifically how it binds to RquA.

My initial goal with the RquA mutants was to determine the atomic resolution structure through x-ray diffraction; however, I was not able to get a good enough yield of RquA with either of the mutants. However, it is still feasible with RquA_HD to carry out structural studies of MBP-RquA_HD. In the past, crystallization with a fusion protein was difficult due to conformational heterogeneity that occurs when a fusion protein is present, however there have been a few crystals created with a fusion tag still attached (Smyth et al, 2003). A good yield of MBP-RquA_HD (2.54 mg) was achieved without detergent. If this method is to be tried, the first thing that needs to be determined is if MBP-RquA_HD can bind SAM. Fluorescence can be used to determine if SAM is able to bind to MBP-RquA_HD to see if the bound form of MBP-RquA_HD can be determined. This can be done by titrating SAM and intrinsic tryptophan fluorescence can be measured from 300 nm to 450 nm to see the change in fluorescence at 340 nm. However, if SAM is no longer binds to MBP-RquA_HD, the unbound structure of MBP-RquA_HD can still be determined. Another strategy to determine the structures of the mutants could be expression without MBP. A plasmid with either a C-terminal or N-terminal His-tag could be created to purify these mutants to remove the issue with the difficult separation of MBP

from RquA. One issue with this strategy is purifying proteins with His-tags is not as specific as purifying proteins with MBP. Ni^{2+}-NTA has an affinity to any proteins that have histidine's, so it would not only purify your protein, but any protein that has histidine's. This was seen when RquA was refolded and purified through Ni^{2+}-NTA with the multiple bands seen on the SDS-PAGE gel after the RquA band.

Once the structure of RquA is determined, future work could determine where both SAM and UQ bind to RquA. We know where the putative SAM-binding location is; however, where UQ might bind remains unknown. I would predict that UQ binds close to the SAM-binding domain, as SAM donates the amino group that replaces the methoxy group on UQ. It would be important to learn where both substrates bind to RquA to learn more about the reaction and how it proceeds. Once the UQ binding site is located, mutagenesis studies can be done to determine the important residues required for the binding of UQ. All these experiments aim to learn more about how the RquA reaction works which currently remains unknown. To fully understand how RquA works, we need to learn how both SAM and UQ interact with RquA acts as substrates to produce RQ.

Bibliography

Aguilar, Z. P. (2013). Types of nanomaterials and corresponding methods of synthesis. Nanomaterials for Medical Applications, 33–82. https://doi.org/10.1016/b978-0-12-385089-8.00002-9

Ahmad, M,. Wolberg, A., and Kahwaji, C.I. (2023). Biochemistry, electron transport chain. Treasure Island (FL): StatsPearks Publishing. Available from: https://www.ncbi.nlm.nih.gov/books/NBK526105/

Alberts, B., Johnson, A., Lewis, J., et al. (2002). How cells obtain energy from food. In: Molecular Biology of the Cell. 4th edition. New York: Garland Science. Available from: https://www.ncbi.nlm.nih.gov/books/NBK26882/

Alcázar-Fabra, M., Navas, P., & Brea-Calvo, G. (2016). Coenzyme Q biosynthesis and its role in the respiratory chain structure. Biochimica et Biophysica Acta (BBA) - Bioenergetics, 1857(8), 1073–1078. https://doi.org/10.1016/j.bbabio.2016.03.010

Allen, J. F. (2002). Photosynthesis of ATP—electrons, proton pumps, rotors, and poise. Cell, 110(3), 273–276. https://doi.org/10.1016/s0092-8674(02)00870-x

Allen, K. N., Entova, S., Ray, L. C., & Imperiali, B. (2019). Monotopic membrane proteins join the fold. Trends in biochemical sciences, 44(1), 7–20. https://doi.org/10.1016/j.tibs.2018.09.013

Amesz, J. (1973). The function of plastoquinone in photosynthetic electron transport. Biochimica et Biophysica Acta (BBA) - Reviews on Bioenergetics, 301(1), 35–51. https://doi.org/10.1016/0304-4173(73)90011-6

Ballard, J. W. O., & Youngson, N. A. (2015). Review: Can diet influence the selective advantage of mitochondrial DNA haplotypes? *Bioscience Reports*, *35*(6). https://doi.org/10.1042/bsr20150232

Bentley, R., & Meganathan, R. (1982). Biosynthesis of vitamin K (menaquinone) in bacteria. Microbiological Reviews, 46(3), 241–280. https://doi.org/10.1128/mr.46.3.241-280.1982

Bernert, A. C., Jacobs, E. J., Reinl, S. R., Choi, C. C. Y., Roberts Buceta, P. M., Culver, J. C., Goodspeed, C. R., Bradley, M. C., Clarke, C. F., Basset, G. J., & Shepherd, J. N. (2019). Recombinant rqua catalyzes the in vivo conversion of ubiquinone to rhodoquinone in escherichia coli and saccharomyces cerevisiae. Biochimica Et Biophysica Acta (BBA) - Molecular and Cell Biology of Lipids, 1864(9), 1226–1234. https://doi.org/10.1016/j.bbalip.2019.05.007

Bhatt, V. (2016). Thermodynamics and kinetics of complex formation. In Essentials of Coordination Chemistry (pp. 111–137). essay, Academic Press.

Birch, J., Axford, D., Foadi, J., Meyer, A., Eckhardt, A., Thielmann, Y., & Moraes, I. (2018). The fine art of integral membrane protein crystallisation. Methods, 147, 150–162. https://doi.org/10.1016/j.ymeth.2018.05.014

Boersch, M., Rudrawar, S., Grant, G., & Zunk, M. (2018). Menaquinone biosynthesis inhibition: A review of advancements toward a new antibiotic mechanism. RSC Advances, 8(10), 5099–5105. https://doi.org/10.1039/c7ra12950e

Bolton, J. L., & Dunlap, T. (2016). Formation and biological targets of quinones: cytotoxic versus cytoprotective effects. Chemical Research in Toxicology, 30(1), 13–37. https://doi.org/10.1021/acs.chemrestox.6b00256

Boyer, P.D. (1998), Energy, life, and ATP (Nobel Lecture). Angewandte Chemie International Edition, 37: 2296-2307. https://doi.org/10.1002/(SICI)1521-3773(19980918)37:17<2296::AID-ANIE2296>3.0.CO;2-W

Brajcich, B. C., Iarocci, A. L., Johnstone, L. A., Morgan, R. K., Lonjers, Z. T., Hotchko, M. J., Muhs, J. D., Kieffer, A., Reynolds, B. J., Mandel, S. M., Marbois, B. N., Clarke, C. F., & Shepherd, J. N. (2010). Evidence that ubiquinone is a required intermediate for rhodoquinone biosynthesis in Rhodospirillum rubrum. Journal of bacteriology, 192(2), 436–445. https://doi.org/10.1128/JB.01040-09

Carpenter, E. P., Beis, K., Cameron, A. D., & Iwata, S. (2008). Overcoming the challenges of membrane protein crystallography. Current Opinion in Structural Biology, 18(5), 581–586. https://doi.org/10.1016/j.sbi.2008.07.001

Chen, H., & Zhang, Y.-H. P. (2020). Enzymatic regeneration and conservation of ATP: challenges and opportunities. Critical Reviews in Biotechnology, 41(1), 16–33. https://doi.org/10.1080/07388551.2020.1826403

Coleman, J. P., & Smith, C. J. (2014). Microbial metabolism. Reference Module in Biomedical Sciences, 1–6. https://doi.org/doi.org/10.1016/B978-0-12-801238-3.05146-1.

Cooper, G.M. (2000) Chapter 2 Photosynthesis, In The cell: A molecular approach. 2nd edition. Sunderland (MA): Sinauer Associates. Available from: https://www.ncbi.nlm.nih.gov/books/NBK9861/

Dairi, T. (2012). Menaquinone biosyntheses in microorganisms. Natural Product Biosynthesis by Microorganisms and Plants, Part A, 107–122. https://doi.org/10.1016/b978-0-12-394290-6.00006-9

Darrouzet, E., & Dupuis, A. (1997). Genetic evidence for the existence of two quinone related inhibitor binding sites in NADH-CoQ reductase. Biochimica et Biophysica Acta (BBA) - Bioenergetics, 1319(1), 1–4. https://doi.org/10.1016/s0005-2728(97)00009-1

Dykens, J. A. (2007). Redox enzymes. (J. B. Taylor & D. J. Triggle, Eds.). Comprehensive Medicinal Chemistry II, 1053–1087. https://doi.org/https://doi.org/10.1016/B0-08-045044-X/00071-7

El-Najjar, N., Gali-Muhtasib, H., Ketola, R. A., Vuorela, P., Urtti, A., & Vuorela, H. (2011). The chemical and biological activities of quinones: Overview and implications in analytical detection. Phytochemistry Reviews, 10(3), 353–370. https://doi.org/10.1007/s11101-011-9209-1

Ferguson, S. J., Jackson, J. B., & McEwan, A. G. (1987). Anaerobic respiration in the Rhodospirillaceae: characterisation of pathways and evaluation of roles in redox balancing during photosynthesis. FEMS Microbiology Letters, 46(2), 117–143. https://doi.org/10.1111/j.1574-6968.1987.tb02455.x

Garavito, R. M., & Ferguson-Miller, S. (2001). Detergents as tools in membrane biochemistry. Journal of Biological Chemistry, 276(35), 32403–32406. https://doi.org/10.1074/jbc.r100031200

Havaux, M. (2020). Plastoquinone in and beyond photosynthesis. Trends in Plant Science, 25(12), 1252–1265. https://doi.org/10.1016/j.tplants.2020.06.011

Hebditch, M., & Warwicker, J. (2019). Web-based display of protein surface and ph-dependent properties for assessing the developability of Biotherapeutics. Scientific Reports, 9(1). https://doi.org/10.1038/s41598-018-36950-8

Heckman, K., Pease, L. Gene splicing and mutagenesis by PCR-driven overlap extension. Nature protocols, 2, 924–932 (2007). https://doi.org/10.1038/nprot.2007.132

Hentges D.J. (1996) Chapter 17 Anaerobes: general characteristics. In: Medical Microbiology. 4th edition. Galveston (TX): University of Texas Medical Branch at Galveston. Available from: https://www.ncbi.nlm.nih.gov/books/NBK7638/

Hinkle, P. C., & McCarty, R. E. (1978). How cells make ATP. Scientific American, 238(3), 104–123. https://doi.org/10.1038/scientificamerican0378-104

Hiraishi, A. (1988). Fumarate reduction systems in members of the family Rhodospirillaceae with different quinone types. Archives of Microbiology, 150(1), 56–60. https://doi.org/10.1007/bf00409718

Igelsrud, D. E. (1989). How living things obtain energy: A simpler explanation. The American Biology Teacher, 51(2), 89–93. https://doi.org/10.2307/4448857

Joseph, M., Trinh, H. M., & Mitra, A. K. (2017). Peptide and protein-based therapeutic agents∗. Emerging Nanotechnologies for Diagnostics, Drug Delivery and Medical Devices, 145–167. https://doi.org/10.1016/b978-0-323-42978-8.00007-3

Jumper, J., Evans, R., Pritzel, A. et al. Highly accurate protein structure prediction with AlphaFold. Nature 596, 583–589 (2021). https://doi.org/10.1038/s41586-021-03819-2

Jurtshuk P Jr.. (1996). Chapter 4 Bacterial metabolism. In: Medical Microbiology. 4th edition. Galveston (TX): University of Texas Medical Branch at Galveston. Available from: https://www.ncbi.nlm.nih.gov/books/NBK7919/

Karavaeva, V., & Sousa, F. L. (2022). Modular structure of complex II: An evolutionary perspective. Biochimica et Biophysica Acta (BBA) - Bioenergetics, 1863, 148631. https://doi.org/10.1016/j.bbabio.2022.148631

Kishi, S., Saito, K., Kato, Y., & Ishikita, H. (2017). Redox potentials of ubiquinone, menaquinone, phylloquinone, and plastoquinone in aqueous solution. Photosynthesis research, 134(2), 193–200. https://doi.org/10.1007/s11120-017-0433-4

Kozbial, P. Z., & Mushegian, A. R. (2005). Natural history of S-adenosylmethionine-binding proteins. BMC structural biology, *5*, 19. https://doi.org/10.1186/1472-6807-5-19

Leibly, D. J., Nguyen, T. N., Kao, L. T., Hewitt, S. N., Barrett, L. K., & Van Voorhis, W. C. (2012). Stabilizing additives added during cell lysis aid in the solubilization of recombinant proteins. PLoS ONE, 7(12). https://doi.org/10.1371/journal.pone.0052482

Ling, G. N. (1981). Oxidative phosphorylation and mitochondrial physiology: A Critical Review of Chemiosmotic Theory, and Reinterpretation by the Association-Induction Hypothesis. Physiological Chemistry and Physics, (13).

Lonjers, Z. T., Dickson, E. L., Chu, T. P., Kreutz, J. E., Neacsu, F. A., Anders, K. R., & Shepherd, J. N. (2012). Identification of a new gene required for the biosynthesis of rhodoquinone in Rhodospirillum rubrum. Journal of bacteriology, 194(5), 965–971. https://doi.org/10.1128/JB.06319-11

Marcia, M., Langer, J. D., Parcej, D., Vogel, V., Peng, G., & Michel, H. (2010). Characterizing a monotopic membrane enzyme. biochemical, enzymatic and crystallization studies on aquifex aeolicus sulfide:quinone oxidoreductase. Biochimica et Biophysica Acta (BBA) - Biomembranes, 1798(11), 2114–2123. https://doi.org/10.1016/j.bbamem.2010.07.033

Mazzei, L., Ciurli, S., & Zambelli, B. (2016). Isothermal titration calorimetry to characterize enzymatic reactions. Methods in Enzymology, 215–236. https://doi.org/10.1016/bs.mie.2015.07.022

Micsonai, A., Wien, F., Kernya, L., Lee, Y.-H., Goto, Y., Réfrégiers, M., & Kardos, J. (2015). Accurate secondary structure prediction and fold recognition for circular dichroism spectroscopy. Proceedings of the National Academy of Sciences, 112(24). https://doi.org/10.1073/pnas.1500851112

Milshteyn, D., Cooper, G., & Deamer, D. (2019). Chemiosmotic energy for primitive cellular life: Proton gradients are generated across lipid membranes by redox reactions coupled to meteoritic quinones. Scientific Reports, 9(1). https://doi.org/10.1038/s41598-019-48328-5

Moraes, I., Evans, G., Sanchez-Weatherby, J., Newstead, S., & Stewart, P. D. (2014). Membrane protein structure determination - the next generation. Biochimica et biophysica acta, 1838, 78–87. https://doi.org/10.1016/j.bbamem.2013.07.010

Moyes, C. D., & Le Moine, C. M. R. (2011). Tissue respiration | mitochondrial respiration. Encyclopedia of Fish Physiology, 959–965. https://doi.org/10.1016/b978-0-12-374553-8.00121-0

Muller, A. W. J. (1983). Thermoelectric energy conversion could be an energy source of living organisms. Physics Letters A, 96(6), 319–321. https://doi.org/10.1016/0375-9601(83)90189-5

Neupane, T., Chambers, L. R., Godfrey, A. J., Monlux, M. M., Jacobs, E. J., Whitworth, S., Spawn, J. E., Clingman, S. H., Vergunst, K. L., Niven, F. M., Townley, J. J., Orion, I. W., Goodspeed, C. R., Cooper, K. A., Cronk, J. D., Shepherd, J. N., & Langelaan, D. N. (2022). Microbial rhodoquinone biosynthesis proceeds via an atypical RQUA-catalyzed amino transfer from S-adenosyl-L-methionine to ubiquinone. Communications Chemistry, 5(1). https://doi.org/10.1038/s42004-022-00711-6

Nowicka, B., & Kruk, J. (2010). Occurrence, biosynthesis and function of isoprenoid quinones. Biochimica et Biophysica Acta (BBA) - Bioenergetics, 1797(9), 1587–1605. https://doi.org/10.1016/j.bbabio.2010.06.007

Salinas, G., Langelaan, D. N., & Shepherd, J. N. (2020). Rhodoquinone in bacteria and animals: Two distinct pathways for biosynthesis of this key electron transporter used in anaerobic bioenergetics. Biochimica Et Biophysica Acta (BBA) - Bioenergetics, 1861(11), 148278. https://doi.org/10.1016/j.bbabio.2020.148278

Sawers, R. G., Falke, D., & Fischer, M. (2016). Oxygen and nitrate respiration in streptomyces coelicolor A3(2). Advances in Bacterial Electron Transport Systems and Their Regulation, 1–40. https://doi.org/10.1016/bs.ampbs.2016.02.004

Schmitz, R.A., Daniel, R., Deppenmeier, U., Gottschalk, G. (2006). The Anaerobic way of life. In: Dworkin, M., Falkow, S., Rosenberg, E., Schleifer, KH., Stackebrandt, E. (eds) The Prokaryotes. Springer, New York, NY. https://doi.org/10.1007/0-387-30742-7_4

Sissi, C., & Palumbo, M. (2009). Effects of magnesium and related divalent metal ions in topoisomerase structure and function. Nucleic acids research, 37(3), 702–711. https://doi.org/10.1093/nar/gkp024

Smyth, M. S., & Martin, J. H. (2000). x ray crystallography. Molecular pathology: MP, 53(1), 8–14. https://doi.org/10.1136/mp.53.1.8

Smyth, D. R., Mrozkiewicz, M. K., McGrath, W. J., Listwan, P., & Kobe, B. (2003). Crystal structures of fusion proteins with large-affinity tags. Protein science: a publication of the Protein Society, 12(7), 1313–1322. https://doi.org/10.1110/ps.0243403

Stairs, C. W., Eme, L., Muñoz-Gómez, S. A., Cohen, A., Dellaire, G., Shepherd, J. N., Fawcett, J. P., & Roger, A. J. (2018). Microbial eukaryotes have adapted to hypoxia by horizontal acquisitions of a gene involved in rhodoquinone biosynthesis. ELife, 7. https://doi.org/10.7554/elife.34292

Stefely, J. A., & Pagliarini, D. J. (2017). Biochemistry of mitochondrial coenzyme Q Biosynthesis. Trends in biochemical sciences, 42(10), 824–843. https://doi.org/10.1016/j.tibs.2017.06.008

Stetsenko, A., & Guskov, A. (2017). An overview of the top ten detergents used for membrane protein crystallization. Crystals, 7(7), 197. https://doi.org/10.3390/cryst7070197

Stouthamer, A. H. (1991). Metabolic regulation including anaerobic metabolism Inparacoccus Denitrificans. Journal of Bioenergetics and Biomembranes, 23(2), 163–185. https://doi.org/10.1007/bf00762216

Thauer, R. K., Jungermann, K., & Decker, K. (1977). Energy conservation in chemotrophic anaerobic bacteria. Bacteriological Reviews, 41(1), 100–180. https://doi.org/10.1128/br.41.1.100-180.1977

Thomson, R. H. (1971). Naturally occurring quinones. Academic Press.

Uno, S., Kimura, H., Murai, M., & Miyoshi, H. (2019). Exploring the quinone/inhibitor-binding pocket in mitochondrial respiratory complex I by chemical biology approaches. The Journal of biological chemistry, 294(2), 679–696. https://doi.org/10.1074/jbc.RA118.006056

Verberne, M. C., Budi Muljono, R. A., & Verpoorte, R. (1999). Chapter 13 - Salicylic acid biosynthesis. Biochemistry and Molecular Biology of Plant Hormones, 33, 295–312. https://doi.org/https://doi.org/10.1016/S0167-7306(08)60493-7

Voidarou, C., Antoniadou, M., Rozos, G., Tzora, A., Skoufos, I., Varzakas, T., Lagiou, A., & Bezirtzoglou, E. (2020). Fermentative foods: microbiology, biochemistry, potential human health benefits and public health issues. Foods (Basel, Switzerland), 10(1), 69. https://doi.org/10.3390/foods10010069

Walther, B., Karl, J. P., Booth, S. L., & Boyaval, P. (2013). Menaquinones, bacteria, and the food supply: the relevance of dairy and fermented food products to vitamin K requirements. Advances in nutrition (Bethesda, Md.), 4(4), 463–473. https://doi.org/10.3945/an.113.003855

Wilman, H. R., Shi, J., & Deane, C. M. (2014). Helix kinks are equally prevalent in soluble and membrane proteins. Proteins, *82*(9), 1960–1970. https://doi.org/10.1002/prot.24550

Yeagle, P. L. (2016). Chapter 10 - Membrane proteins. In The Membranes of Cells (3rd ed., pp. 219–268). essay, Academic Press.

Zhang, J., & Zheng, Y. G. (2016). SAM/SAH analogs as versatile tools for SAM-dependent methyltransferases. ACS chemical biology, 11(3), 583–597. https://doi.org/10.1021/acschembio.5b00812

Zhu, Y., Jiang, X., Wang, C., Liu, Y., Fan, X., Zhang, L., Niu, L., Teng, M., & Li, X. (2016). Structural insights into the methyl donor recognition model of a novel membrane-binding protein ubig. Scientific Reports, 6(1). https://doi.org/10.1038/srep23147

Zimmerman, J. J., von Saint André-von Arnim, A., & McLaughlin, J. (2011). Chapter 74 - Cellular respiration. In Pediatric Critical Care (4th ed., pp. 1058–1072). essay, Mosby.